Conversion of Molecular Architectures Using [2+2]-Cycloaddition Reactions and Its Applications to Photo-functional Materials

[2+2]環化付加反応による構造変換と光機能性材料への応用

February, 2023

Moeka INADA

稲田　萌花

Conversion of Molecular Architectures Using [2+2]-Cycloaddition
Reactions and Its Applications to Photo-functional Materials

[2+2]環化付加反応による構造変換と光機能性材料への応用

February, 2023

Waseda University Graduate School of Advanced Science and Engineering

Department of Advanced Science and Engineering, Research on Life
Science and Medical Bioscience

Moeka INADA
稲田　萌花

Contents

Chapter 3 *Photo-conversion of multi-branching structures based on [2+2]-cycloaddition reactions*……………………………………………………….63

List of figures

List of tables

List of schemes

List of abbreviations

^{1}H-NMR	Proton (^{1}H) nuclear magnetic resonance spectroscopy
^{13}C-NMR	Carbon (^{13}C) nuclear magnetic resonance spectroscopy
^{29}Si-NMR	Silicon(^{29}Si) nuclear magnetic resonance spectroscopy
3D-	Three-dimensional
4D-	Four-dimensional
BA	Boronic acid
CA	Cinnamic acid
CAA	Cinnamylideneacetic acid
CAC	Critical aggregation concentration
CH_2Cl_2	Dichloromethane
DCB	Dynamic covalent bond
DCM	Dichloromethane
DCTB	trans-2-[3-(4-tert-butylphenyl)-2-methyl-2-propenylidene]malononitrile
DCvC	Dynamic covalent chemistry
DFT	Density functional theory
DLS	Dynamic light scattering
DMF	N, N-dimethylformamide
DNA	Deoxyribonucleic acid
DNN	Dual dynamic network
DoD	De-bonding on-demand
DPDA	Diphenyl diacetylene
DSC	Differential scanning calorimetry
EDC	1-ethyle 3 -(3-dimethylamonopropyl) carbodiimide hydrochloride
FT-IR	Fourier-transform infrared
G'	Storage modulus
G"	Loss modulus
GPC	Gel permeation chromatography
HCl	Hydrogen chloride
HOBt	1-hydroxybenzotriazole monohydrate
HOMO	Highest occupied Molecular Orbital
HRMS(ESI)	High-resolution Mass spectrometry (Electrospray ionization)
K_2CO_3	Potassium carbonate
LUMO	Lowest Unoccupied Molecular Orbital
MALDI-TOF	Matrix Assisted Laser Desorption/Ionization-Time of Flight
MAT	Macromolecular architectural transformations
MM calculation	Molecular Mechanics calculation
$MgSO_4$	Magnesium sulfate
MOFs	Metal-organic frameworks
NaCl	Sodium chloride
$NaHCO_3$	Sodium hydrogen carbonate
NMR	Nuclear magnetic resonance

PDI	**P**yri**d**inedi**i**mine
PE	**P**oly**e**thylene
PET	**P**oly**e**thylene **T**erephthalate
PMMA	**P**oly**m**ethyl **m**eth**a**crylate
PP	**P**oly**p**ropylene
PTFE	**P**oly**t**etra**f**luoro**e**thylene
RT	**R**oom **t**emperature
S_0	Ground state
S_1	Singlet excited states
T_1	**T**riplet excited states
T1	Longitudinal relaxation time, spin-lattice relaxation time
T2	Transverse relaxation time, spin-spin relaxation time
TEM	**T**ransmission **e**lectron **m**icroscope
T_g	Glass transition temperature
TG-DTA	**T**hermo**g**ravimetry **d**ifferential **t**hermal **a**nalysis
THF	**T**etra**h**ydro**f**uran
UV	**U**ltraviolet
UV/Vis	**U**ltraviolet-**V**isible

Abstract

Polymers incorporating dynamic covalent bonds, which can be reversibly combined and broken repeatedly, have the potential to be used as environmentally friendly materials. In this study, [2+2] cycloaddition reactions, known as light-driven dynamic covalent bonds, were focused on. The polymers incorporating these bonds were designed and synthesized through several polymerization reactions. Particular attention was concentrated on the monomer structure for polymerization, elucidating the correlation between the molecular structure and the functionality imparted by the structure. The polymerization conditions were searched and controlled to develop the polymeric materials for applications to self-healing, de-bonding on demand, and shape memory polymer materials.

Chapter 1

General introduction

Introduction

Our societies have been supported by numerous materials produced in the 20th century by mass production. However, most of these materials are yet to be made and optimized for recyclability. Consequently, global environmental problems, including waste disposal issues, have emerged. Sustainable material-cycle societies, represented by a circular economy, require the development of recyclable materials that are easily degradable and have a long lifetime. Material design for maximum functionality is an important step to achieve this goal, which starts from the molecular design stage.

Traditionally, molecular synthesis in organic chemistry has relied on irreversible reactions with molecules and kinetic control mechanisms. Compared to irreversible bonds, reversible non-covalent and covalent bonds have a "dynamic" nature.[1, 2] Supramolecular polymers, among the polymers, have dynamic properties, consisting of weak non-covalent bonds that spontaneously rearrange themselves into the most conformational thermodynamically advantageous forms.[3] However, supramolecular polymers are said to be unstable and unsuitable for applications where higher robustness is required. For applications requiring greater robustness, dynamic covalent bonds have emerged as an attractive alternative to the unstable supramolecular polymer.[4] In dynamic covalent bonds, the strength of common covalent bonds is combined with the reversibility of non-covalent bonds, in which bonds are formed and broken irreversibly by external stimuli.[1] Polymers incorporating dynamic covalent bonds can reversibly break and recombine and can polymerize and depolymerize autonomously because of external stimuli, such as heat and light (Figure 1.1). Due to their ability to reorganize after polymerization, such polymers are expected to be used as self-healing materials [5], biodegradable materials [6], and recyclable polymers [7, 8] which have attracted much attention in recent years.
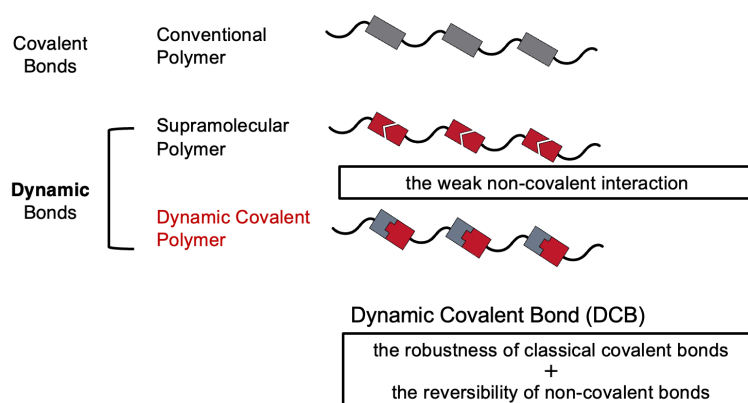
Figure 1.1 Schematic of polymer systems with a) covalent bonds and b) dynamic bonds (based on the reference from H. Otsuka *et al.* [9, 10])

1.1. Dynamic covalent chemistry (DCvC)

1.1.1 Principles of dynamic covalent bonds

Rowan *et al.* defined dynamic covalent chemistry as a thermodynamically controlled bond, wherein all components are in equilibrium. [1, 9, 11] The dynamic covalent bond (DCB) process is a dynamic exchange of molecular components in equilibrium to reach thermodynamical stability. It can also be described as stimulus-responsive chemistry, as the library composition changes in response to the reaction environment, including the reaction medium (solvent) and physical factors (such as temperature, light, electricity, and mechanical stress).[12] As shown in Figure 1.2, covalent bonding is generally irreversible, and hence it is induced under kinetic control. In contrast, covalent bonds are formed under thermodynamic control when the equilibration process is sufficiently fast and stabilized by external stimuli.[9] This reaction is governed by the relative stabilities of the resulting products (ΔG_B, ΔG_c) rather than the relative magnitudes of the transition states ($\Delta G_B^{\ddagger}$, $\Delta G_c^{\ddagger}$). Dynamic chemical systems are accomplished simply in the following ways. The first is to incorporate a specific function into the starting material. For example, constitutional, steric, or electronic effects stabilize the desired product and promote equilibrium to the thermodynamically most stable product. A second approach is to use an excess of one of the starting materials or to remove the condensation product. Thus, the equilibrium of the reaction can be directed toward producing the desired product.
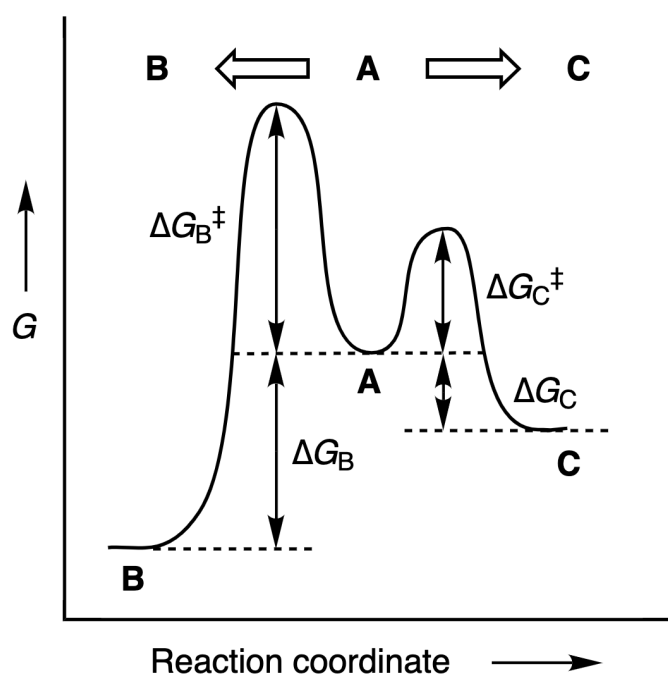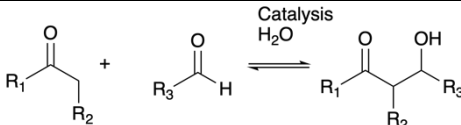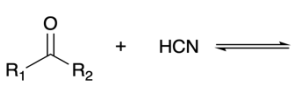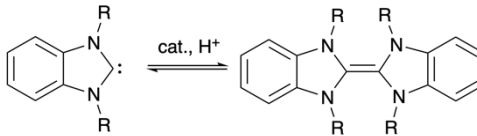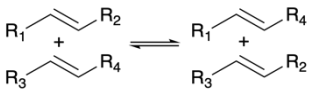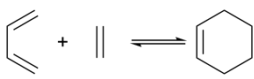
Figure 1.2 Diagram illustrating kinetic and thermodynamic control of a product distribution depicted with free energy. Free energy profile illustrating kinetic (A→C) versus thermodynamic (A→B) control of the product distribution: in part from ref 1, with permission from Wiley Online Library.[1]

Dynamic covalent bonds also require a catalyst for equilibration, as the thermodynamically stable products take longer to progress in the reaction than non-covalent supramolecules.[1] External stimuli such as temperature, concentration, pressure, and light can also induce reversible reactions. It is generally recognized that reversible dynamic covalent bonds can be classified into two types[12]: (1) exchange reactions and (2) formation reactions to form new bonds. Thus, the DCBs are classified by bond and summarized in Table 1.1-5.

1.1.2 Summary of dynamic covalent bonds

i)   C-C bonds

Table 1.1 Summary of dynamic covalent bonds based on C-C bond.

Reaction type		Chemicals	Condition	Ref
C-C bonds	Aldol reaction		Chemical	13
	Cyanohydrin formation		Chemical	14
	Carbene dimerization		Chemical and heat	15, 16
	Friedel-Crafts alkylation		Chemical	17
	Olefin metathesis		Metal catalyst	18
	Diels–Alder reaction		Heat	19, 20
	Cycloaddition reactions		UV-light, heat	21, 22

ii) C-N bonds

Table 1.2 Summary of dynamic covalent bonds based on C-N bond.

Reaction type		Chemicals	Condition	Ref.
C–N bond	Imine exchange		pH	23
	Imine condensation		pH	23
	Amide exchange		Catalysis, heat	24

iii) C-O bonds

Table 1.3 Summary of dynamic covalent bonds based on C-O bond.

Reaction type		Chemicals	Condition	Ref.
C–O bond	Ester-exchange		Chemical	25
	Acetal-formation/ exchange		Chemical	25
	Nicholas ether-exchange		Chemical	26
	Hemiaminal ether-exchange		Chemical	27
	Alkoxyamine-exchange		Heat	28

iv) C-S bonds

Table 1.4 Summary of dynamic covalent bonds based on C-S bond.

Reaction type		Chemicals	Condition	Ref
C–S bond	Thioacetal exchange		Heat, acid	[25, 29]
	Thiazolidine exchange		Catalysis	[30]
	Thia-Michael reaction		Catalysis	[31, 32]

v) Others

Table 1.5 Summary of dynamic covalent bonds (Others).

Reaction type		Chemicals	Condition	Ref
B–O bond	Boronic acid condensation		Chemical	[33]
S–S bond	Disulfide exchange		RT or mild temperature	[34]
Siloxane	Siloxane silanol exchange reaction		Catalyst	[35, 36]
Diselenide	Diselenide exchange		Visible light	[34]

1.1.3 Chemical dynamic covalent bonds

A chemical dynamic covalent bond is typically formed by a catalytic reaction and induced by changes in pH.

(1) Catalyst-induced reactions

Most of the functional groups involved in dynamic covalent bonds are initiated by catalysts and maintain equilibrium with their surroundings. As a result of these dynamic covalent bonding reactions, the covalent bonds are equilibrated in a time-dependent manner to produce a thermodynamically stable product. [37]

Olefin metathesis reactions: Olefin metathesis is one of the oldest known catalytic dynamic covalent bonds. These are catalytic reactions in which bond recombination occurs between two different olefins.[18] One example is the formation of a four-membered ring metallacyclobutane complex from a carbene complex and an olefin, followed by another carbene complex and olefin.[38] In this reaction, the olefin moiety reacts selectively, yielding complex olefins from simple raw materials, and even in the case of intermolecular reactions, selective cross-metathesis products are obtained depending on the substrate, which is of high synthetic value.

Ester exchange: The ester-exchange reaction occurs when alcohols, carboxylic acids, and other esters exchange acyl and alkoxy groups to form new esters. Trace amounts of alkali and inorganic acids act as catalysts in this reaction. The reaction is accelerated using large quantities of alcohol. Transesterification is usually accomplished by reacting an ester with alcohol in the presence of an acid catalyst.

(2) pH-induced reactions

Boronic acid condensation and imine bonds are dynamic covalent bonds in which the pH is changed by the addition of an acid or base.

Reversible boronate ester formation: Boronic acid (BA) derivatives can readily interact with cis-diols, which are abundant in biomolecules such as sugar and ribose, by reversibly forming boronic acid esters in an aqueous solution.[39]

Imine bond formation/exchange: Imine bond formation occurs when a water molecule is lost within a single molecule or between two molecules containing an amino group and a carbonyl group, resulting in an intramolecular or intermolecular C=N double bond. The addition of water to an imine causes hydrolysis and condensation to proceed in the opposite direction, giving rise to a reversible reaction. These reactions can also be triggered by acid catalysis. There are several external factors that influence the equilibrium state of an imine-bonded reaction, including solvent, concentration, pH, temperature, and steric and electronic factors.[40]

1.1.4 Thermally dynamic covalent bonds

Thermo-responsive dynamic covalent bonds, represented by the Diel-Alder reaction in pericyclic reactions, are known to break/join bonds in a thermally responsive manner.

Reaction mechanism of a Diel-Alder reaction: Pericyclic Reactions were discovered by R.B.Woodward and R.Hoffman in 1964 to explain the symmetry of molecular orbitals,[41] and also Kenichi Fukui described this reaction by frontier orbit theory in 1981.[42] The Diehl-Alder reaction is a [4+2] reaction in which an unsaturated six-membered ring is formed by the addition of an alkene to a conjugated diene (Figure 1.3). This reaction proceeds by heat, in which there are two π-connections disappearance and the occurrence of two σ-connections.[19, 20]
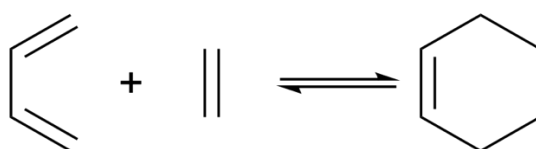
Figure 1.3 Scheme of Diel-Alder reactions.

Alkoxyamine exchange: In the case of alkoxyamine units derived from stable nitroxide radicals, one of the thermally reversible reactions is the reversible formation of C-ON bonds between the units. When the covalent C-ON bond is homolyzed by the heating process, the alkoxyamine derivative can produce a nitroxide radical with carbon.[10]

1.2 Photodynamic covalent bonds

While the previous section examined several dynamic covalent bonds in detail, this section focuses particularly on photochemical reactions. A photochemical reaction is a chemical reaction that is initiated by light as an energy source; the process is initiated by the absorption of photon energy by the molecules of a substance.[43] Frequently, this photochemical reaction is compared and discussed with thermo-induced reactions. Photochemical reactions are characterized by the ability of "direct" remote irradiation and leaving no residues, herein, those reactions are considered as the green synthesis pathway. Thus, a critical role is played by light-induced covalent bonding in the development of smart materials that respond to environmental stimuli. [43-46] It is known that many photochemical reactions exist, such as photoisomerization [48] and photo-dimerization. [47, 48]

The following section discusses a type of pericyclic reaction, photocycloaddition reaction, in which dynamic covalent bonds are formed between molecules by light. Thus, a critical role is played by light-induced covalent bonding in the development of smart materials, that respond to environmental stimuli.[47, 48] To understand the mechanism of these photochemical reactions, it is important to understand the energy state of the molecules. Figure 1.4 shows the Jablonski diagram, which demonstrates the possible transitions that can occur after the molecule is photoexcited. [49]
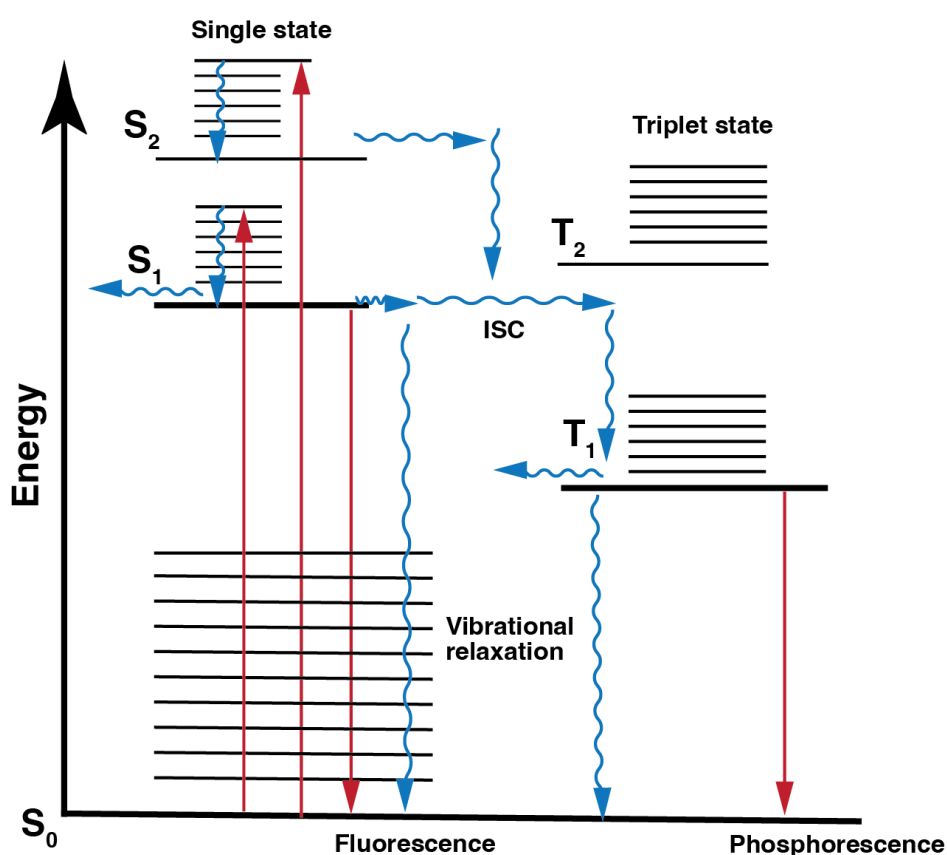
Figure 1.4 Scheme of Jablonski diagram based on Frackowiak *et al.* [49]

As the light energy is absorbed by a ground-state molecule (S_0), the electrons in the highest occupied molecular orbital (HOMO) become excited to form lowest unoccupied molecular orbital (LUMO). There are two types of excited states: singlet excited states (S_1), in which the spin states of the HOMO and LUMO are inversely parallel, and triplet excited states (T_1), in which they are parallel. Excited molecules generated by photoexcitation have high energies and different electronic configurations compared to ground-state molecules. Therefore, electron transfer processes that do not occur in the ground state often also occur in the excited state. The excited molecules lose their excitation energy through decomposition, isomerization, luminescence, non-radiative transitions, energy transfer to other molecules, deactivation, and addition reactions. [49] The following section discusses a type of pericyclic reaction, photocycloaddition reaction, in which dynamic covalent bonds are formed between molecules by light.

1.2.1 Cycloaddition reactions

The history of photocycloaddition reactions dates back to the [4+4] dimerization of anthracene reported by Fritzschein in 1867.[50] Subsequently, Riiber reported the mechanism of photoinduced [2+2] dimerization.[51] Ciamician and Silber also reported dimerization of cinnamic acid, stilbene, and coumarin in the solid phase and in the solution.[21, 52, 53] A subsequent study suggested pyrimidine, a component of DNA, could dimerize when exposed to UV light, leading to skin cancer.[54] This led to extensive research into the mechanism of photo-reversible addition. Recently, these reactions were applied for the click chemical reaction[55] and photopolymerization. [48, 56] Table 1.6 summarizes examples of photochemical cycloaddition reactions.

Table 1.6 Overview of the moieties that undergo photochemical cycloaddition. [21]
*Stereoisomers are not included in this schematic.

[4+4] cycloaddition reactions	Photoreaction	Ref
Anthracene		57
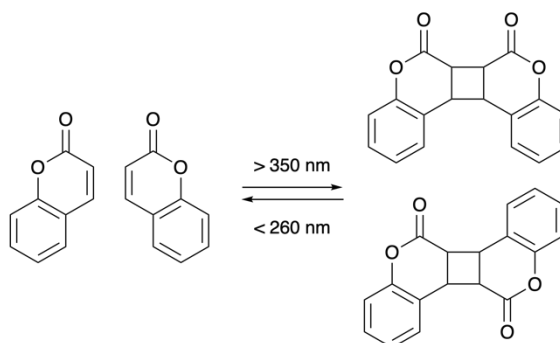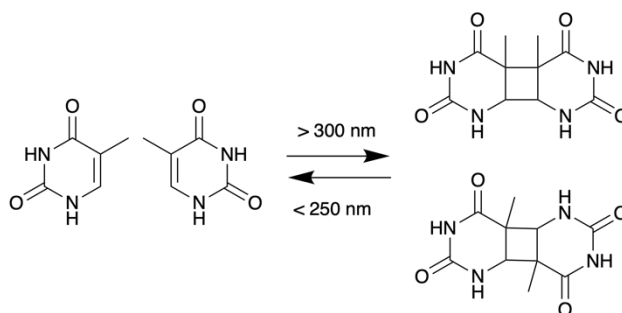
[2+2] cycloaddition reactions	Photoreaction	Ref
Coumarin		58, 59
Thymine		60
Stilbene		61
Cinnamic acid		62
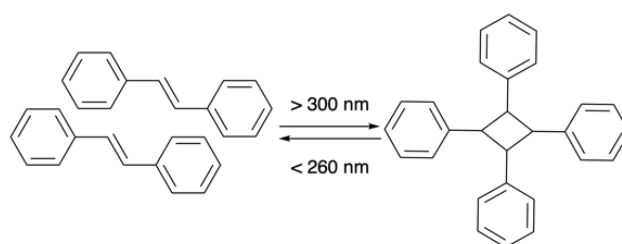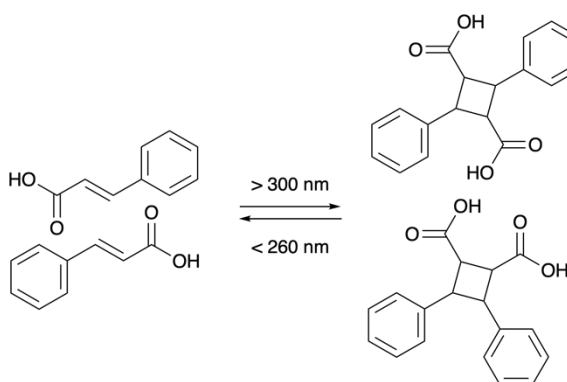
1.2.2 [2+2] cycloaddition reactions

In the [2+2] photoaddition reaction, the conjugated alkene undergoes an intersystem crossover from the ground state (S_0) to the excited singlet state (S_1) and from there to the triplet state (T_1). Specifically, the $\psi 1$ orbital, the HOMO of one ground state, moves to the $\psi 2^*$ orbital, the HOMO of the excited state, and when the HOMO of the excited state of the other alkene interacts it's LUMO, a [2+2]-cycloaddition reaction occurs. In the case of photoinduced cycloaddition reactions, a transient diradical species is produced when a photon raises one of the electrons to the LUMO, resulting in an allowed reaction with the same symmetry of HOMO and LUMO (Scheme 1.5).[63]
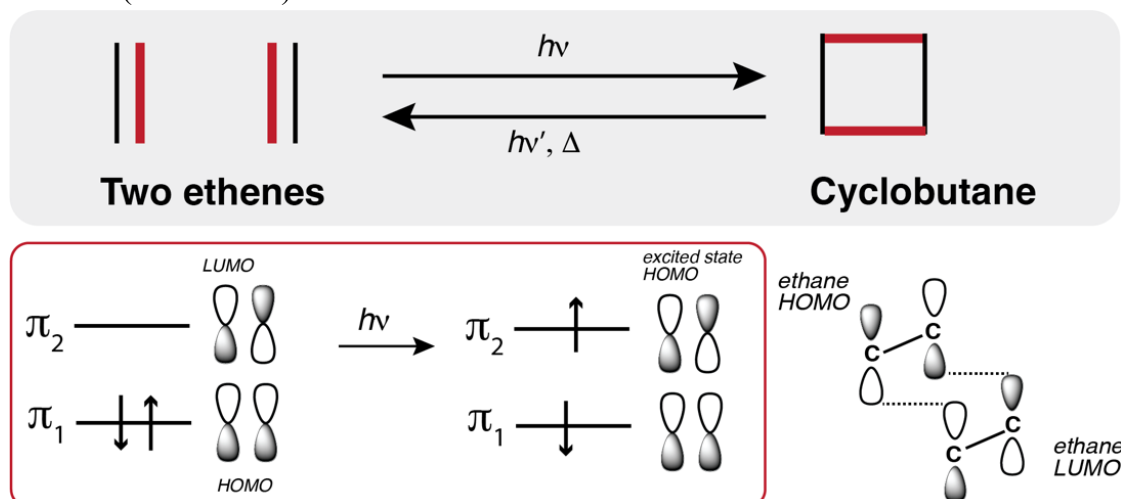
Figure 1.5 Scheme of the mechanism of photo-cyclization is based on the references. [64]

Reversible photoreactions: Photocycloaddition reactions can return to their original initial species by irradiation with light of a lower wavelength than cycloaddition reactions. [48, 56, 58] However, irreversible optical processes may occur during the excitation of a molecule by UV irradiation.[48, 58, 60, 65] In addition, the absorption bands of the photoreactive seeds overlap with that of the cycloaddition product. Thus, low-wavelength irradiation often leads to the simultaneous excitation of the cyclization rearrangement and cycloaddition reaction, resulting in reduced quantum yields. [22.]

1.2.3 Thymine chemistry

Thymine, a base segment of DNA, is known to exhibit a photo-reversible reaction, wherein two olefin sites of thymine generate cyclic cyclobutane when irradiated with UV light above 300 nm, which revert to their original olefins when irradiated with 254 nm light. It is also known to exhibit a photo-reversible reaction back to the original olefin when irradiated with 254 nm light. UV-induced damage to DNA mostly forms cyclobutane dimers and pyrimidine-primidone (6-4) photoproducts (Figure 1.6). [54, 66] As thymine dimerization progresses in the body, this damage triggers the creation of rigid tangles in the DNA. This is believed to induce cell mutations and trigger carcinogenesis when the cell's DNA replicates. Thymine chemistry is consequently a vital part of research from a biological viewpoint. [67]
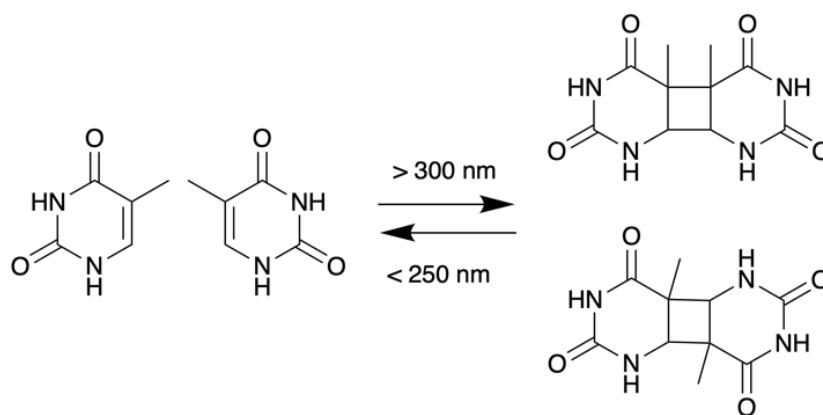
Figure 1.6 Photoproducts of thymine.

In a paper by Wulff and Fraenkel in 1969, it was reported that four stereoisomers of the thymine photo dimer were formed. Four distinct mixtures of the main isomers of the photo dimer that can be produced by photoirradiation were found to exist in thymine solution as shown in Figure 1.7. [60]
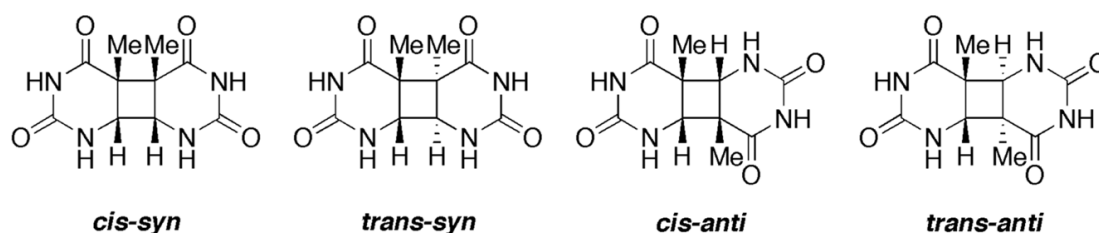
Trans-syn and *cis-anti* thymine dimers exist as enantiomeric pairs.

Figure 1.7 Thymine photo-isolation from Ref 68. The figure is reproduced with permission from Spring Nature. [68]

However, the generation of thymine dimerization in an aqueous solution is quite challenging. Therefore, thymine dimerization was attempted in freeze-dried aqueous solutions.[60] The removal of water by freeze-drying triggers thymine agglomeration and/or crystallization, resulting in the dimerization of thymine due to the proximity of the thymine molecules. In this process, the stereochemical control of thymine aggregation is known to lead to a cis-syn structure. [60, 69]

1.2.4 Coumarin chemistry

Coumarins are aromatic compounds with a lactone skeleton and are widely distributed in nature, mainly in plants.[58] Unsubstituted coumarins seldom show fluorescence itself, in contrast to the introduction of an electron-donating group at 7-position, which is characterized by strong photo absorption and luminescence. Coumarins are also known to exhibit reversible [2+2] cycloaddition reactions. The [2+2] cycloaddition reaction of coumarins was reported by Ciamician and Silber in 1902.[70] In this reaction, dimerization proceeds under UV irradiation at 365 nm, and the cyclobutane structure of the coumarin dimer is cleaved under UV irradiation at 280 nm. In addition, it proceeds under sunlight and visible light, although dimerization requires more time, thus it is expected to be a practical technology available under sunlight.[59]
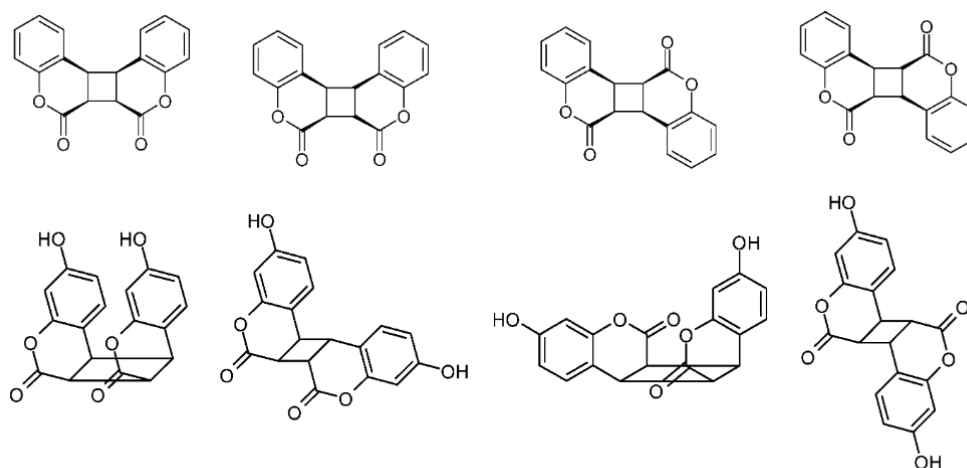
Figure 1.8 Coumarin photo-isolation reprinted in part from ref 58, with permission from American Chemical Society.[58]

In Figure 1.8, four possible dimers of coumarin formed by UV irradiation are indicated. The selectivity of the dimeric structure depends on the amounts of light exposure, solvents, and concentrations. [58]

In selecting molecules for the [2+2] cycloaddition reaction, it is crucial to evaluate the advantages and disadvantages relative to the intended application. Coumarin, for instance, boasts a longer reaction wavelength, approaching that of sunlight, and a faster reaction rate. However, it is also more susceptible to oxidation reactions and the generation of by-products. On the other hand, thymine has demonstrated promising results in vivo, making it a suitable candidate for biological applications. Despite this, its relatively slow reaction time necessitates the use of photosensitizers or other catalysts to enhance the reaction rate. Additionally, the proximity of the wavelength of the forward and reverse reactions, as well as the presence of isomers, can impede the reversibility of non-cyclic alkenes.

1.2.5 Topochemical polymerization

Topochemical polymerization is a solid-state polymerization in which monomer crystals are driven to retain their crystalline state, producing polymers.[71, 72] Within the monomer crystal lattice, topochemical reactions are intermolecularly constrained, allowing precise control over the tacticity, packing, and crystallinity of the polymers produced in the polymerization process. [73-75] Thus, the position in the crystal can be precisely controlled, and the products can be obtained with high yield, selectivity, and specificity. In addition, compared to conventional polymer synthesis in solution, topochemical reactions proceed without the use of solvents or catalysts, thus reducing the use of fossil resources and creating an environmentally friendly synthetic route. Topochemical reactions are mainly known as [2+2] photocycloaddition cyclization by light, [76] intramolecular rearrangements and isomerization by heat. [77]

Schmidt's topochemical postulate: For [2+2] photocycloaddition reactions to occur, the double bonds must be parallel, and their distance must not >4.5 Å. This hypothesis was explained by G.M.J. Schmidt in 1964. [78, 79] In a series of articles, Schmidt explained the topochemical postulate, the so-called "solid-phase reactions occur by minimal movement of atoms and molecules.". Specifically, in the dimerization of siliceous acid derivatives, a type of [2+2] cyclic-addition reaction, the result showed that a) the reaction can only be performed within a certain distance and b) molecular structure is determined by its geometric correlation.

Arranging olefin-bonded pairs in solids: As mentioned earlier, for a solid-state photochemical reaction to proceed, a pair of olefin bonds in the ligand must be parallel in the Pz orbital and overlap at 4.2 Å, as proposed by Schmidt *et al*. There are two ways of arranging olefin-bonded pairs in solids, face-to-face and slip-stacking, respectively, at least. In the case of photodimerization of facing olefin bond pairs, as shown in Fig. 1.9 b), the dimerization reaction does not proceed along the chain, and a dimer rather than a polymer is formed. Therefore, the olefin-bonded pairs must be arranged in a slip-stack configuration and be on a step, allowing successive [2+2]-cycloaddition reactions to occur. (Fig 1.9 c). [76]
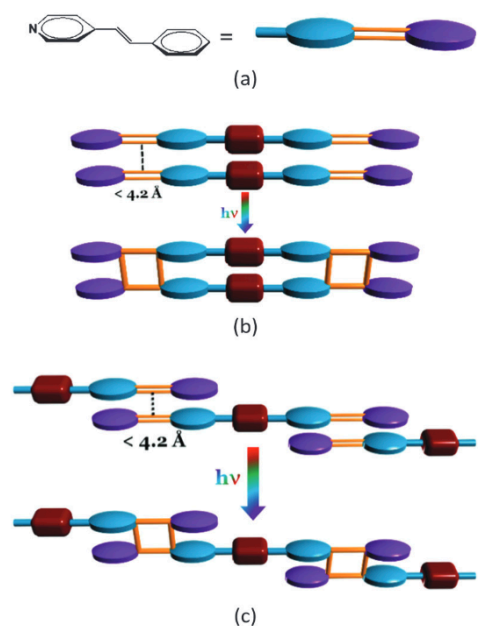
Figure 1.9 Configuration of olefin pairs in solids. (a) Typical monodentate ligand with olefinic bonds. (b) "Face-to-face" olefin bond pairs. (c) "Slip-stack" arrangement of olefin bond pairs leading to polymerization: in part from ref 77, with permission from Royal Society of Chemistry.[77]

Various single-molecule designs have been attempted in crystal engineering to achieve the "slip-stack" arrangement of olefin bond pairs, which is a key requirement for solid-phase polymerization as described above. In the solid phase, the packing state of molecules in the crystal lattice dominates the polymerization, and interactions such as "hydrogen bonding, stacking, and weak interactions such as halogen-halogen" control the arrangement to bring the reactive functional groups closer together.[74] However, controlling reaction selectivity to synthesize polymers with different structures is quite challenging, and various applications of solid-phase reactions require more precise adjustment of the arrangement of reactants in the solid. Therefore, topochemical polymerization reactions in more flexible and diverse confined spaces are being explored.

Metal-organic frameworks: Metal-organic frameworks (MOFs) are structures in which organometallic ligands interact with each other to form a porous coordination network structure. Compared to crystals, MOFs provide excellent confinement spaces for a variety of reactions, including selective, multipoint, and reversible olefin/olefin cyclization reactions. [80, 81] Besides having a variety of pore structures suitable for confining reactants, MOFs have the "flexibility" to deform their own framework in response to molecular adsorption and desorption. [82] Recently, MOFs with strong coordination bonds and competing for intra-skeletal dispersion forces responsible for structural rigidity have been found to exhibit frustrated flexibility. [83] Vittal *et al.* demonstrated that [2 +2] photopolymerization within MOFs forms syndiotactic organic polymeric ligands.[69] In addition, the polymer was shown to be reversibly de-polymerizable by cleavage of the cyclobutane ring formed via heating.

Self-assembly: Self-assembly is a spontaneous molecular assembly of molecules with a well-defined structure. Self-assembly of supramolecular molecules has shown to be an effective method for preparing materials with nanometer-order structural properties.[84-86] Frauenrath *et al.* showed that diacetylene derivatives form nanometer-sized self-assemblies using β-sheet-type hydrogen bonding networks, and topochemical polymerization occurs within these self-assemblies. [87] Kim *et al.* demonstrated the use of photopolymerization to "capture" metastable intermediates in a self-assembly process. Specifically, they showed that metastable intermediates can be effectively trapped by UV-accelerated polymerization of chiral perylene diimide with diacetylene-containing alkyl chains, prior to the formation of thermodynamically stable tubular structures. [88] Zhu *et al.* have demonstrated that rotaxane-based molecules containing diphenyl diacetylene (DPDA) monomers can self-assemble in an aqueous solution and form polymers/oligomers by topochemical reactions in this self-assembly. The structural transformation by this stimulation results in the capping of the host-guest structure, which can be tracked by changes in the luminescence signal. [89]

Bulk: Bulk polymerization process employs only monomer molecules and polymer initiators. In general, they are stirred for the appropriate mass transfer and heat transfer to initiate polymerization. [90] As the polymerization proceeds, the viscosity of the medium increases, making the blending process gradually difficult, and the molecular weight distribution becomes wider. [2+2] cycloaddition reactions do not require initiators and have the potential for bulk polymerization without the need for physical agitation. As shown above, there are a variety of reported cases of [2+2] cycloaddition progressing in the solid phase (in crystals) [91], but in recent years, some photochemical [2+2] polymerization of liquid-phase monomers[92] and polymerization in films[93] have also been reported.

1.3 Applications of dynamic polymer

1.3.1 Dynamic polymer networks

In previous sessions, specific examples of dynamic covalent bonding have been outlined. Polymers with this dynamic covalent bond implanted between monomer units are called dynamic polymers. These dynamic polymers can be reversibly polymerized/de-polymerized by external stimuli and are attracting considerable attention as smart polymers. The bonding concept, where the crosslinking points of polymers comprise reversible factors, is known to constitute a wide variety of polymer architectures.[65] In this paper, three broad categories are presented. [94]

Reversible linear polymer: First, dynamic covalent bonds are incorporated into the linear polymeric main chain. These dynamic covalent bonds between monomer units can be dissociated/combined repeatedly, allowing the linear polymer to be partially degraded and further re-polymerized. These polymers are expected to have applications in chemical recycling, as the degraded fragments can be repolymerized. [95] Chemical recycling is necessary to recycle monomers and oligomers that can be used to produce new products after decomposition without degradation of performance. [96] In recent years, it has also shown promise as upcycling to produce materials with improved performance compared to raw materials. There are almost no reported examples of such reversible linear polymers, as loop defect is often generated, and the sequence is difficult to control.[4]

Reversible crosslinked polymer: Second, side chains with dynamic covalent bonds are introduced into the copolymer backbone. Side chains can reversibly crosslink with linear polymers, allowing networks to form structures as shown in Figure 1.10 b.[97] Third, a reversible network is formed by hyperbranched chains without requiring a copolymer backbone as shown in Figure 1.10 c. Multiple binding sites increase the binding potential and enable the desired network structure to be obtained. Compared to linear polymers, reversibly crosslinked polymers can form network structures and exhibit complex behavior. Therefore, they have been reported to provide network polymers with recyclability and reparability.[4] A critical factor in the design of crosslinked polymers is the presence of dynamic reaction sites and the number of functional groups present. As the amount of crosslinking increases, the width of the cavities between the networks shrinks, which can be disadvantageous for the mobility of the networks. Conversely, a high proportion of functional groups within the monomer units can have a strong influence on the overall thermal and mechanical properties, i.e., on the increase of the glass transition temperature (T_g).
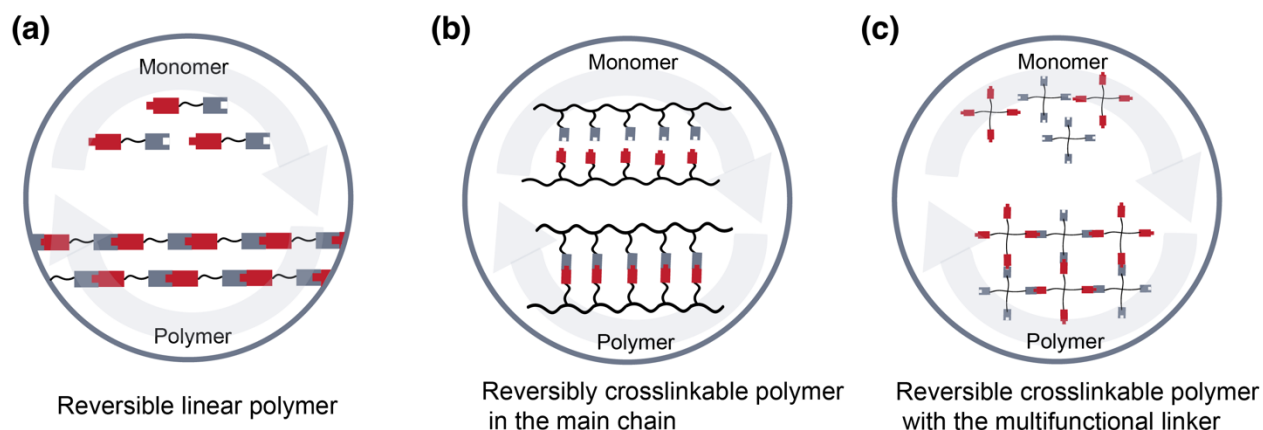
Figure 1.10 Types of reversible polymers: (a) Reversible linear polymer (b) Reversibly crosslinkable polymer in the main chain (c) Reversible crosslinkable polymer with the multifunctional linker. This figure is based on references from J. Dahlke *et al.* [94]

The dynamic covalent bond networks described above have been deployed in new functional applications such as chemical recycling and self-healing materials due to their dynamic nature. Specific applications are reviewed, focusing on examples of photo-reversible [2+2]-cycloaddition reactions.

1.3.2 The molecular architecture of dynamic polymer

In designing polymers incorporating dynamic covalent bonds, the factors to be considered are categorized below. There are two important factors in designing the molecular structure.

(1) The location of the dynamic covalent bonds and number of reaction sites
Monomer structures with two reaction sites produce linear or cyclic polymers when the bonding sites are linked and reactive sites are introduced in multiple branches or on the sides of the main chain, which produce crosslinked polymers.

(2) The structure and function of the monomer backbone
Structures other than the bonding sites can control their reactivity by the interaction between molecular chains and their molecular weight. This is the decisive factor in preventing topological defects due to intramolecular reactions and allowing intermolecular reactions to proceed and produce polymers.
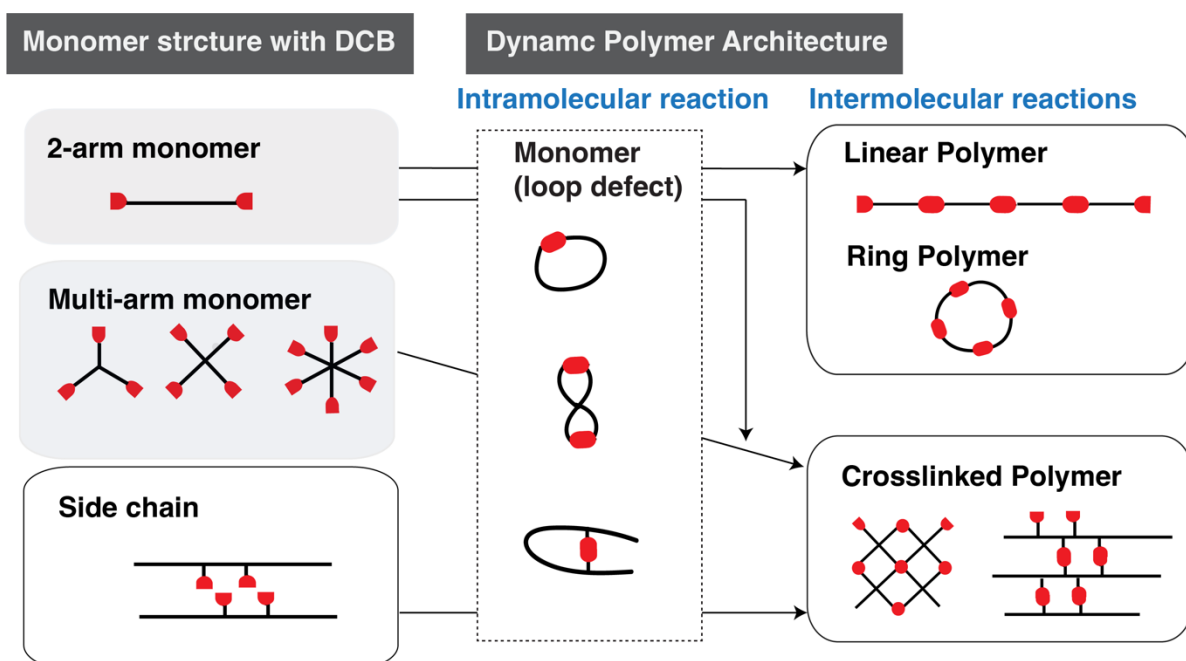
Figure 1.11 Classification of nonlinear polymer topologies is based on the reference from Y. Tezuka *et al.* [98]

Multi-arm monomer: As shown in Figure 1.11, multi-armed monomers are known to form a three-dimensional network of polymer chains given the presence of binding reaction sites at the ends.[99] Early studies on such 3D model networks date back to the 1970s. This early work reported that linear telechelic polymers and functional small molecule crosslinkers are linked by conjugation reactions.[100] Subsequently, star-shaped polymers were discovered to replace linear polymers, and efforts have been devoted to better control of the functionality of the branching points. [101] In particular, the number of steps in the formation process differs depending on whether the reaction at the chain end is hetero or homo.[99] The [2+2] cycloaddition reaction is a highly efficient process due to the homo-molecular of the binding site and the occurrence of the reaction in a single step.

1.3.3 Application 1: chemical recycling

Mechanical recycling is currently the most widespread recycling technique; however, its applications are limited owing to some disadvantages, such as considerable loss in value with each cycle and production of inferior materials after the cycle has been completed. [45] It is possible to recycle plastics chemically, which creates monomers and other value-added products from plastics, as an alternative to plastic recycling. This section highlights selected examples of photochemical polymer structures aimed at chemical recycling.

Chirik *et al.* previously developed a hetero [2+2] cycloaddition of dienes and alkenes using PDI iron complexes.[102, 103] They succeeded in performing cyclization reactions with high regioselectivity and diastereoselective by the highly developed umbrella-shaped iron complexes. Furthermore, sequential [2+2] cycloaddition cyclization of the raw olefins with pyridine (diimine)-coordinated iron catalysts resulted in cyclobutyl rings linked at positions 1

and 3 to form oligomeric chains.[102] The butadiene formed in the [2+2] reverse cycloaddition reaction was considered difficult to coordinate with the iron catalyst and to isolate from the reaction field. Therefore, decomposed butane was enclosed in a 5 Å molecular sieve to collect the monomer, which was achieved by repeated upcycling.

1.3.4 Application 2: shape memory polymer materials

Shape memory polymers are defined as polymers that can be enabled to change shape, in a pre-defined manner, when exposed to stimuli such as heat and light. Recently, shape memory polymers have also been used in 3D printers and are attracting attention in 4D printing because of their ability to change the shape after printing in a time-dependent manner. [104]

Lendlein *et al.* reported that shape-memory polymers have achieved the effect of light stimulation by incorporating a reversible photoreactive molecular switch. [105] To introduce photosensitivity into shape memory polymers, cinnamic acid (CA) or cinnamylideneacetic acid (CAA) moieties, which act as photo-trigger switches, have been incorporated into the polymer structure. Upon the UV irradiation, a [2+2] cycloaddition reaction occurs between these photosensitive moieties, forming a cyclobutane ring which is covalently cross-linked. Irradiation with lower wavelength light cleaves the newly formed bonds.

1.3.5 Application 3: self-healing materials

Self-healing polymers have been inspired by biological systems and describe polymers that repair mechanical damage, such as scratches, cracks, and holes in polymers.[106][107] In general, the self-repair mechanism of polymers consists mainly of two interactions. [108] The first point is to consider the self-healing reaction from a physical point of view: self-healing requires the generation of fluidity within the polymer for filling the damaged area. This physical fluidity is described by the free volume of the polymer and depends on the type of damage, the healing conditions applied, and the chemical behavior of the crosslinking. The other is to consider the chemical point of view: self-healing requires the restructuring and reconnection of the polymer network. Therefore, one strategy has been considered to incorporate polymer networks with dynamic covalent bonds. [5]

Sanjib *et al.* reported that the 3-arm PIB polymers containing a coumarin functional group at the terminal end were confirmed to heal under sunlight, with photocleavage occurring upon UV irradiation reversibility.[109] Hughes, Abdallh *et al.* confirmed that 4-arm coumarin-functionalized monomers polymerized when irradiated with 365 nm light and repaired surface scratches when irradiated with 254 nm light. [110-112]

1.3.6 Application 4: de-bonding on-demand materials

Reusable adhesive polymeric materials are one of the most attractive materials due to their ability to be bonded and debonded as required, which extends their lifespan. An approach to obtaining DoD materials is the incorporation of dynamic covalent bonds in polymer networks. Intermolecular interactions between interfaces within the adhesive and/or at the adhesive/substrate interface can be deliberately disturbed to achieve macroscopic changes in physical properties by controlling adhesive interactions.[72, 73] Kaiser *et al.* have reported the reversibility of the [4+4]-cycloaddition reaction of anthracene applied to the construction of a dry adhesive with switchable adhesive properties.[113] The hydrogenated nitrile butadiene rubbers with a photoresponsive anthracene group were produced by one-pot synthesis. Photolysis and thermal decomposition achieved adhesive recoveries of 75% and 80%, respectively.

Summary

In the general introduction, the concept of dynamic covalent bonding was outlined, including its types and repetition of bonding and dissociation. In particular, the [2+2] cycloaddition reaction, a photodynamic covalent bond reaction, which is a green synthetic pathway under ambient temperature and pressure, was explained as an example. Furthermore, polymer transformation consisting of dynamic covalent bonding was discussed in terms of its type and reaction field. Furthermore, the molecular design of monomers was described as the dominant factor controlling the polymer morphology. Understanding the design of monomers with dynamic covalent bonds is essential for generating polymers with efficient bonding and non-bonding properties.

1.4 Objectives of this thesis

In this research, the monomer structure of polymers with light-driven dynamic covalent bonds was investigated; more concretely, the correlation between the molecular structure of monomer and the functions provided by the resultant polymer structure was explored considering applications to various materials. Intermolecular photoreactions, such as cycloaddition reactions described in 1.2.1, are only possible provided that the reaction sites of the molecules are at a suitable distance for the reaction. For increasing the efficiency of intermolecular photoreactions, the following two methods are discussed:

1. Sequence control of reaction sites: to intentionally control the relative positions of photocyclization reaction sites by creating a restricted space using intermolecular interactions.

2. Multi branching of reaction sites: to increase the reaction probability by increasing the number of molecular binding sites.

Using each of the two methods, the following was investigated 1) creation of linear polymers using dynamic covalent bonding of monomers in non-covalent supramolecular space, and 2) the application of crosslinked polymers consisting of multibranched monomers to desorption materials, respectively. Based on the results obtained by these approaches, the influence of the design of monomers, incorporating dynamic photochemical reaction sites on the structural changes of the polymers and the materials properties was demonstrated (Figure 1.12).

Chapter2

1) Sequence control of reaction sites.

Linear Polymer

Chapter3

2) Multi-branching of the reaction site.

Crosslinked Polymer

Photo-functional Materials

Reversible linear polymer

DoD materials
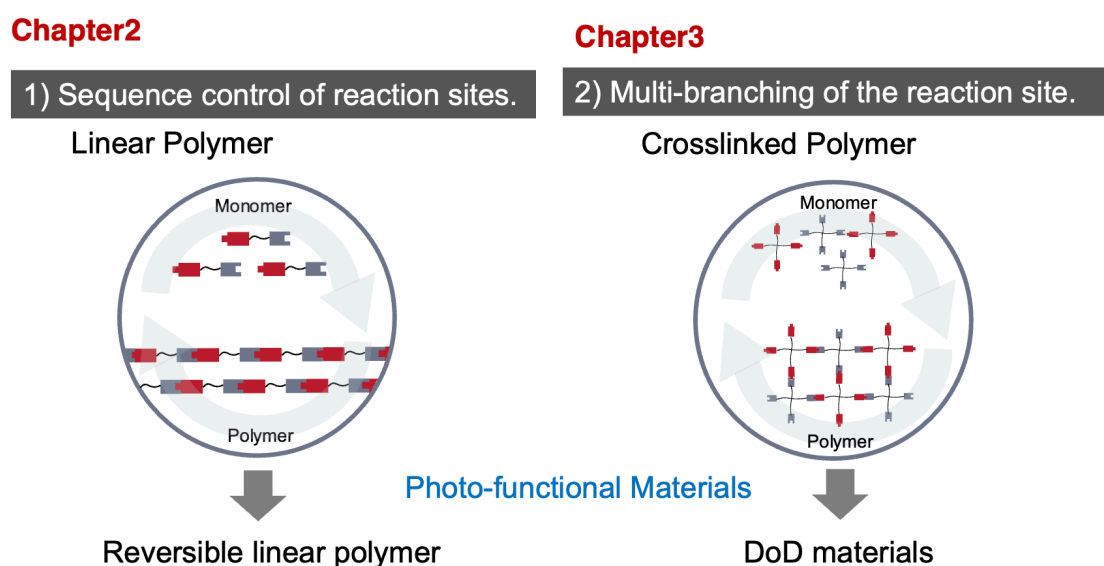
Figure 1. 12 Schematic diagrams of the concept of this thesis.

1.5 Overview

This doctoral thesis is composed of four chapters. The following provides an overview of each chapter. Chapter 1 introduces the topic of dynamic covalent bonding. It begins with a review of significant prior research in this area and discusses the factors that contribute to the design of materials for recycling. The principle and previous studies of the [2+2] cycloaddition reaction, which is the focus of this thesis, are then outlined. The chapter also provides examples of the applications of polymers with dynamic covalent bonds and discusses the relationship between their characteristic molecular structures and the factors to consider in material design.

In chapter 2, research on the creation of linear polymers using dynamic covalent bonds between molecules in supramolecular space was reported. Chapter 2.1 outlines the advantages and importance of using controlled spaces, such as crystals and supramolecular chemistry, to maintain a constant distance between reaction sites in [2+2] cycloaddition reactions. Within the restricted space, molecules are highly ordered and aligned, allowing highly efficient photochemical reactions to proceed, which results in the formation of characteristic three-dimensional structures. Molecular linkages between linear polymers by intermolecular cycloaddition reactions have been reported in a few cases and, if successful, are expected to contribute to recyclable linear polymers. These reasons are explained and important previous studies on photocycloaddition reactions in confined spaces are described. Chapter 2, Section 2 describes the experimental and analytical methods used in this study. In Section 2.3, the conversion of supramolecular self-assembled structures into continuous linear polymer structures was investigated by linking self-assembled molecules using [2+2] cycloaddition reactions. For this purpose, an amphiphilic monomer with thymine as the photochemical reaction site is required to construct the self-assembled structure, and the cycloaddition reaction was designed to occur using the interaction between two adjacent monomers in the constructed structure. The monomeric thymine-based bora amphiphiles were designed and synthesized using different phenylene spacers based on the ortho-, meta-, and para-aromatic substituents. These molecules were self-assembled in water and their structures were characterized by transmission electron microscopy and dynamic light scattering, which showed that they formed ribbon-like self-assembled structures in water. The [2+2] cycloaddition of thymine within the self-assembled structure was subsequently studied by UV spectroscopy, and its molecular weight was identified using MALDI-TOF-MS. Furthermore, molecular mechanics simulations were used to predict the arrangement of single molecules in the self-assembled structure and to discuss the frequency of inter- and intramolecular cycloaddition reactions with different aromatic substituents. As a result, it is predicted that the distance between the intermolecular photoreaction sites (thymine-olefin bonds) at ortho- and meta-positions is narrower at the meta-position than at the ortho-position. In other words, the meta-position retains more favorable conditions for the formation of polymer structures by intermolecular cycloaddition reactions than the ortho-position, indicating that the covalent structures by cycloaddition reactions can be controlled from the design stage through single-molecule structural control.

In Chapter 3, the application of crosslinked polymers synthesized from multibranched monomers by [2+2] cycloaddition reaction to self-healing and de-adhesive materials is reported.

Here, the possibility that dynamic covalent bonding and the functional groups of the multibranched monomers, which form the core of the dynamic covalent bonding, contribute to the material properties of the dynamic polymers is discussed. Chapter 3.2 describes the experimental and analytical methods. Chapter 3.3 mainly reports on the reversible cycloaddition of four-arm siloxane monomers with coumarin, and the polymer-based systems created by the reaction, including the characterization of physical properties and the evaluation of self-healing and adhesive properties. The four-arm monomers induce polymeric structural transformation by increasing the number of dynamic covalent bonding sites, forming denser and more reproducible polymer networks. To achieve this macromolecular structural transformation, the monomer must possess two characteristics: 1) fluidity and 2) dynamic covalent bonding sites. In this study, we designed a liquid monomer whose central moiety consists of cyclic siloxanes. The coumarins located at each end of this monomer are reversible [2+2] cycloaddition antagonists, which allow light-induced changes in the stiffness and fluidity of the material. The monomer undergoes reversible crosslinking and de-crosslinking under 365 nm and 254 nm light irradiation at room temperature, and the two polymeric structures obtained show a glass transition temperature (T_g) above room temperature and a low T_g value, respectively. The polymeric structures alternately increased and decreased their adhesion to substrates, such as quartz, when irradiated with similar light at two different wavelengths. To examine the mechanism of this reversible adhesion, the dynamic elastic moduli (storage modulus representing elasticity and loss modulus representing viscosity) of the four-chain monomer were measured before and after light irradiation at 365 nm and 254 nm, and their frequency dependence was observed. The results show that the rheological behavior changes before and after light irradiation and that the bond strength is not only due to the microscopic intermolecular bonding but also due to the light-induced change in the macroscopic stiffness of the whole material. The results of this study show that multibranched monomers, represented by four-chain siloxane monomers, can be applied as a sustainable material, a DoD adhesive, through reversible cycloaddition reactions.

Chapter 4 provides summarizes this doctoral thesis and future perspectives. The results show that in the design of monomers constituting polymers using dynamic covalent bonding, the arrangement of the binding sites in the reaction field and their chemical structures are important and directly contribute to the polymer structural transformation. In particular, the precise molecular design of monomers is again shown to be an important element in the construction of materials, as it leads to the control of the three-dimensional structure. In addition, the previously reported examples of polymers constructed using dynamic covalent bonding are compared with the polymers created in this study, and their potential for industrialization as materials and adaptation to industrial processes are discussed. In the design of circulating materials in this study, although there are advantages in using photocycloaddition reactions, which is a green synthetic route, the application of polymers with light-driven dynamic covalent bonds still has some limitations, such as the need to use light-permeable materials as substrates and the difficulty in increasing the size of the equipment and the inability to deploy on a large scale. There are still some limitations. Including these points, the current issues in

the application of photocycloaddition reactions are discussed, and the elements necessary for industrialization in the field of advanced materials are discussed.

Chapter 2

Photo-conversion of self-assembled structures
into continuous covalent structures
via [2+2]-cycloaddition reactions※
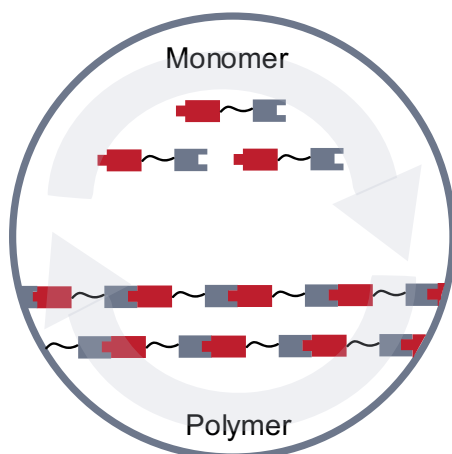
Abstract

In this study, the conversion of self-assembled structures into continuous polymeric structures by linking the self-assembled molecules using the [2+2]-cycloaddition reaction was investigated. Synthesized bio-inspired thymine-based bolaamphiphilic molecules were designed to force the interactions between two molecules to engage two thymines in their self-assembled structure to undergo a cycloaddition reaction. Thymine-based bolaamphiphilic molecules were designed and synthesized using different phenylene spacers based on aromatic substituents (ortho-) (meta-) (para-), and alkyl-chain. The formed self-assembled structures from these molecules were characterized and compared using molecular mechanical simulations. Simulations were performed to discuss the relationship between the inter- and intramolecular cycloaddition sensitivity to different substituents. This study provides a strategy for creating higher molecular weight linear polymers by controlling the photocyclization sites within the self-assembly by spacers between thymines.

Chapter 2 describes studies on the creation of linear polymers by using dynamic covalent bonds in a supramolecular.

2.1 Introduction

Photochemical reactions in confined spaces have attracted considerable interest in the preparation of photoresponsive self-assemblies, which are well-controlled as nanomaterials. Self-assembly is a system in which molecules are spontaneously held together by non-covalent bonds, such as hydrogen bonding, van der Waals interactions, or π-π stacking. The system is particularly applicable to emulating biological systems, such as DNA helical structures, ribosomes, and cytoskeletons. [115-119] Most studies on stimuli response have focused on changing 3D structures using light stimuli to control the strength of the interaction between molecules. [84, 120-125] Within a confined space, molecules are highly ordered and aligned and can undergo photochemical reactions efficiently to form unique 3D materials.

Photochemical reactions in Self-assembled structure
Photochemical reactions are attracting attention from the viewpoint of green chemistry because they can proceed at room temperature (RT) and atmospheric pressure, and specific sites can be remotely stimulated.

Cage-like self-assembly structure : Yoshizawa *et al.* reported that the Diels–Alder and [2+2]-cycloaddition reactions within cage-like self-assembled structures, where two reactant molecules are confined in the self-assembly, effectively yield the product. [126, 127]

Metal-organic framework : Vittal *et al.* reported the synthesis of 3D structure-controlled polymers inside a metal-organic framework using a [2+2]-photopolymerization reaction.[76, 128]

Single-chain nanoparticle : Barner-Kowollik *et al.* introduced the formation of single-chain nanoparticles via [2+2]- and/or [4+4]-cycloaddition reactions in confined environments. [129, 130]

Intermolecular [2+2]-cycloaddition reaction
Intermolecular photoreactions require an appropriate distance between reactive sites. According to Schmidt et al., an intermolecular [2+2]-cycloaddition occurs when the reactive sites of adjacent molecules coincide with a separation distance of 3.5 Å-4.2 Å in a crystal, where the confined spaces determine the reaction distance.[78, 79]

Recently, Kei Saito and coworkers reported that the morphology of self-assemblies can be transformed from ribbon-like structures to spheres via a [2+2]-cycloaddition reaction.[131] This was successful because of the creation of thymine-incorporated bolaamphiphilic compounds capable of self-assembly in water. Upon irradiation, the adjacent thymines, which are known as one of the DNA bases, were photodimerized by the [2+2]-cycloaddition reaction and

changed the entire morphology of the self-assembly. Inspired by our previous works, [48, 91, 131-135] several novel bora amphiphiles were synthesized that are expected to self-assemble and undergo continuous 'intermolecular' [2+2]-addition cyclization reactions, in which the thymine groups in their structures are closely linked. This 'intermolecular' [2+2]-cycloaddition reaction was able to link the self-assembled molecules and form a polymeric structure. This paper describes the conversion of a self-assembled structure into a continuous covalent structure.

2.2 Materials and methods

2.2.1 Materials and equipment

All chemicals were purchased from Tokyo Chemical Industry Co., Wako Pure Chemical Industries Ltd, and Sigma-Aldrich, Japan. ^{1}H NMR and ^{13}C NMR spectra were recorded on a JEOL ECZ500 spectrometer. Electrospray ionization high-resolution mass spectra were employed on a JEOL AccuTOF-CS electrospray mass spectrometer. The morphology of the self-assembly of bolaamphiphiles was observed using Transmission Electron Microscopy (TEM, JEM-1011, JEOL) at an accelerating voltage of 100 kV. UV crosslinkers (CL1000 302 nm, UVP, and CL1000 254 nm, UVP) were used to carry out the photochemical reactions. The molecular weights of the photoproducts were analyzed using matrix-assisted laser desorption/ionization time-of-flight mass spectrometry (MALDI-TOF-MS; AUTOFLEX III, BRUKER). The photoproducts of bolaamphiphiles **1a** and **1b** after UV-light irradiation at 302 nm, which were corrected as a liquid by the evaporation of water, were dissolved in chloroform mixed with trans-2-[3-(4-tert-butylphenyl)-2-methyl-2-propenylidene]malononitrile (DCTB) at a concentration of 10 mg/mL as a matrix.

2.2.2 Synthesis

Methyl-3-{3-[(2-{[3-(3-methoxy-3-oxopropyl)5-methyl-2,6-dioxo-1,2,3,6-tetrahy dropyrimidin-1-yl] methyl}phenyl)methyl]-5-methyl2,4-dioxo1,2,3,4tetrahydropyrimidin-1-yl} propanoate (**4a**), methyl 3-{3-[(2-{[3-(3-methoxy-3-oxopropyl)-5-methyl-2,6-dioxo-1,2,3,6-tetra-hydro-pyrimidin-1-yl]methyl} phenyl) methyl]-5-methyl2,4-dioxo-1,2,3,4-tetrahydropyrimi-din-1-yl}propanoate (**4b**), and methyl 3-{3-[(4-{[3-(3-methoxy3-oxopropyl)-5-methyl-2,6-dioxo1,3-diazinan-1yl]methyl} phenyl)methyl]-5-methyl-2,4-dioxo1,2,3,4-tetrahydropyrimi-din-1-yl} propanoate (**4c**),3,3′-((1,2-phenylenebis(methylene))bis-(5meth-yl-2,4-dioxo-3,4-dihydro-pyrimidine-3,1(2H)-diyl))dipropionic acid (**5a**), 3,3′-((1,3-phenylenebis(methylene))-bis(5-methyl-2,4-dioxo-3,4-dihydropyrimidine -3,1(2H)-diyl))dipropionic acid (**5b**) and 3,3′-((1,4-phenylene-bis(methylene))bis(5-methyl-2,4-dioxo-3,4-dihydropyri-midine-3,1(2H)-diyl))dipropionic acid (**5c**) and 2-(2-(2-methoxyethoxy)ethoxy) ethan-1-amine (**TEGNH₂**) were synthesized according to previously reported procedures.[132, 133, 136]

3,3'-((1,2-phenylenebis(methylene))bis(5-methyl-2,4-dioxo-3,4-dihydropyrimi-dine-3,1(2H)-diyl))bis(N-(2-(2-(2-methoxyethoxy) ethoxy)ethyl)propanamide)(1a) [136] a round-bottom flask **5a** (0.495 g, 0.72 mmol), 1-hydroxybenzotriazole monohydrate (HOBt; 0.340 g, 2.2 mmol) and DMF were mixed in a round-bottom flask and the mixtures were cooled in an ice bath and added 1-ethyl-3-(3-dimethylaminopropyl) carbodiimide hydrochloride (0.421 g, 2.2 mmol) was added to the mixture, followed by the addition of **TEGNH₂** (0.385 g, 2.40 mmol). After stirring for 2 h in an ice bath, the reaction was allowed to proceed at RT for 2 d. The mixture was evaporated to remove DMF. The residue was taken up in CH₂Cl₂, washed

with a saturated aqueous $NaHCO_3$ solution (3 × 100 mL) and brine with low pH adjusted with concentrated HCl, and dried over $MgSO_4$. After filtration, the filtrate was evaporated to obtain a brownish, viscous residue. The crude product was purified by column chromatography (chloroform: methanol: ethyl acetate = 5:1:3) to yield the pure product. Yield: 0.661 g, 85%. ^{1}H NMR (500 MHz, CDCl$_3$, δ): 1.92 (s, 6H), 2.58–2.64 (t, J = 5.8 Hz, 4H), 3.35 (s, 6H), 3.37–3.34 (m, 3H), 3.47–3.63 (m, 21H), 4.00–4.06 (t, J = 6.0 Hz, 4H), 5.42 (s, 4H), 6.51–6.57 (t, J = 5.3 Hz, 2H), 7.13−7.25 (m, 6H). ^{13}C NMR (125 MHz, CDCl$_3$, δ: 13.10, 34.85, 39.37, 41.88, 46.43, 58.96, 70.15–71.85, 109.28, 127.40, 128.47, 135.06, 140.10, 151.60, 164.05, 170.06. HRMS(ESI) m/z: [M + Na]$^+$ calculated for $C_{38}H_{56}N_6O_{12}$+Na$^+$: 788.3956; found: 811.3845.

3,3'-((1,3-phenylenebis(methylene))bis(5-methyl-2,4-dioxo-3,4-dihydropyrim-idine-3,1(2H)-diyl))bis(N-(2-(2-(2-methoxyethoxy) ethoxy)ethyl)propanamide)) (1b) [136]

The compounds in **1b** were synthesized and purified using the same procedure as in **1a**. Yield: 0.677 g, 87%. ^{1}H NMR (500 MHz, CDCl3, δ): 1.87 (s, 6H), 2.65–2.68 (t, 5.8 Hz, 4H), 3.34 (s, 6H), 3.35–3.56 (m, 24H), 4.02–4.05 (t, J = 6.0 Hz, 4H), 5.06 (s, 4H), 7.02–7.04 (t, J = 5.3 Hz, 2H), 7.17−7.24 (m, 3H), 7.30–7.35 (m, 3H).^{13}CDCl3 (125 MHz, CDCl3, δ): 12.98, 34.72, 39.41, 44.30, 46.63, 58.97, 69.63–71.86, 109.32, 128.13, 137.26, 140.20, 163.66, 170.11. HRMS(ESI) m/z: [M + Na]$^+$ calculated for $C_{38}H_{56}N_6O_{12}$+Na$^+$: 788.3956; found: 811.3842.

3,3'-((1,4-phenylenebis(methylene))bis(5-methyl-2,4-dioxo-3,4-dihydropyrim-idine-3,1(2H)-diyl))bis(N-(2-(2-(2-methoxyethoxy)ethoxy)ethyl)propanamide) (1c) [136]

The compounds in **1c** were synthesized and purified using the same procedure as in **1a**. Yield: 0.545 g, 70%. ^{1}H NMR (500 MHz, CDCl$_3$, δ): 1.88 (s, 6H), 2.55–2.61 (t, J = 5.8 Hz, 4H), 3.34 (s, 6H), 3.40–3.42 (m, 10H), 3.48-3.55(m, 8H), 3.58–3.62 (m, 12H), 3.92–4.01 (t, 4H), 5.06 (s, 4H), 6.32–6.36 (t, J = 5.3 Hz, 2H), 7.18–7.21 (m, 2H), 7.37–7.39 (m, 4H). ^{13}CDCl3 (125 MHz, CDCl$_3$, δ): 0.06, 13.07, 14.28, 34.83, 39.45, 44.25, 46.25, 59.03, 70.23, 70.46, 70.54, 71.94, 76.85, 77.10, 77.35, 109.42, 129.21, 136.34, 140.06, 151.60, 163.87, 170.02. HRMS(ESI) m/z: [M + Na]$^+$ calculated for $C_{38}H_{56}N_6O_{12}$+Na$^+$: 788.3956; found: 811.3842.
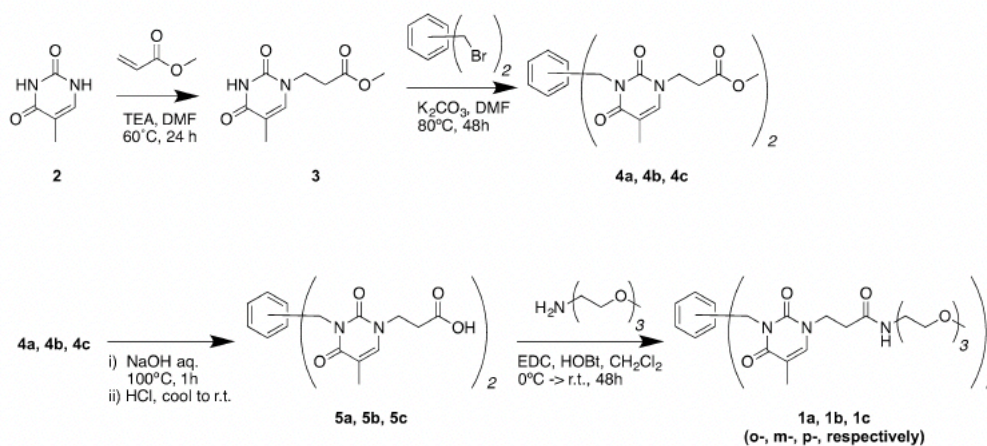
Scheme 2.1 Syntheses of **1a**, **1b**, and **1c**. This scheme is a reprinted version from scheme 2 of M. Inada *et.al*, 2022. [114]

TEGNH$_2$ was synthesized according to previously reported procedures. [136, 137]

3-(Thymine-1-yl)propanoic acid methyl ester (thymine propanoate)

Thymine (6.3 g) was dissolved in 70 mL of DMF in a 200 mL round bottom flask and triethylamine (10 mL) was added and stirred. After 5 min, methyl acetate (7.8 mL) was added dropwise to the stirred mixture and stirred for 24 h at room temperature. The solvent was drained off by an evaporator and a white liquid remained. This liquid was recrystallized with 50:50 ethanol and hexane and filtered. The residue was dried for 24 hours under a vacuum. %. ^{1}H NMR (500 MHz, CDCl$_3$, δ): 1.89 (d, 3H), 2.77 (t, 2H), 3.69 (s, 3H), 3.94 (t, 2H), 7.13 (s, 1H).

3,3'-(3,3'-(butane-1,4-diyl) bis(5-methyl-2,4-dioxo-3,4-dihydropyrimidine-3,1(2H)-diyl))-di-propanoate (butyl-bis-thymine)

Thymine propanoate (8.0 g) was added to DMF (15 mL solution, 7.0 g K$_2$CO$_3$) in a 100 mL round bottom flask and stirred for 5 minutes. The mixture was added diiodobutane (1.0 mL) and stirred at 70 °C for 48 hours. After 48 hours, the reaction was stopped and cooled to room temperature. 75 mL of water was added to the reaction product and the precipitated white mass was filtered and recrystallized with ethanol by the temperature drop method to give the product. The product was dried in vacuum for 1 day. Yield: 0.518 g, 76%. ^{1}H NMR (500 MHz, CDCl$_3$, δ): 1.59 (s, 4H,), 1.90 (d, 6H), 2.73 (t, 4H), 3.90 (s, 6H), 4.00 (t, 8H), 7.69 (d, 2H).

3,3'-(3,3'-(Butane-1,4-diyl) bis(5-methyl-2,4-dioxo-3,4-dihydropyrimidine-3,1(2H)-diyl))di-propanoic acid (butyl-bis-thymine dicarboxylic acid)

Butyl-bis-thymine dicarboxylic acid and 125 mL of a 2% NaOH solution were added to a 250 mL round bottom flask and refluxed for 1 hour. The impurities precipitated in the flask were filtered out, hydrochloric acid was added until the pH was below 7 and the flask was cooled down in an ice bath for 2 hours. The precipitate was filtered and rinsed twice with cold pure water to yield the product and was vacuum dried for 1 day. Yield: 0.518 g, 76%. ^{1}H NMR (500 MHz, CDCl$_3$, δ): 1.48 (br, 4H), 1.78(s, 6H), 2.61 (t, 4H), 3.78 (t, 4H), 3.87 (t, 4H) 7.57 (s, 2H), 12.41 (s, 2H).

3,3'-(butane-1,4-diylbis(5-methyl-2,4-dioxo-3,4-dihydropyrimidine-3,1(2H)-diyl)) bis(N-(2-(2-(2-methoxyethoxy)ethoxy)ethyl)propanamide) (1N)

Butyl-bis-thymine dicarboxylic acid (1.0 g), 1-hydroxybenzotriazole monohydrate (HOBt; 0.765 g) and DMF (100 mL) were added to a round bottom flask and stirred in an ice bath. 1-ethyle 3 -(3-dimethylamonopropyl) carbodiimide hydrochloride (EDC; 0.946 g) and **TEGNH$_2$** (0.849 g) were added during stirring, the mixture was stirred in an ice bath for 2 h and allowed to react at room temperature for 2 days. The solvent was skimmed off using an evaporator and the residue was dissolved in CH$_2$Cl$_2$ and aliquoted three times with saturated NaHCO$_3$. The organic layer was acidified with HCl and divided three times with NaCl, and MgSO$_4$ was added to the organic layer to exclude water and filtered. The residue was evaporated with an evaporator and vacuum-dried for 1 day. The product was purified by column chromatography (expansion solvent: chloroform ethyl acetate methanol 5:3:1). Yield: 0.518 g, 51%. ^{1}H NMR (500 MHz, CDCl$_3$, δ): 1.64-1.68 (s, 12H), 1.88(t, 8H), 2.61(t, 4H), 3.37–3.44 (m, 6H), 3.51–3.70 (m, 24H), 3.97 (t, 4H), 4.07 (t, 4H), 6.54 (t, 2H), 7.18 (m, 2H). ^{13}C NMR (125 MHz, CDCl$_3$, δ): 13.03, 25.10, 34.91, 39.45, 41.04, 46.34, 53.50, 59.05, 69.66, 70.25, 70.49, 71.95, 109.24, 139.98, 151.53, 163.98, 170.18. ESI-MS m/z: [M-H]$^-$ calculated for C$_{34}$H$_{56}$N$_6$O$_{12}$: 740.8414; found:739.60.
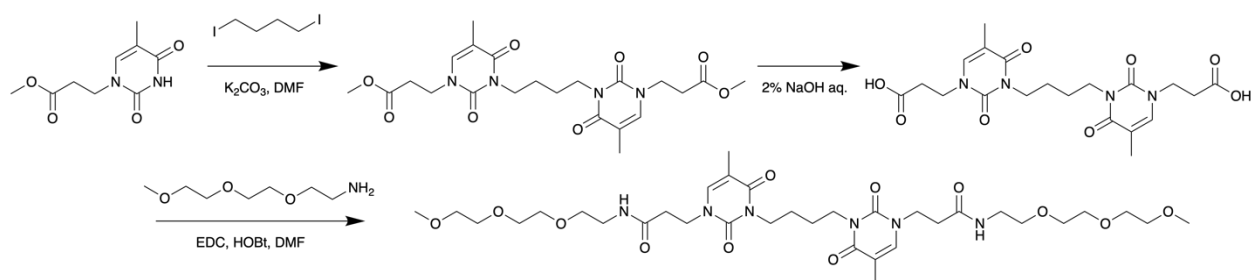
Scheme 2.2 Syntheses of **1N**.

2.2.3 Sample preparation

Bolaamphiphiles **1a** and **1b** were dissolved in pure water at a concentration of 1.8×10^{-3} M. The solutions were heated for 1 h at 70 °C and allowed to cool to RT (25 °C) for 3 weeks except for the Critical aggregation concentration measurement and gel permeation chromatography, for which self-assembled bolaamphiphiles were prepared by sonication for 1 h without the process of heating and cooling.
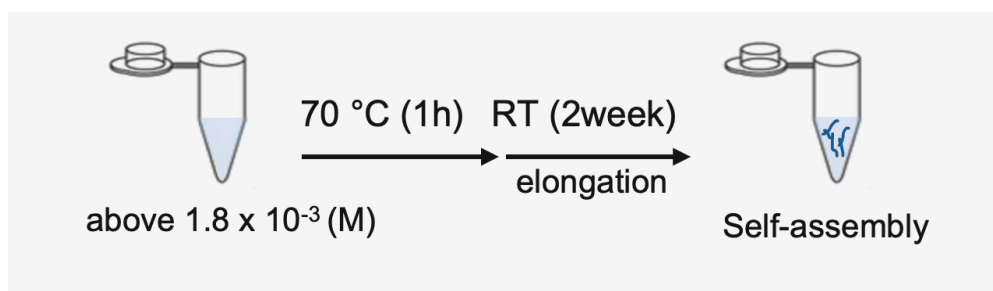
Figure 2.1 Process of creating a self-assembly structure.

2.2.4 Photoreaction of bolaamphiphiles

Bolaamphiphiles were dispersed in an aqueous solution at a concentration of 1.8×10^{-3} M and filled into quartz cuvettes. A lamp producing mid-range UV light with wavelengths from 280 to 320 nm was used to irradiate the cuvettes with mid-range UV light for several hours. UV-Vis spectrometers (V-550, JASCO) were used to study photochemical reactions. UV/Vis samples were diluted because the absorbance of the solution was saturated at 1.8×10^{-3} M.

2.2.5 Molecular and self-assembly modelling

The self-assembled structures of bolaamphiphiles **1a** and **1b** were simulated by molecular mechanics (MM) molecular modelling on BIOVIA Materials Studio 2019 using the Forcite geometry optimization module with a DREIDING force field. A pair of **1a** and **1b** molecules was placed in a unit cell and calculated under periodic boundary conditions. Repeating structures were visualized using the Mercury CSD 4.3.1 software.

2.3 Results and discussion

2.3.1 Design and synthesize of 1a, 1b, 1c and 1N

Three bolaamphiphile compounds comprising two thymine molecules separated by a phenylene spacer linked by two oligo (ethylene glycol) molecules using amide bonds were synthesized. Phenylene spacers with different aromatic substituent patterns (ortho- (**1a**), meta- (**1b**), and para- (**1c**)) were used for each compound (Scheme 2.3). The hypothesis here is to enforce "intermolecular" [2+2] cycloaddition through π-π stacking between the benzene rings in the spacer and hydrogen bonding between the amide bonds in adjacent molecules within the self-assembly structure.
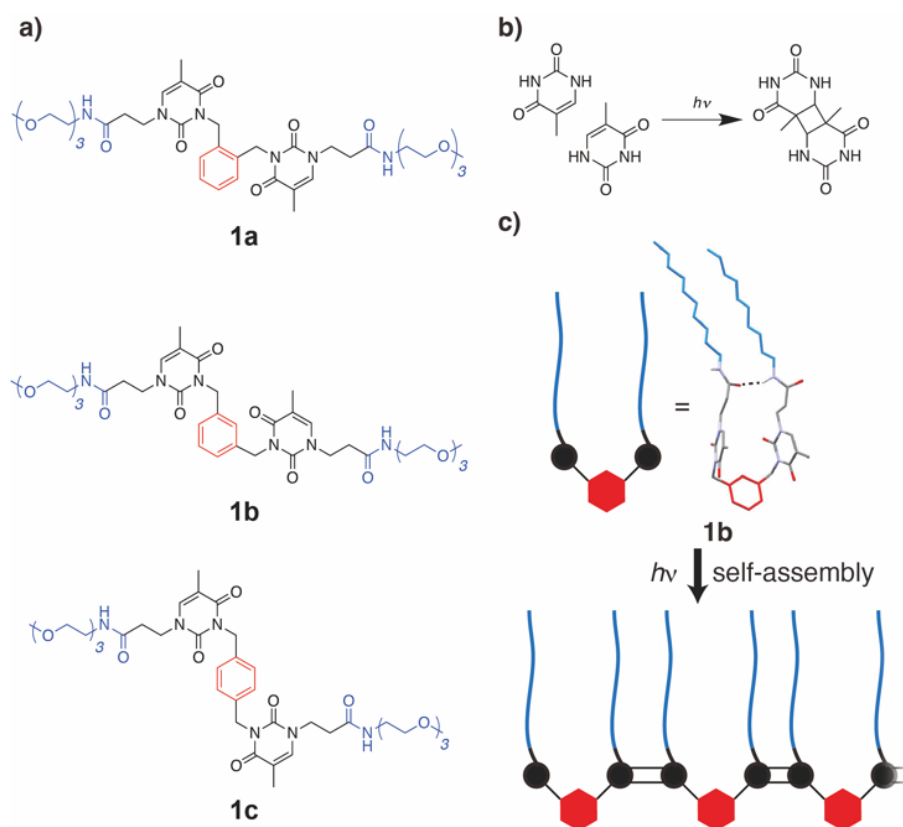
Scheme 2.3 a) Chemical structures of bolaamphiphiles **1a**, **1b** and **1c**. b) Photodimerization scheme of thymine. c) Scheme strategy of this study for producing continuous covalent structures using an intermolecular [2+2]-cycloaddition reaction. The 3D molecular structures were simulated by MM calculation. The dotted lines show intermolecular hydrogen bonds. This scheme is a reprinted version from scheme 1 of M. Inada *et al.*, 2022. [114]
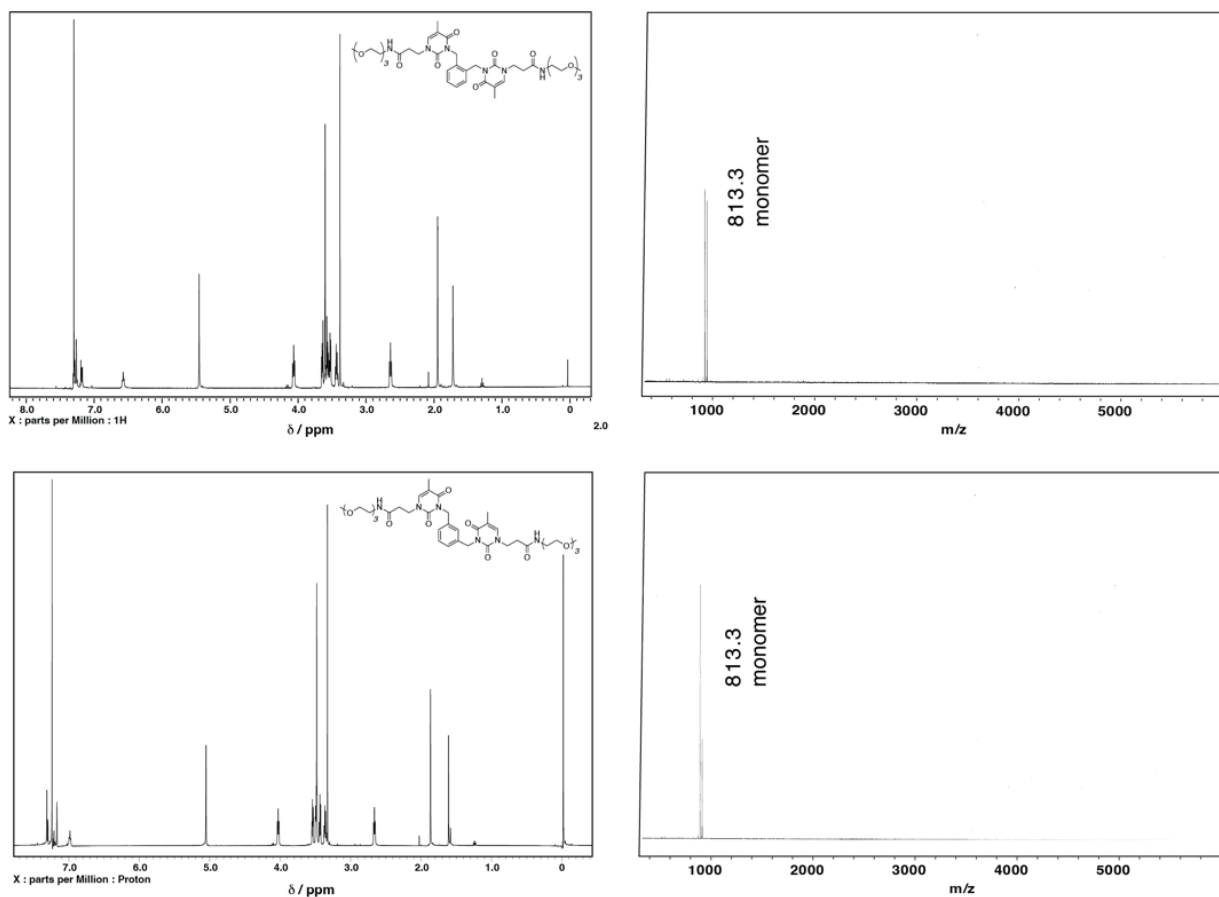
Figure 2.2 NMR spectra and MALDI-TOF-MS spectra of **1a** and **1b**

2.3.2 Self-assembly formation of bolaamphiles

Self-assembly structures

To observe a more explicit self-assembled structure using TEM, each **1a** and **1b** molecule was sonicated for 1 h above CAC (at 1.8×10^{-3} M) and then heated at 70 °C for 1 h and cooled to RT to form a self-assembled structure. The prepared sample was dropped onto a Cu grid and stained with an aqueous samarium acetate solution, and the morphology of the self-assembly was observed using TEM. [138]
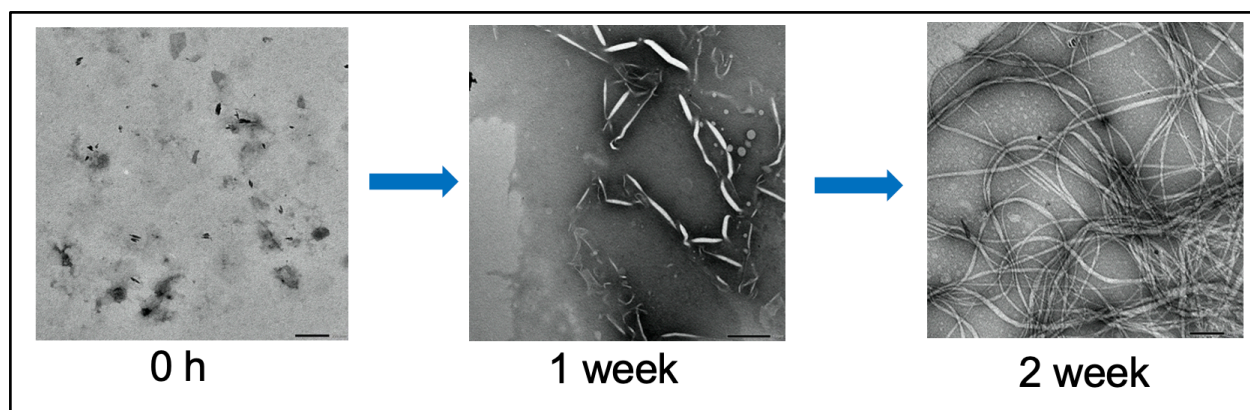
Figure 2.3 The process of self-assembly elongation of **1b**.

The images of both bola amphiphiles **1a** and **1b** show the formation of ribbon-like self-assembled structures (Fig. 2.4 a and Fig. 2.4 b) in water. The ribbon-like structures in both **1a** and **1b** are >~300 nm in length (blue), ~20 nm in width (red), and <10 nm in thickness (green).
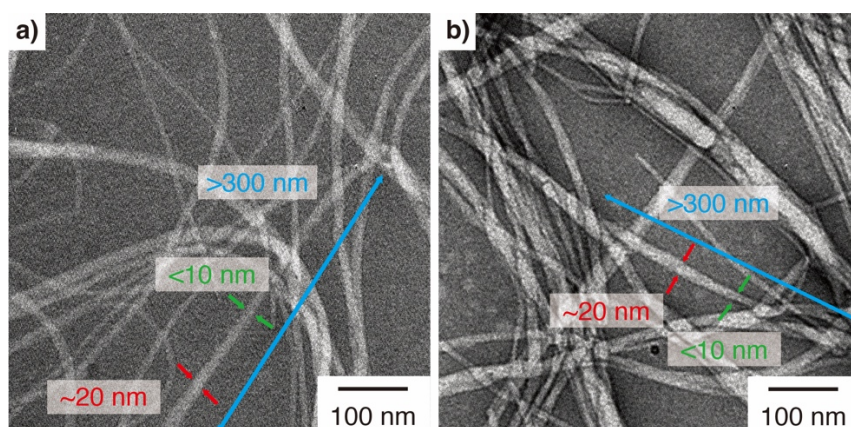
Figure 2.4 TEM images of the self-assembled nanoribbons of (a) **1a** and (b) **1b** in an aqueous solution at 1.8×10^{-3} M without UV irradiation. The measured values of length, width, and thickness are indicated in blue, red, and green, respectively. This figure is a reprinted version from Figure 1 of M. Inada *et al.*, 2022. [114]

In addition, dynamic light scattering (DLS) was carried out to confirm that the self-assembly of **1a** and **1b** existed in solution. DLS data showed that the average size of bolaamphiphile **1a** and **1b** (at 1.8×10^{-3} M) were 269.8 nm and 259.7 nm, respectively (Table 2.1).

Table 2.1 Mean particle size (z-average) of the self-assembled structures at 1.8×10^{-3} M and at 1.8×10^{-5} M. This table is a reprinted version from Table S1 of M. Inada *et al.*, 2022. [114]

Bolaamphiphile	Average size (nm) at 1.8×10^{-3} M	Average size (nm) at 1.8×10^{-5} M
1a	269.8 nm	N/D
1b	259.7 nm	N/D

2.3.3 Photochemical reactions of bolaamphiphiles

Next, self-assembled **1a**, and **1b** were irradiated under UV lamps which had the highest intensity wavelength at 302 nm in an aqueous solution. To monitor the [2+2]-cycloaddition reaction of thymines in the self-assembled structure, the UV absorption spectrum was measured to characterize the change in the absorption spectra. The total intensity of continuous light irradiation until the 270 nm peak completely decreases. As shown in Figure 2.5, the absorption bands at ~270 nm in **1a** and **1b**, which originate from the double bond site of the pyrimidine ring structure in thymine, decreased by approximately 90% of the equilibrium value at 168 h and 240 h respectively. The disappearance of the long-wavelength absorption of the thymine upon irradiation does not necessarily mean that all thymines are produced photoproducts by [2+2]-cycloaddition reactions because it is possible to occur the competing reactions. Regarding **1c** molecular, the self-assembly of the **1c** was not observed in water, whereas those of **1a** and **1b** molecules were observed. Indeed, the **1c** solution which could not be observed self-assembly was irradiated under the same condition (Figure 2.5 c). The absorption of 270 nm decreased by approximately only 20%. This result indicates that [2+2]-cycloaddition reactions are less likely to occur for **1c**. Hence, results from **1a** and **1b** are reported below.
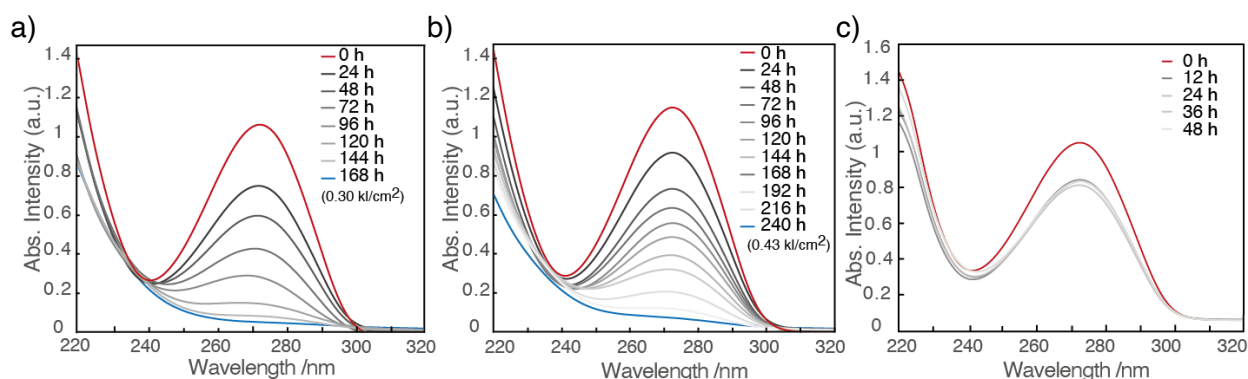
Figure 2.5 UV–Vis absorption spectra of (a) **1a** and (b) **1b** (c) **1c** at a concentration of 1.8×10^{-3} M after UV irradiation. This Figure is a revisited version from Figure 2 and Figure S1of M. Inada *et al.*, 2022. [114]

One of the competing reactions of photo dimerization is the formation of (6-4) photoproduction. However, this competing reaction is not considered to have occurred as there was no UV absorbance observed with a peak at 325 nm from the photo products[139] (Figure 2.6). These results suggest that the [2+2]-photocycloaddition reaction between thymines within the self-assembly proceeded almost completely.
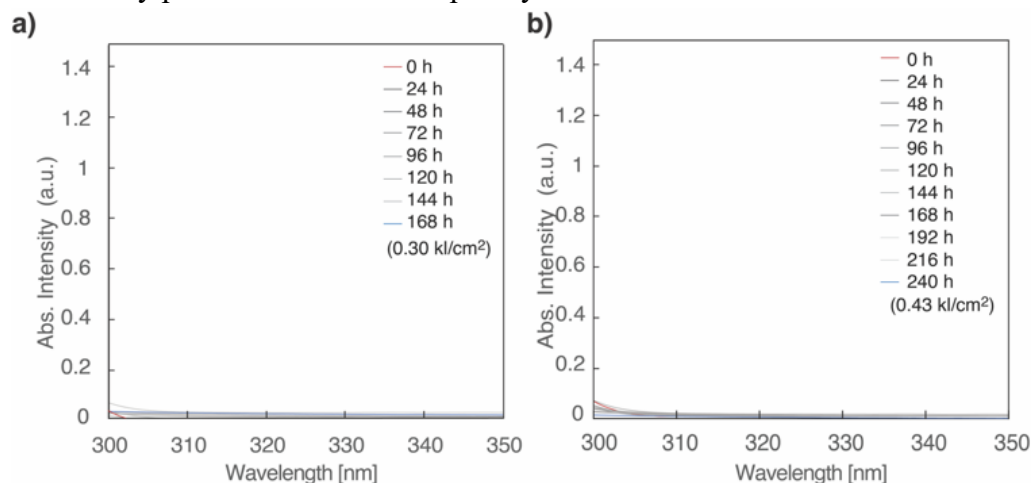
Figure 2.6 UV-Vis absorbance spectra of **1a** and **1b** from 300 nm to 350 nm. The competing reactions of photodimerization is not considered to have occurred as there was no UV absorbance observed with a peak at 325 nm from the (6-4) photoproducts. This figure is a reprinted version from Figure S3 of M. Inada *et al.*, 2022.[114]

When self-assembled structures are transformed into continuous polymeric structures by [2+2]-cycloaddition reactions, the molecular weight of the photoproduct increases relative to that of the original monomer. The molecular weights of the photoproducts after UV irradiation were analyzed using MALDI-TOF mass spectrometry to confirm the increase in molecular weight. The molecular weight of the photoproducts of **1a** (ortho-substitution) also increased up to the trimer level (three repeating units), as shown in Supporting Information (Fig. 2.7). The molecular weight of photoproduct **1b** (meta-substitution) was found to increase to a pentamer of the original molecule (Fig. 2.8 a). This result indicates that five molecules of **1b** are linked by [2+2]-cycloaddition reactions and form a continuous covalent structure. In addition, the morphology of the self-assembly of **1b** was observed as ribbon-like structures, even after UV irradiation, as shown in the TEM image (Fig. 2.8 b). This also supports the observation of the formation of continuous covalent structures within the self-assembled structure.
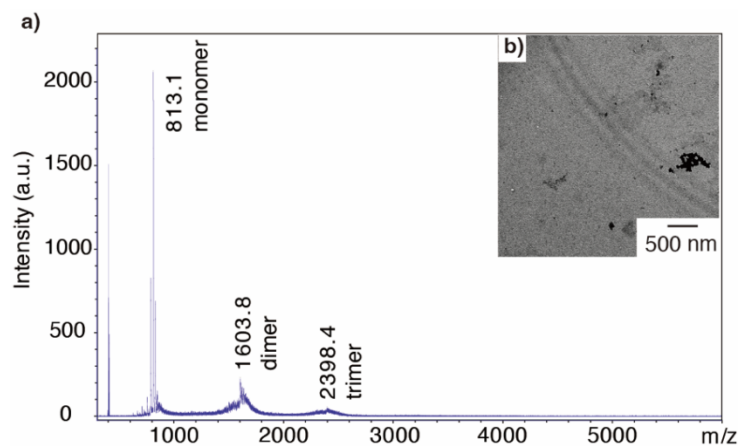
Figure 2.7 a) MALDI-TOF MS spectrum of the photoproducts of **1a** after UV irradiation with a total light intensity of 0.30 kJ cm^{-2}. b) TEM image of the photoproducts of **1a**. This figure is a reprinted version from Figure S5 of M. Inada *et al.*, 2022.[114]
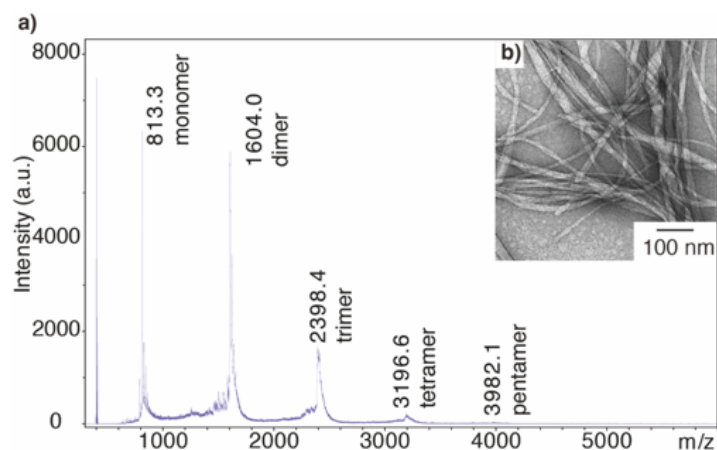
Figure 2.8 a) MALDI-TOF MS spectrum of the photoproducts of **1b** after UV irradiation with a total light intensity of 0.43 kJ cm^{-2}. b) TEM image of the photoproducts of **1b** This figure is a reprinted version from Figure 3 of M. Inada *et al.*, 2022.[114]

2.3.4 MM calculations

The molecular arrangement was predicted using MM simulations (Scheme 2.3 c) shows that a single molecule could be predicted to have a folded shape, with two arms extending from the benzene ring of the spacer point in the same direction. The structure of the single molecule (**1a** or **1b**) was optimized and confirmed from the MM studies, revealing that they are in a folded structure and have both intramolecular and intermolecular C=O···H–N hydrogen bonds between single molecules. Fig. 2.9 presents the modelled self-assembly structure as determined from the MM calculation considering the length axis in parts 10a (**1a**) and 10d (**1b**), as well as from the width axis in parts 10c (**1a**) and 10f (**1b**).
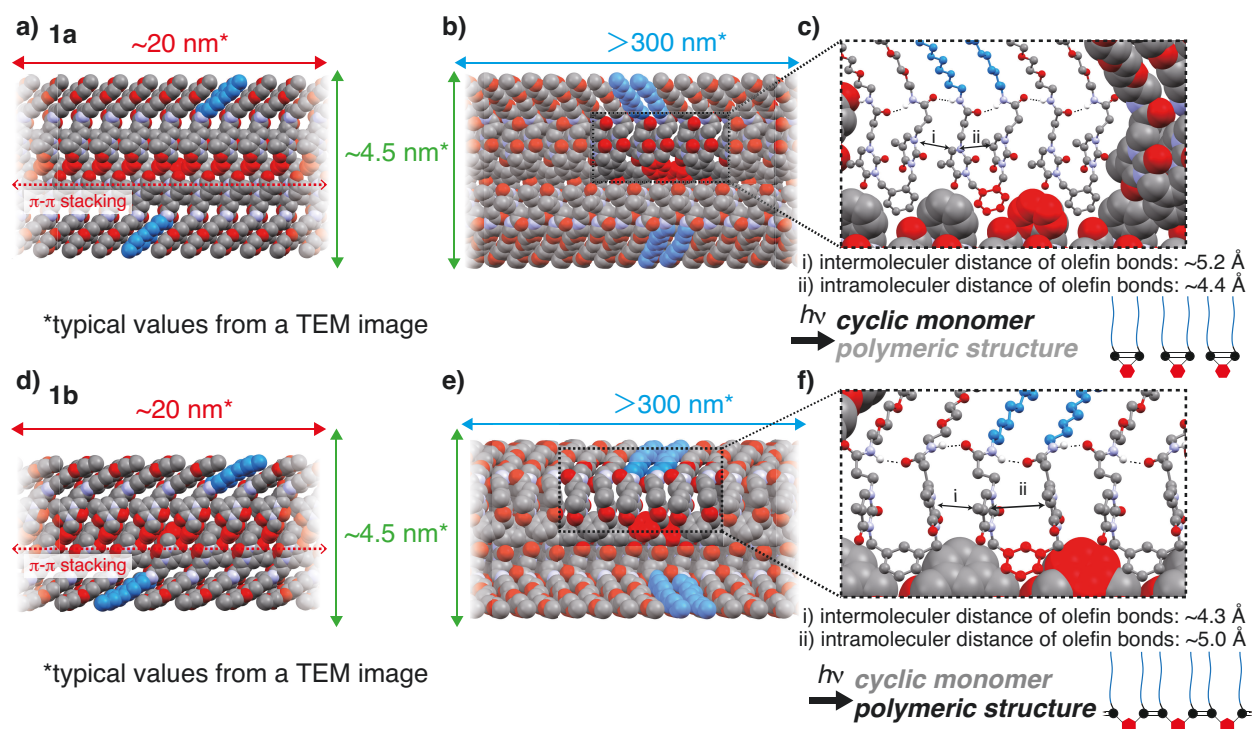
Figure 2.9 Proposed models for molecular packing from the MM calculations of **1a** and **1b** inside a supramolecular nanoribbon in the view from (a, d) length and (b, e) width axes (C: gray, N: cyan, O: red, and H: white). The enlarged images of molecular alignment and expected photoproduct of (c) **1a** and (f) **1b**. Hydrogen atoms except for the amide bonds of focused molecules were omitted for clarity. The dotted lines show hydrogen bonds. The intermolecular and intramolecular distances of olefin bonds are indicated with i and ii, respectively. This figure is a reprinted version from Figure 4 of M. Inada *et al.*, 2022.[114]

As single molecules are repeatedly aligned and stacked in a continuous array via the CO···H–N bonds between amide bonds and the π–π stacking interactions between the benzene rings, self-assembly forms a 3D nanoribbon-like structure, which correlates with the TEM images. Most importantly, we found that **1a** and **1b** are packed slightly differently and recognized that the distances between the photoreactive sites (thymine olefin bonds) also differ between **1a** and **1b** (Fig. 2.9 c and 10f). For **1a**, the intramolecular distance between olefin bonds is closer within a single molecule (4.4 Å) than that between olefin bonds in two molecules (5.2 Å). In contrast, for **1b**, the intermolecular distance between olefin bonds in two molecules (4.3 Å) is shorter than that within one (5.0 Å). From these MM simulation results, **1b** has more favorable conditions than **1a** for undergoing the intermolecular cycloaddition reaction to form a polymeric structure. This could be the reason why a more extended covalent structure was detected in **1b** (meta-substitution) than in **1a** (ortho-substitution).

2.3.5 Comparison of photoreaction efficiencies for different spacers (1N)

In this study, the morphology and efficiency of photopolymerization of boraamphiphile derivatives with the addition of a benzene ring as a spacer were investigated, and MM calculations suggested that the π–π stacking of this aromatic ring is involved in the formation of self-assembly and that this molecular packing controls the intermolecular distance of the reaction site. Therefore, this study further investigated whether benzene rings can be involved in self-assembly and discussed the role of spacers in controlling intermolecular distance (Scheme 2.4). Therefore, an alkyl group was substituted for the benzene ring in the spacer.
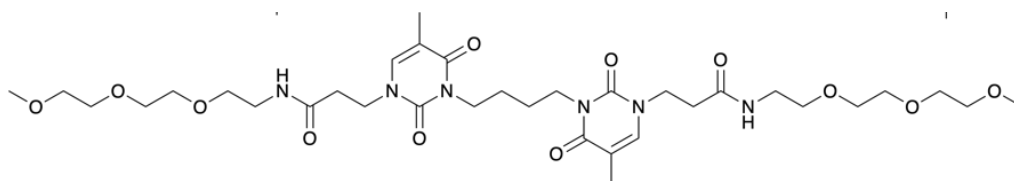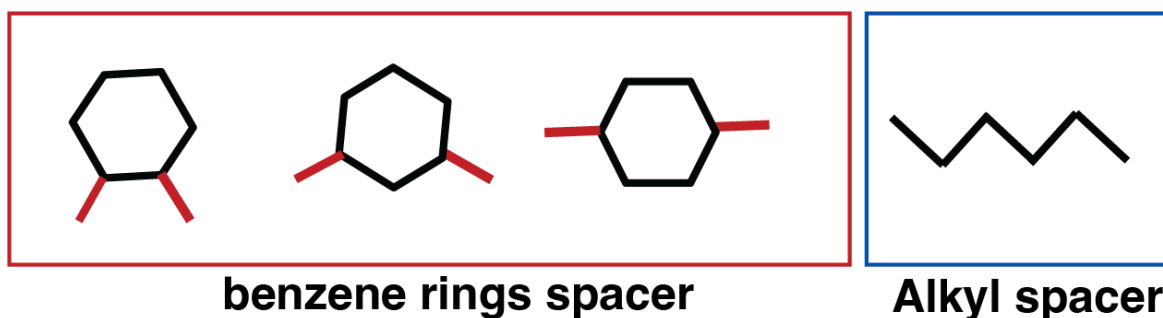
Scheme 2.4 Chemical structures of bolaamphiphiles **1N.**

1N was dissolved in pure water to a concentration greater than CAC, heated at 70°C, then returned to room temperature, and observed by TEM (Figure 2.10 left). As the TEM images show, a micelle-like morphology of around 100 nm was observed. The DLS results also suggest that these micelles have an average size of 114.2 nm.
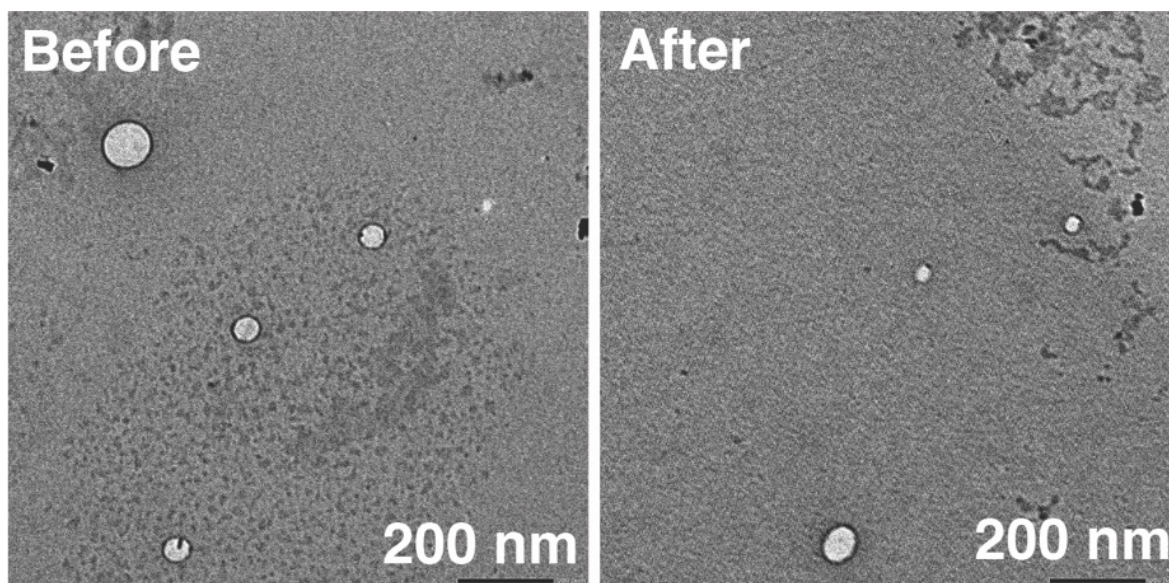
Figure 2.10 TEM images of **1N** before UV irradiation and after UV irradiation.

The samples prepared above CAC (0.94 x 10^{-3} M) were placed in a quartz cell and irradiated with UV light (302 nm) using a high-pressure mercury vapor lamp for several hours. The photochemical reaction was traced by measuring the UV absorption spectrum. The decrease in absorption (270 nm) due to the double bond site of the pyrimidine ring structure indicates that the [2+2]-photocycloaddition reaction was in progress for 14 minutes. Acetone is widely applied as a photosensitizer in which the singlet-triplet transition occurs relatively easily. [144.] The addition of a small amount of acetone as a photosensitizer accelerated the photochemical reaction rate (Figure 2.11).
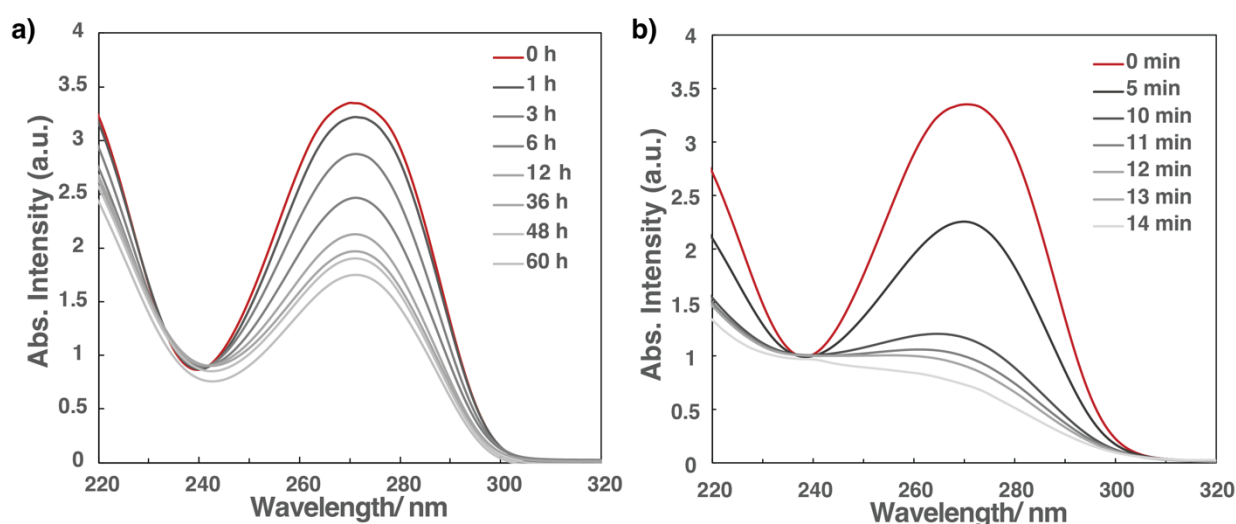
Figure 2.11 UV-vis spectra of 1N at a)302 nm and b) 302 nm UV irradiation with 2.5 mol% acetone as a photosensitizer.

^{1}H NMR measurements were performed to compare the structures of the amphiphilic bis-thymine derivatives before and after UV irradiation (Figure1.12). In the NMR spectrum before UV irradiation, a peak around ppm7 appeared, which was attributed to the double bond of the thymine skeleton. However, in the NMR spectrum after UV irradiation, this peak disappeared. This suggests that the [2+2] photocycloaddition reaction was promoted by UV irradiation. Furthermore, a new peak appeared near ppm4 after UV irradiation, which is a cyclobutane-derived peak formed by the [2+2] photocycloaddition reaction. The peak associated with the methyl group of the thymine ring shifted to the right after UV irradiation, indicating that the [2+2] photocycloaddition reaction had proceeded. Thus, the NMR results indicate that the double bond moiety derived from the thymine backbone disappeared and cyclobutane was formed, indicating that the [2+2] photocycloaddition reaction proceeded. Thymine dimers can be classified into four conformational isomers: cis-syn, cis-anti, trans-syn and trans-anti.[79] The results of ^{1}H-NMR identified which isomer of the Bis-thymine derivative (**1N**) was formed by photochemical reactions in the self-assembly. The proton peak at the methyl group of the thymine ring was divided into four peaks, indicating that the trans-syn isomer was mainly produced.[65, 140] According to the NMR integrated values, 92 % of the total trans-syn form was produced by the photochemical reaction.

Before UV irradiation

X : parts per Million : 1H δ / ppm

After UV irradiation

X : parts per Million : 1H δ / ppm
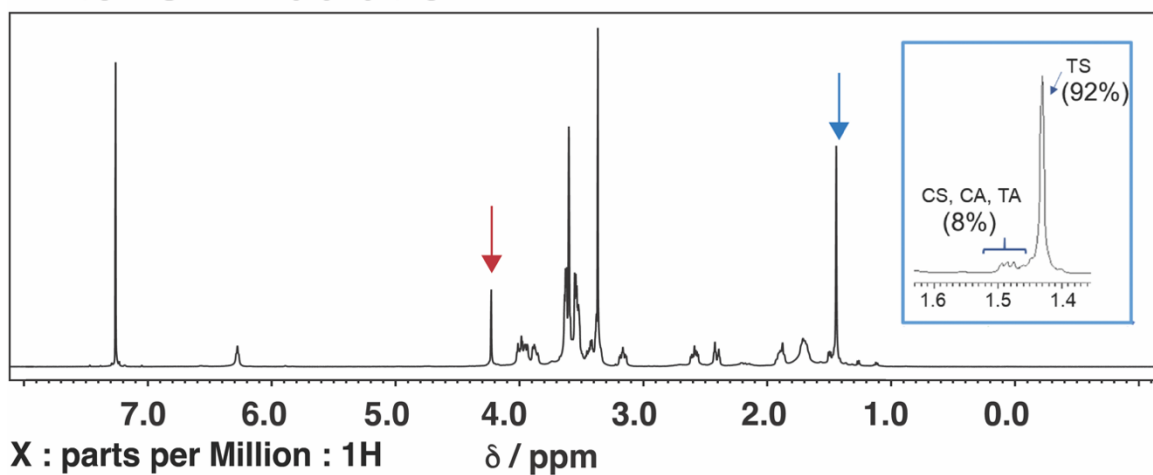
Figure 2.12 ^{1}H-NMR spectra of **1N** before and after UV irradiation.

MALDI-TOF-MS was used to measure the mass of **1N** after UV irradiation at 302 nm for measuring the mass of polymers. The molecular weight of **1N** was found to be elongated to the dimer by UV irradiation at 302 nm (Figure 2.13).
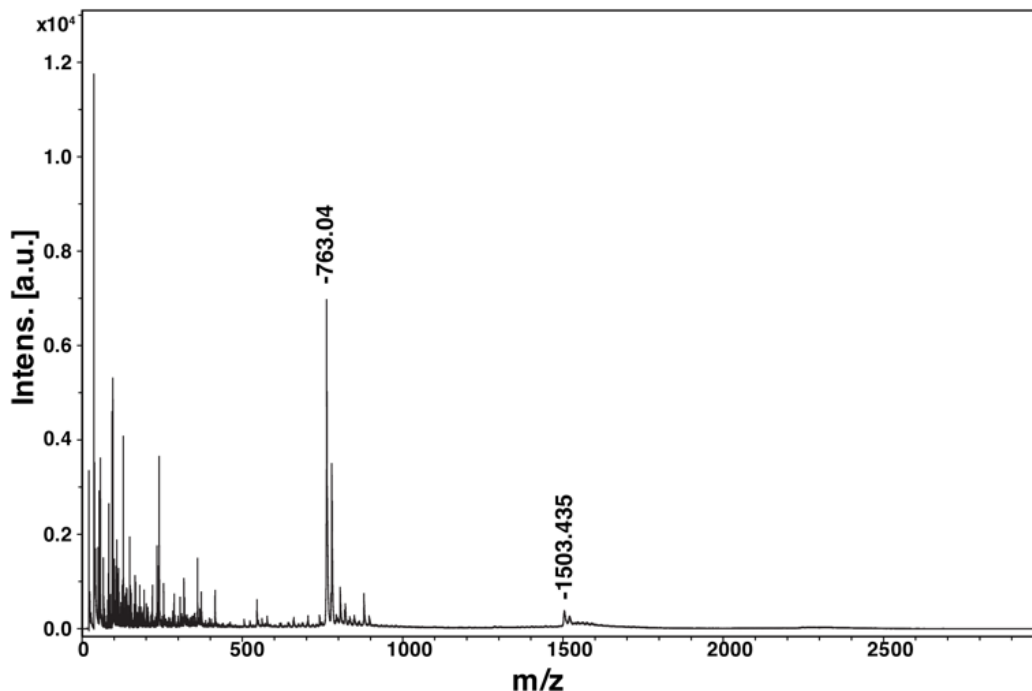
Figure 2.13 MALDI-TOF-MS spectrum of **1N** after UV irradiation.

These results indicate that in the molecular design of bolaamphiphiles, the morphology of the self-assembly can be controlled by the difference in the functional group (aromatic ring, alkyl group) of the thymine ring spacer in the hydrophobic moiety. However, this study lacks a quantitative assessment of the strength of intermolecular forces and does not provide substantial evidence that the addition of functional groups can control the stability of self-assembly. The strength of intermolecular interactions in self-assembly can be determined by analyzing the vibrational frequencies of the molecules using techniques such as Infrared spectroscopy (IR) and Raman spectroscopy. Additionally, by using small angle X-ray scattering (SAXS), the size and shape of self-assembled aggregates can be determined, which can also provide information on the strength of intermolecular interactions.

2.3.6 Stability of the self-assembly before and after UV irradiation

The transformation of nanostructures in-situ conditions is fascinating as it means that the dynamic behavior of nanostructures can be controlled at the nano-size level. Therefore, we investigated the changes in the dynamic behavior of self-assembled 3D structures before and after light irradiation. Nanostructures before and after UV irradiation were heat-stimulated at 90°C and their sizes were investigated using DLS (Table 2,2).

Table 2.2 Mean particle size (z-average) of the self-assembled structures before and after UV irradiation under heating.

	Average size (nm)
Before UV irradiation	269.8 nm
Before UV irradiation and heating at 90 °C for 1 hour	78.8 nm
After UV irradiation and heating at 90 °C for 1 hour	342.2 nm

The average particle size of the self-assembled bodies before UV irradiation was 269.8 nm, but after heating at 90°C for 1 hour, the size changed to 78.8 nm. When the self-assemblies were heated at 90°C for 1 hour before UV irradiation, the average particle size was 342.2 nm. These results suggest that self-assemblies converted to a conventional continuous structure by light stimulation are stable and do not undergo dynamic changes due to heat. However, DLS is a method to calculate particle size distribution from the Brownian motion of materials suspended in water. Since the molecules in the present study have a ribbon-like self-assembled morphology, there is a limit to discussing the stability of self-assembly from this slight change in size behavior due to thermal stimulation.

2.3.7 Photo-reversibility of bolaamphiphiles

The [2+2] cycloaddition reaction is a reversible reaction. As the figure in Figure 2.14 shows, irradiation with 254 nm light reconstituted only about 20% of the double bonds, and the absorption intensity at 271 nm did not completely increase back.
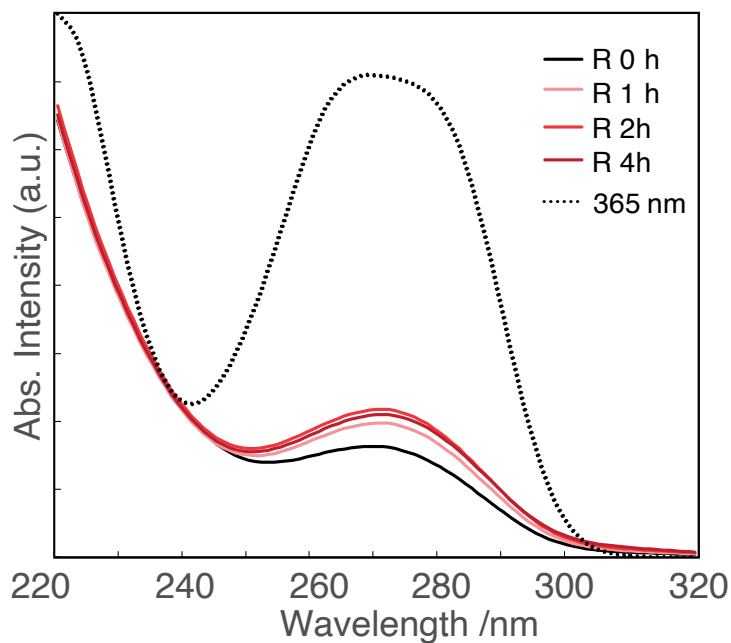
Figure 2.14 UV-vis spectra of **1b** by UV irradiation at 365nm and 254 nm.

2.4 Conclusion

In this study, a boraamphiphilic bisthymine molecule was designed and synthesized, wherein the [2+2] cycloaddition reaction proceeds in a confined ribbon-like self-assembled structure. This analysis revealed that the **1b** (meta-substitution) molecule formed a continuous covalent structure up to pentamers by linking self-assembled molecules without changing their overall 3D shape. Furthermore, the photoproducts have different molecular weights because of differential molecular packing caused by differences in the three-dimensional structure of the self-assembled molecules (Figure 2.15). There were differences in the shape of the self-assemblies between the **1N** and **1a** and **1b** self-assemblies, which were micellar and rod-shaped. The structure of the self-assemblies was attributed to the monomeric structure, suggesting that clever design of linker sites between thymine motifs could control the structure of the self-assemblies and even the intra/intermolecular [2+2] cycloaddition. This finding provides insight into the conversion of non-covalent supramolecules to covalently linked molecules; furthermore, it can potentially provide a basis for the development of novel stimuli-responsive nanomaterials for drug delivery systems, nanodevices, and other applications. In contrast to crystalline and other solid phases, self-assemblies are believed to exhibit a degree of instability in their assembly due to the presence of covalent bonding between constituent molecules. To address this issue, it has been proposed that redesigning the spacer moieties to be more rigid, through the incorporation of more bulky aromatic spacers, may lead to improved self-assembly.

1. Sidechain structure
 bolaamphiphiles→ self-assembly

2. Bis-Thymine (DCB site)
 → continuous linear oligomer

3. Spacer		
Polymerized Molecules	Trimer	Pentamer
Morphology	Fiber	Fiber
Photoreaction site distance	Intramolecular < Intermolecular ~4.4 Å ~5.2 Å	Intramolecular > Intermolecular ~5.0 Å ~4.3Å
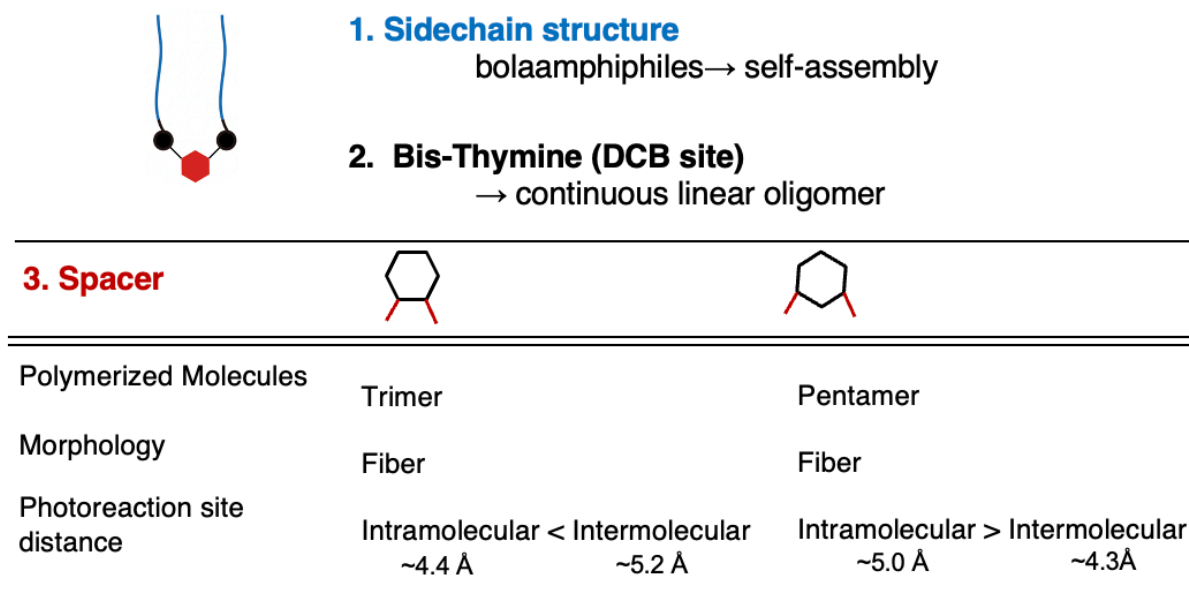
Figure 2.15 Monomer design for the formation of linear polymer structures.

Molecular design

From the perspective of molecular design, three factors were considered in creating the linear polymer structure.

(1) Side-chain structures

Bolaamphiphiles structures were designed as the side chain structure for self-assembly, and a well-defined ribbon-shaped self-assembly was achieved. To investigate the conditions for self-assembly in water, a flexible and hydrophilic polyethylene glycol (PEG) structure was introduced, leading to dissolution in the aqueous phase and a transition to the ribbon structure.

(2) DCB sites

Two photoreaction sites on thymine were placed in the molecule. At the beginning of the design, the molecular design assumed that the thymine double bond would be placed in a ladder-like configuration, similar to the topological reactions in crystals that have been reported in the past. [65, 132] However, as suggested by the morphology of the self-assemblies and MM calculations obtained in this study, the spacers between thymines in the solvent-interacting self-assemblies are flexibly bent and the two side chains are arranged to face each other. Therefore, the spacers between thymines contribute significantly to the regulation of intra/intermolecular reactions.

(3) Spacers

Aromatic spacers were introduced to enable intermolecular bonding. We found that the different arrangement of the aromatic substituents controls the intra-/intermolecular reactivity of the [2+2] cyclic-addition reaction.

Polymer properties

The obtained pentameric molecules and larger ones did not confirm the physical properties (behavior different from that of small molecules) generally observed with polymeric molecules. The main reason was that the self-assembly in water was in minute quantities and therefore could not be obtained in the quantities needed for analysis.

Chapter 3

Photo-conversion of multi-branching structures based on [2+2]-cycloaddition reactions ※
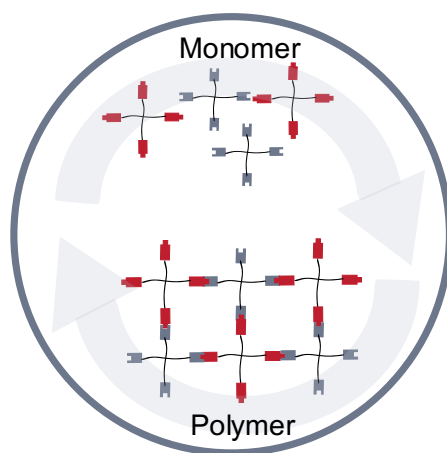
Chapter 3 describes studies on the creation of cross-linked polymers by using dynamic covalent bonds.

3. 1. Introduction

Adhesives are widely used in mechanical bonding methods and have been implemented in various daily applications. Over the past decade, debonding-on-demand (DoD) systems with a variety of bond strengths according to requirements have been developed in the medical, automotive, micro, and soft electronics fields. [141-145] These DoD adhesives are required to possess switchable adhesiveness, that is, they should be sufficiently strong to hold and bond adherends when in use, while decreasing in strength sufficiently to be peeled off from the adherends after use. For example, acrylic- and silicone-based adhesives are mainly used as peelable wound dressings in the biomedical field.[146-148] In the automotive field, a temporary adhesive tape is typically used as an in-process masking tape; recently, a DoD mechanism has been considered for easy material retrieval from end-of-life electronic devices.[149-152] The most attractive mechanism for developing DoD adhesives that are reversibly detachable on demand is incorporating a system of reversible bond breaking and forming into the material design.[143-145] Dynamic covalent bonds, which are distinguished by their reversibility and responsiveness to external stimuli such as heat, light, electricity, and pH, can control the degree of polymerization, crosslink density, and viscoelastic properties of polymeric materials. [11, 153] Recently, stimulus-responsive dynamic covalent bonding has been shown to be applicable to adhesives in terms of controlling adhesiveness. [154, 155] Notably, current DoD adhesives are mainly based on thermo-reversible reactions such as Diels–Alder[156-159] and transesterification reactions,[160, 161] which limit their application at room temperature. In contrast, photoinduced processes that enable "direct" remote manipulation of the macroscopic properties of materials by irradiating light of specific wavelengths and intensities are useful for DoD adhesives under ambient conditions.[141]

Typically, photo-reversible covalent bonding reactions include [2+2]- and [4+4]-type photochemical cycloadditions of thymine,[162] coumarin, [163-165] and anthracene, [166-171], trans-cis photoisomerization of azobenzene,[172] and photolysis of trithiocarbonates.[173-176] Dynamic covalent polymer networks incorporating these light-induced reversible reactions have a wide range of applications, including self-healing polymers [109, 177-183] and shape memory materials.[184-187] Herein, the cycloaddition reaction of coumarin and its derivatives is one of the most promising reactions applicable to DoD adhesives. It is expected to provide a light-responsive reversible change in adhesiveness and exhibit stability under sunlight owing to its properties, such as irradiation with ultraviolet (UV) light with a wavelength of 365 nm or longer, inducing the cyclodimerization of coumarin, leading to the formation of a dimer with a cyclobutane ring, whereas the reverse photocleavage reaction occurs by irradiation with light at wavelengths below 254 nm, recovering the original monomers. Although polymers with coumarins have been used in self-healing and shape-memory materials, only a few have been used to create reversible adhesives. In addition, most of the adhesives developed with

coumarins are based on block polymers, and their synthetic pathways are exceedingly complex.[163, 164]

In this study, we report a DoD system based on a coumarin-terminated four-arm monomer with a siloxane (–Si–O–Si–) backbone. Four-arm monomers are known to induce macromolecular architectural transformations (MAT) by increasing the number of dynamic covalent bonding sites, forming denser and more reproducible polymer networks.[92, 188-191] To achieve MAT, two features are important: i) flowability (ability to be fluidized); and ii) intermolecular bonding (ability to form networks). In the molecule we synthesized (**SS1**, Fig. 1a), a central moiety consisting of cyclic siloxane appears suitable as a liquid monomer and has a high glass transition temperature (T_g) in its polymerized state, and each terminal coumarin motif includes the photo-reversible intermolecular bonding; this structure is designed to enable light-induced change in the rigidity and fluidity of the materials. The synthesis of the four-arm monomer **SS1** was achieved by selecting a simple epoxy ring opening reaction of 2,4,6,8-tetramethyl-2,4,6,8-tetrakis(propylglycidylether)cyclotetrasiloxane with 7-hydroxycoumarin. A dynamic covalent polymer network derived from **SS1** was demonstrated to possess reversible adhesive properties, exhibiting a strong potential as a DoD adhesive.
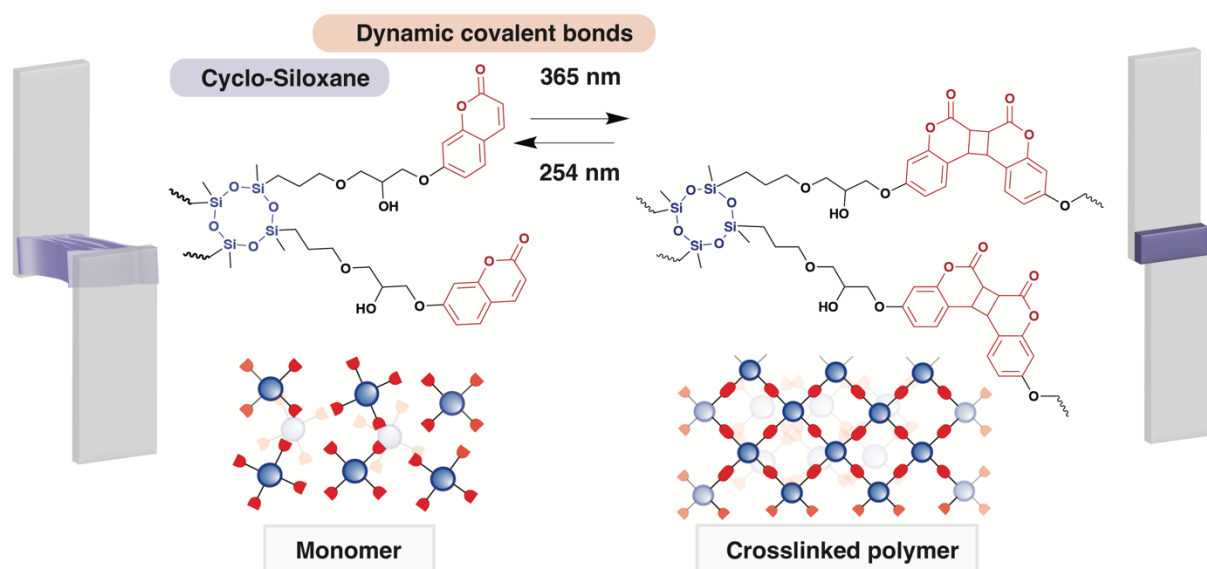
Figure 3.1 Four-arm SS1 adhesives. Schematic diagram of a photoinduced debonding-on-demand system of **SS1**. This figure is a revised version of Figure 1 of M. Inada *et al.*, 2023. ※

3.2. Materials and methods

3.2.1 Materials

7-hydroxycoumarin was purchased from Tokyo Chemical Industry Co., Ltd.; anhydrous potassium carbonate and N, N-dimethylformamide (DMF) were purchased from FUJIFILM Wako Pure Chemical Corporation; and 2,4,6,8-tetramethyl-2,4,6,8-tetrakis(propylglycidylether)cyclotetra-siloxane was purchased from Sigma–Aldrich. The other solvents were purchased from FUJIFILM Wako Pure Chemical Corporation.

3.2.2 Equipment and characterization

Photochemical reactions were performed using a UV crosslinker (CL1000 365 nm, UVP and CL1000 254 nm, UVP). ^{1}H-NMR spectroscopy was performed on a Varian INOVA 400 spectrometer. Fourier-transform infrared (FT-IR) spectra were acquired using a Nicolet 6700 FT-IR spectrometer. The spectra were measured directly on the sample in the frequency range of 4000–500 cm^{-1}. Differential scanning calorimetry (DSC) analyses were conducted using a PerkinElmer DSC8000 at a rate of 50 °C min^{-1} for heating and cooling under an N2 atmosphere. The UV spectra were measured using a JASCO V-550 UV-vis spectrometer. The molecular loss was determined by gel permeation chromatography (GPC) at 40 °C using a Showa Denko Shodex KF-804L column and a JASCO RI-4030 refractive index detector calibrated with a polystyrene standard. Tetrahydrofuran (THF) with a stabilizer was used as the eluent at a flow rate of 1.0 mL min^{-1} and a calibration curve were prepared using Shodex PMMA standards. Optical microscopy images were obtained using a Keyence VW-6000. The depths of the scratches before and after UV irradiation were measured using a Bruker Co. Dektak XT-S stylus profiler. The lap-shear test was performed using a universal testing machine equipped with a 5 kN load cell (Autograph AG 25 TB, Shimadzu Co.) with a stretching rate of 10 mm min–1. Dynamic rheology was performed using a rotary rheometer (MCR 101, Anton Paar) with a 50 mm parallel plate at a gap of 0.5 mm. During the measurements, a frequency sweep (0.1–100 rad s^{-1}) was performed at a strain of 50 Pa. The water contact angle of **SS1** polymer was analyzed by using a contact angle meter (DMs-301, Kyowa Interface Science Co. Ltd).

3.2.3 Synthesis of SS1 monomer
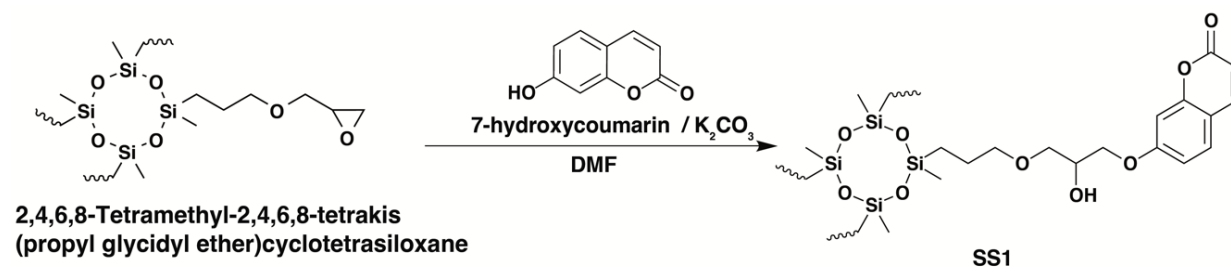
Scheme 3.1 Synthetic scheme for **SS1**. This figure is a revised version of Figure 1 of M. Inada *et al.*, 2023. ※

7-hydroxycoumarin was dissolved in DMF, and anhydrous potassium carbonate was added. The mixture was stirred for 5 min and heated to 105 °C under N2. 2,4,6,8-tetramethyl-2,4,6,8-tetrakis(propylglycidylether)cyclotetrasiloxane was dissolved in DMF (15 mL), added to the flask over 3 h, and stirred for 48 h under constant heating. The reaction mixture was cooled to room temperature and diluted with DMF. The solids were removed by filtration, and the sediments of the product were dropped in ether at set intervals. The ether was poured out and the residues (sticky) were redissolved in DCM and stirred overnight at room temperature. The solution was washed thrice with water (pH 10) and then dried over MgSO4. The solvent was evaporated, and the product was purified by column chromatography with methanol and dichloromethane (20/1). Finally, the sticky brown products were collected by evaporation.

Final mass = 0.9 g, 24% yield. ^{1}H-NMR (CDCl$_3$): 0.07 ppm (12H, br, –Si(CH$_3$)–); 0.53 ppm (8H, m, –SiCH$_2$CH$_2$CH$_2$–); 1.63 ppm (8H, m, –SiCH$_2$CH$_2$CH$_2$–); 3.46 ppm (8H, m, –SiCH$_2$CH$_2$CH$_2$–); 3.58–4.1 ppm (20H, O–CH$_2$–CH(OH)–CH$_2$–O–); 6.23 ppm (4H, d, ArH); 6.81–6.91 ppm (8H, m, ArH); 7.34 ppm (4H, d, ArH); and 7.60 ppm (4H, d, ArH). ^{13}C-NMR (CDCl$_3$):1.65, 13.65, 23.68, 69.49, 70.22, 72.11, 74.68, 102.18, 113.44, 113.88, 114,28, 129.45, 143.92, 156.33, 161.76, 162.42ppm. ^{29}Si-NMR (CDCl$_3$): –19.89 pm. FT-IR: 3411, 2931, 2870, 1724, 1706, 1666, 1608, 1556, 1508, 1479, 1456, 1429, 1402, 1350, 1292, 1281, 1279, 1230, 1198, 1159, 1119, 1045, 989, 891, 831, 798, 750, 685, 664, 6323, 615, 544–565, and 521cm^{-1} (Fig. 2b). MALDI-TOF/mass: *m/z* 1368.51[M+Na]$^+$

3.2.4 Preparing photocrosslinked polymer

The synthesized SS1 monomer was used to produce a crosslinked polymer. The monomer was cast directly onto glass slides and irradiated with UV light at 365 nm in a UV crosslinker at room temperature. For the UV-vis spectra and adhesion tests, the monomer solution (THF, 10 wt.%) was spin-coated onto the quartz glass. After irradiation at 365 nm for 1 h, the crosslinked polymers were obtained.

3.2.5 Self-healing test

The **SS1** monomer was cast onto the glass directly and irradiated with UV light at 365 nm for 16 h. Subsequently, the polymerized **SS1** film surface was scratched with a razor blade and observed using optical microscopy. To confirm the self-healing properties, the membrane was irradiated with 254 nm UV light, and the scratch healing was observed by optical microscopy. Moreover, the depth of damage was measured using a Dektak profiler before and after membrane healing.

3.2.6 Tensile test

To prepare for the adhesion test, the **SS1** monomer (THF, 0.05 M) was spin-coated onto a 25 x 10 mm2 masked glass (quartz, 1 mm thick). Another substrate was then placed over the previously spin-coated substrate and the joint was hand-pressed. The crosslinked polymers were then irradiated with 365 nm light. To measure the adhesion strength of the polymers, a lap-shear test was performed using a universal testing machine (Autograph AG 25 TB, Shimadzu) equipped with a 5 kN load cell. At a stretching rate of 10 mm min^{-1}, each substrate was stretched until it peeled off, and the lap-shear strength was measured (Figure 3.2). After the test, adhesive strength (kPa) was calculated by dividing the maximum load (N) by the lap area (A). Further attempts were made to produce an adhesive after curing. After the shear test, a THF solution (1 μL) was dropped to one of the separated interfaces to add fluidity to the sample on the surface. The glass was placed on top of each other, and hand-pressed pressure was applied. Subsequently, repeated shear tensile tests were performed under the same conditions.
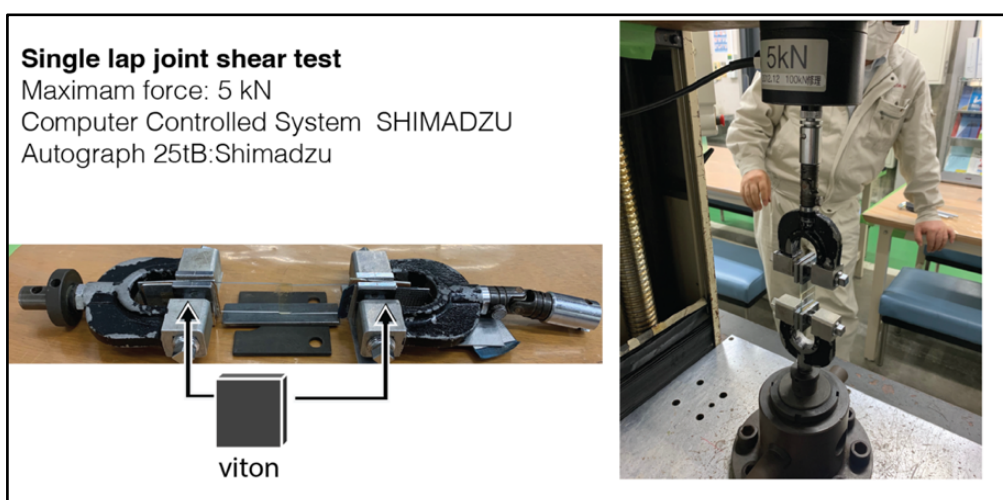
Figure 3.2 The picture of the setup for the single-lap shear test.

3.1 Results and discussion

3.1.1 Spectroscopic characterization of light-induced reversible reactions of SS1

As mentioned in the Introduction, a tetrafunctional monomer (**SS1**) was designed with a structure consisting of a cyclic siloxane core and a photoreactive coumarin attached to the terminus. **SS1** was synthesized by a one-step epoxy ring opening at the end of the side chain with the addition of coumarins. The product was obtained as a liquid and characterized using ^{1}H nuclear magnetic resonance (NMR) spectroscopy (Fig. 3.3)
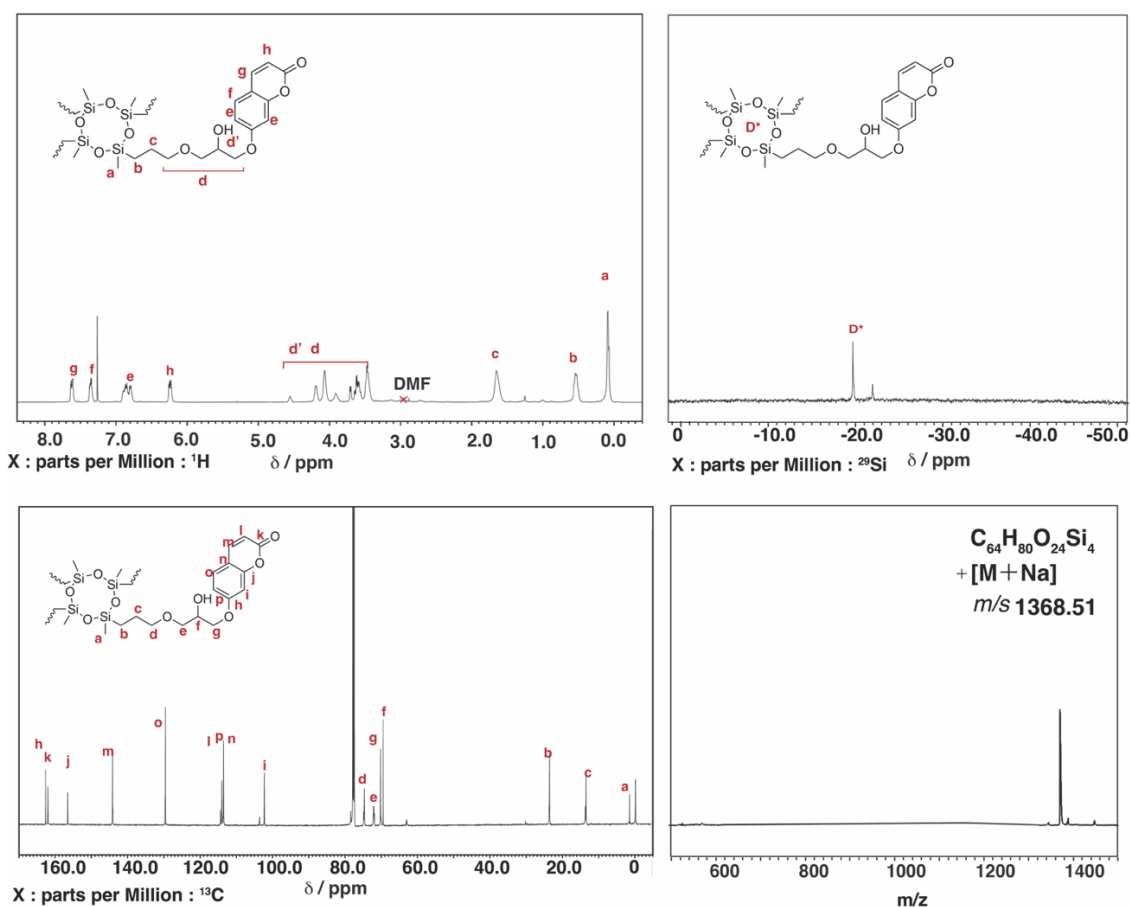
Figure 3.3 ^{1}H NMR spectrum, ^{29}Si NMR spectrum, ^{13}C NMR spectrum, and MALDI-TOF-MS spectrum of **SS1**. This Figure is a reprinted version from Figure S1 of M. Inada *et al.*, 2023. ※

To obtain crosslinked cured polymers, the **SS1** monomer was cast onto glass slides and irradiated with 365 nm UV light. The monomer was placed directly on a glass slide and irradiated in a UV-crosslinking device under ambient temperature and pressure. After irradiation at 365 nm, the resultant polymer film was self-standing. The relevant photoreaction

processes were tracked using infrared (IR) and UV-visible (UV-vis) spectroscopy separately, and the reversibility of the polymers crosslinked by dynamic bonding was demonstrated. The IR spectra of the three types of **SS1** samples, prior to light irradiation, and irradiated at 365 and 254 nm, are shown in Fig. 3.4. Compared to the spectrum prior to UV, the peak assigned to C=O stretching of the coumarin moiety, observed at 1749 cm^{-1} in pre-UV, shifted to 1723 cm^{-1} with an increase in peak intensity owing to the influence of dimer formation (inset of Fig. 3.4). The peak assigned to the cyclobutane ring, not observed in the pre-UV spectrum, appeared at 1555 cm^{-1} owing to the formation of a cyclobutane-based dimer. The peak at 1580 cm^{-1}, assigned to the C=C stretching of the pyrone moiety decreased, whereas the peaks at 1620 and 1510 cm^{-1}, assigned to the C=C stretching of the aromatic ring, were observed both before and after irradiation. After subsequent irradiation at 254 nm, causing photocleavage of the cyclobutane ring, the C=O peak shifted back to 1749 cm^{-1} with a decreased intensity, the peak assigned to the cyclobutene ring at 1555 cm^{-1} disappeared, and the peak originating from the pyrone moiety at 1580 cm^{-1} became clear again. These FT-IR results accompanied by the irradiation at 365 and 254 nm confirm the crosslinking and decrosslinking of **SS1**. [111, 112, 181, 182, 191]

The progress of the polymerization reaction of **SS1** was determined from the UV-vis spectra by comparing the intensity of the absorption peak before and after light irradiation, for which samples were prepared by spin-coating the **SS1** monomer solution on quartz glass. A series of UV-vis spectra were obtained after each exposure to 365 nm UV light (irradiation intensity: 0.28 Jcm^{-2} min^{-1}) every 5 min in a UV crosslinker. As shown in Fig. 2d, a gradual decrease in the absorbance at 321 nm, corresponding to the π–π* transition of the pyrone structure with the double bond in coumarin, was observed upon light irradiation at 365 nm. This indicates the progress of the [2+2] cyclic-addition reaction, resulting in the formation of a cyclobutene-based dimer accompanied by the cleavage of the pyrone structure double bond. As shown in Fig. 2d, a gradual decrease in the absorbance at 321 nm, corresponding to the π –π* transition of the pyrone structure with the double bond in coumarin, was observed upon light irradiation at 365 nm. The absorption decrease was attributed to the cleavage of the double bond in the pyrone structure and the collapse of the conjugated π-system, indicating that the [2+2] cyclic-addition reaction proceeded and a cyclobutene dimer was formed. [192, 193] The photochemical conversion of these coumarin moieties within **SS1** was estimated using Eq. (1): [182]

$$\text{Coumarin conversion (\%)} \;=\; 1 \,-\, (A_{t}{}^{321}/A_{0}{}^{321})\, \text{x}\, 100 \qquad\qquad (1)$$

where $A_t{}^{321}$ denotes the absorbance observed for the sample at a certain time (t) during irradiation and $A_0{}^{321}$ the absorbance prior to irradiation. After 60 min irradiation, ~74% of the coumarin units were estimated to undergo photocyclization; that is, ~23% of the coumarin remained unreacted. In contrast, irradiation with UV light at 254 nm every 1 min resulted in a rapid increase in absorption at 321 nm (Fig. 3.5). A similar estimation indicates that ~67% of the coumarin motifs were in a decrosslinked state after irradiation at 254 nm (irradiation intensity: 0.28 Jcm^{-2} min^{-1}) for as short as 6 min, and thus, the residual ~33% was still crosslinked. Subsequently, irradiation with 365 nm light decreased the absorbance at 321 nm again, thus confirming that the [2+2] cycloaddition reaction occurred repeatedly (Fig. 3.5). The

coumarin conversion rates for different light exposure times, calculated from equation (1), are shown in Fig.3.6. As the photoconversion rate of photocrosslinkable units is correlated with the crosslink density,[194] the relationship between photoconversion rate and light exposure time shown in Fig. 3.6 suggests that the crosslink density changes with light exposure.
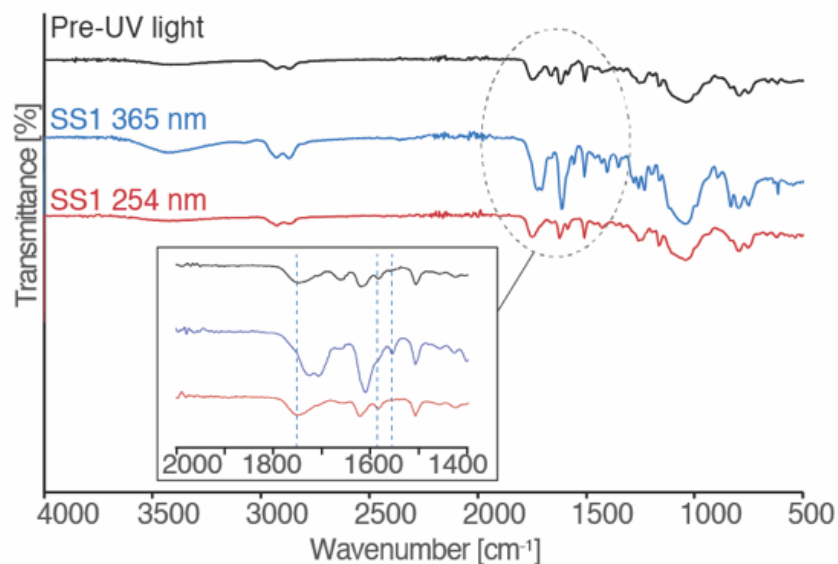
Figure 3.4 Fourier-transform infrared spectrum. This figure is a revised version from Figure 2b of M. Inada *et al.*, 2023. ※
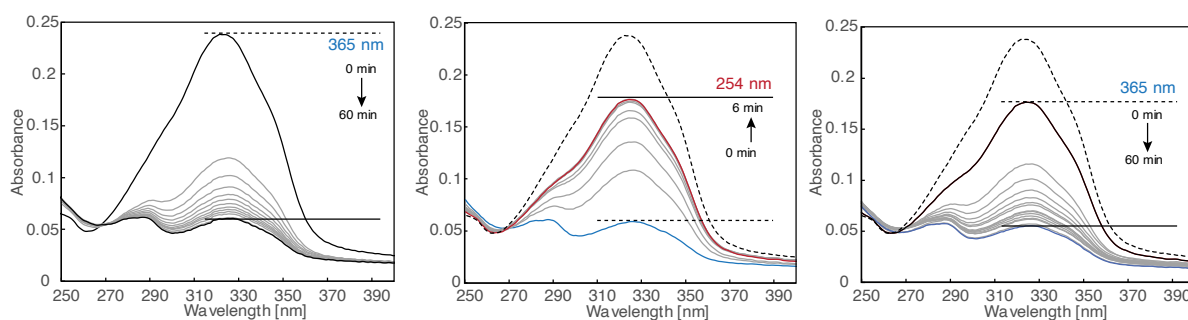
Figure 3.5 UV-vis spectra of the samples after UV irradiation with 365 nm for 60 min, 254 nm for 6 min, and 365 nm (again) for 60 min. The blue and red lines indicate the minimum intensity after 365 nm UV irradiation and the maximum intensity after irradiation with 254 nm, respectively. This figure is a revised version from Figures 2d, 2e, and 2f of M. Inada *et al.*, 2023. ※
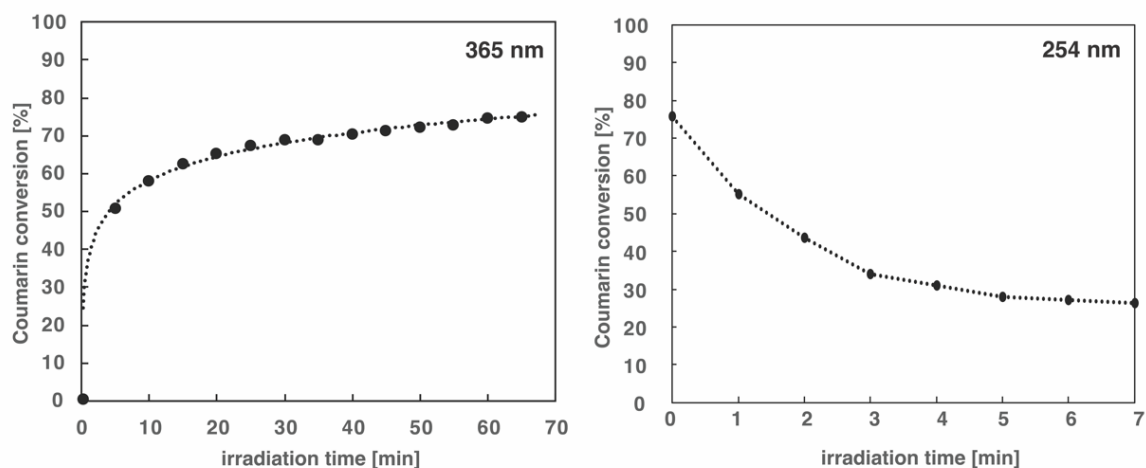
Figure 3.6 Photo-conversion ratio of **SS1** after (left panel) 365- and (right panel) 254 nm irradiation. Reaction progress can be monitored by following the absorbance changes at 321 nm using **Equation 1**(Irradiation intensity: 0.28 Jcm^{-2} min^{-1}). This figure is a reprinted version from Figure S2 of M. Inada *et al.*, 2023. ※

3.3.2 Analysis of thermal properties

The thermal behavior induced by the [2+2] cycloaddition of the terminal coumarin moiety upon photoirradiation of **SS1** confirmed thermogravimetry differential thermal analysis (TG-DTA) (Figure 3.7) and differential scanning calorimetry (DSC) (Fig 3.8). TG-DTA results indicated that photocrosslinked **SS1** was thermally stable. The T_g of the four-arm monomers with a coumarin skeleton can be controlled by changing the wavelength.[92, 141, 180, 189, 190] The T_g of **SS1** before and after UV irradiation at 365 nm (polymerized) and 254 nm (depolymerized) were determined by DSC. The T_g of the monomer was –14.2 °C and that of the crosslinked polymer was as high as 128.3 °C, confirming the achievement of a significant difference in T_g before and after polymerization as designed. After being irradiated with 254 nm UV light to enable the reverse photocleavage of the cyclobutene ring, the T_g of the decrosslinked polymer was determined to be 16.5 °C, which is higher than that of the original monomer but lower than room temperature. This is attributed to the monomer not completely returning to the decrosslinked state and the oligomers being mixed in the polymer. Gel permeation chromatography (GPC) revealed the presence of oligomers (Table 3.1). It was demonstrated that the irradiation with UV light at ambient conditions could reversibly convert between two states of **SS1**: the hard crosslinked state with a T_g of ~130 °C, and the soft decrosslinked state with a T_g below room temperature.
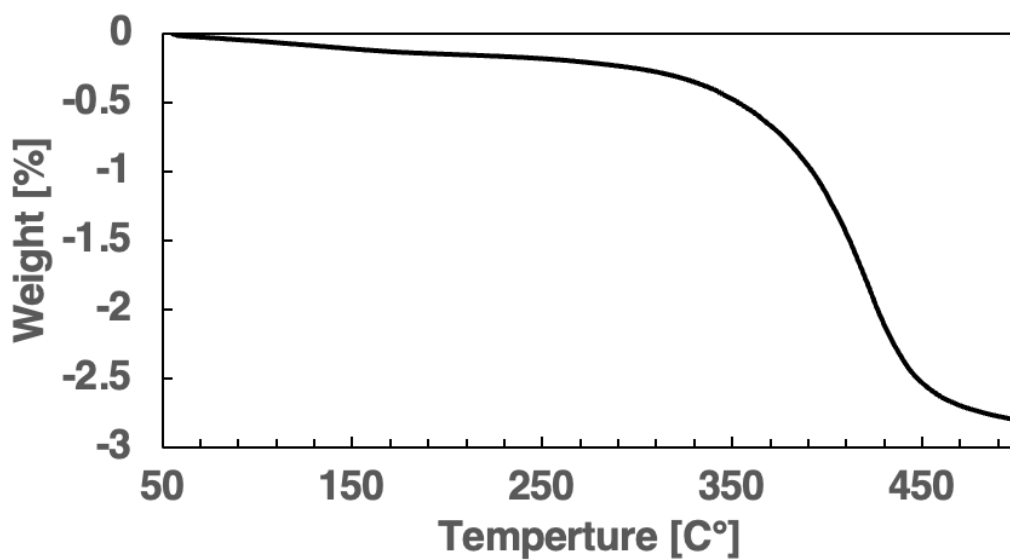
Figure 3.7 TG-DTA curve of **SS1**.
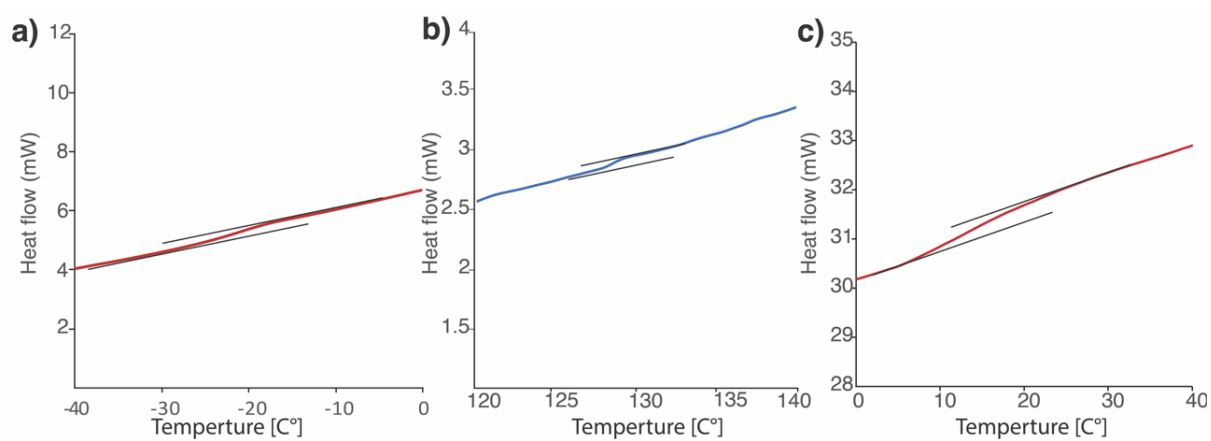
Figure 3.8 DSC curves of **SS1**. This figure is a revised version from Figure S3 of M. Inada *et al.*, 2023. ※

3.3.3 Solubility test

The dependence of the degree of polymer decrosslinking on the duration of UV irradiation was monitored by the solubility testing of **SS1** in THF.42 From the UV-vis and DSC results discussed in the preceding section, UV irradiation at 254 nm for opening the cyclobutane ring of the coumarin motif in the crosslinked part is considered to result in the decrosslinking of the monomers and oligomers. Because these low molecular-weight oligomers are soluble, the mass loss of the samples by dissolution in the solvent was monitored every 1 h during irradiation. After every 1 h, the samples were irradiated with 254 nm UV, completely dissolved in THF solvent, dried, and weighed. The mass loss of the samples was plotted vs. the irradiation exposure time (Fig. 3.9). The mass loss was ~70% after irradiation for 1 h, was as high as ~90% after 2 h, and gradually increased to 96% after 6 h. As suggested from the GPC results (Table 3.1), it is considered that decrosslinking progressed and monomers and oligomers were formed.
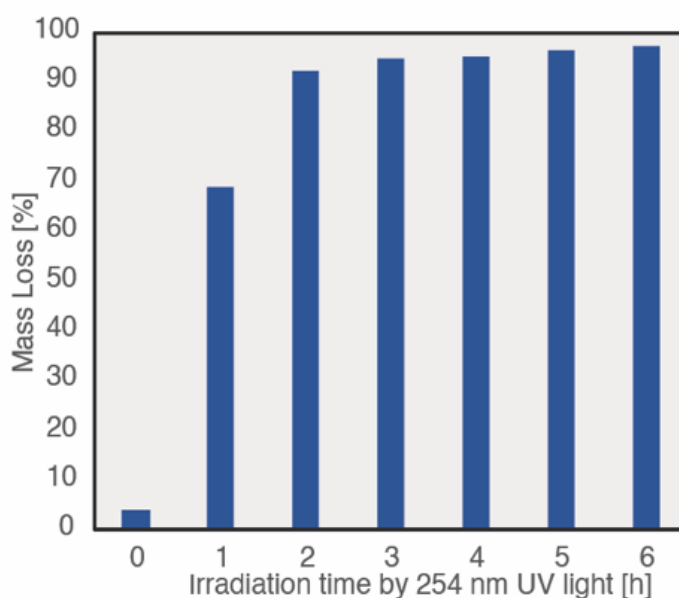
Figure 3.9 Solubility test of **SS1**. UV irradiation at 254 nm increased the mass of the crosslinked polymer dissolved in THF and decreased the mass left over. This figure is a reprinted version from Figure 2c of M. Inada *et al.*, 2023. ※

Table 3.1 Summary of decrosslinked **SS1** polymer. This Table is a reprinted version from Table S1 of M. Inada *et.al*, 2023. ※

	M_n	M_w	M_z
0h	371000	6200000	31800000
1h	1760	1850	1980
2h	651	1160	2780
3h	1560	1580	1590

3.3.4 Moisture sensitivity

Furthermore, the moisture sensitivity of the material was analyzed by measuring the moisture tolerance of **SS1** polymer and the contact angle of its surface (Figure 10 a). Nor like polyethylene glycol-based hydrogel, the weight of the **SS1** polymer under the moisture tolerance analysis did not increase. In addition, the contact angle of the polymer film was 59.8° (Figure 3.10 b).
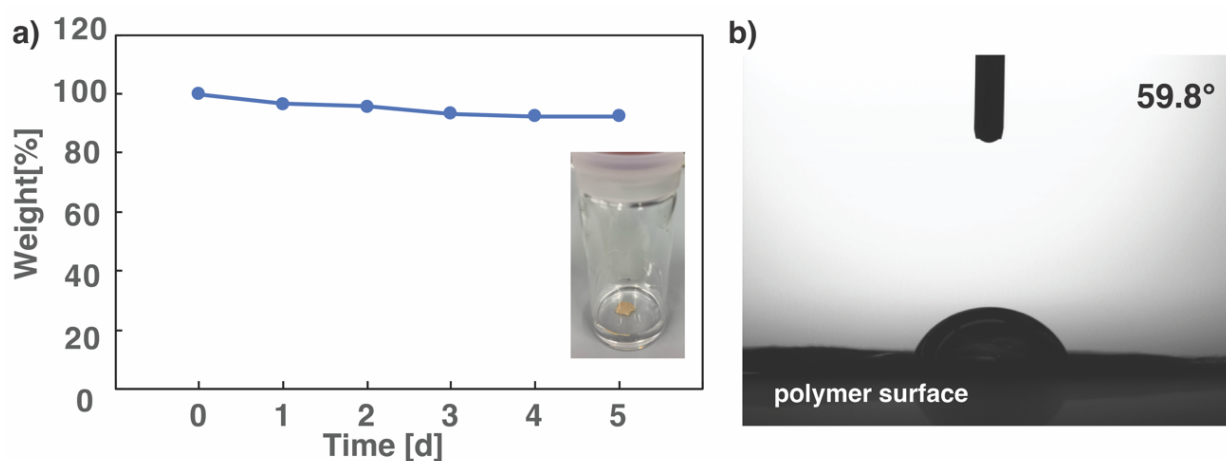
Figure 3.10 a) Weight retention rate versus time in aqueous solution. b) A water contact angle measurement on **SS1** polymer surface. This figure is a reprinted version from Figure S4 of M. Inada *et al.*, 2023. ※

3.3.5 Self-healing ability

The self-healing property of defects on the film upon external stimuli, which contributes to reducing the maintenance cost of polymeric films, is one of the attractive features in the practical applications of DoD adhesives. [177-179] As the **SS1** four-arm monomer was designed for this purpose, similar to the DoD adhesives, the light-induced self-healing properties of the membrane damage were examined using optical microscopy and a Dektak profiler. The monomer was cast on a glass substrate and irradiated with 365 nm light for 2 h (until cured) to prepare the film samples. A 40 μm wide scratch was made on the **SS1** film surface with a razor blade, and the images before and after UV irradiation at 254 nm are shown in Fig. 3.11 a and 3.11 c, respectively. As shown in the Dektak profiles (Fig. 3.11 b and 3.11 d), irradiation with 254 nm UV light at room temperature led to the complete healing of scratches. The results of the thermal measurement described in Section 2.2 confirm that the photoresponsivity of the four-arm polymer adjusted its T_g below room temperature by cleaving the monomer end-junctions into oligomers and monomers after 254 nm UV irradiation. Thus, the light-induced fluidization of the **SS1** film is related to the induction of macroscopic molecular flow and the migration of molecular chains by 254 nm UV irradiation, ultimately leading to scratch repair.
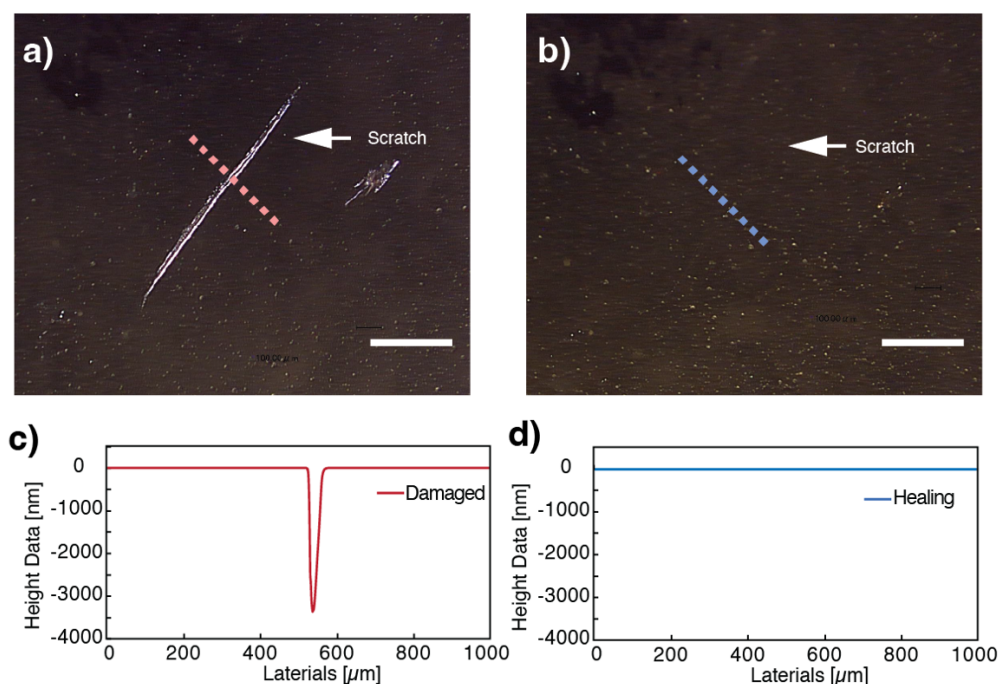
Figure 3.11 Characterization of the self-healing and DoD adhesion properties of **SS1** films. Optical microscopy images of a) scratch on the surface (scale bar: 300 μm), and b) healing on the surface after 254 nm irradiation (scale bar: 300 μm). Dektak profiles of **SS1** film c) before healing, and d) after healing.

However, there are several limitations in terms of constant self-repair. In terms of repairing surface damage, it is extremely challenging to control the depth of damage caused by cutting, and repair of damage that is excessively deep has not been confirmed, hence reproducibility is not always guaranteed.

3.3.6 Light-controlled reversible adhesion

As mentioned in the previous section, for the self-healing property, the stiffness of the **SS1** films was controlled by the degree of crosslinking with 365 and 254 nm UV irradiation. Therefore, considering the potential of **SS1** films as DoD adhesives, the effects of this reversible photo responsive property at room temperature on adhesiveness were investigated. The quartz glass substrates were bonded together by irradiating them with 365 nm UV light and applying a weight of 1 kg (two 500 mL plastic bottles filled with water was suspended at the end of the quartz glass) (Fig3.12); the weight remained suspended for more than 30 min. The glass was then irradiated with 254 nm light and again suspended with a weight; the bonded quartz glass peeled off owing to the weight. In addition, lap-shear tests were performed to quantitatively evaluate adhesive strength behavior. A 10 wt.% **SS1** solution dissolved in THF was prepared for spin-coating, and the reversible light-controlled adhesive strength of the resultant films was evaluated by uniaxial shear tests and stress–strain measurements by a five-step procedure (Fig. 3.12). The monomer solution (10 µL) was cast onto a single glass slide (quartz) with an area of 250 mm2 divided with masking tape (Step 1) and spin-coated at 5000 rpm (Step 2). Another glass plate was then placed on the cast area of the **SS1** monomer and pressure was applied to the contact area (Step 3). Subsequently, 365 nm UV light was irradiated for 5, 10, 15, and 30 min (Step 4), and the shear strength was measured (Step 5).
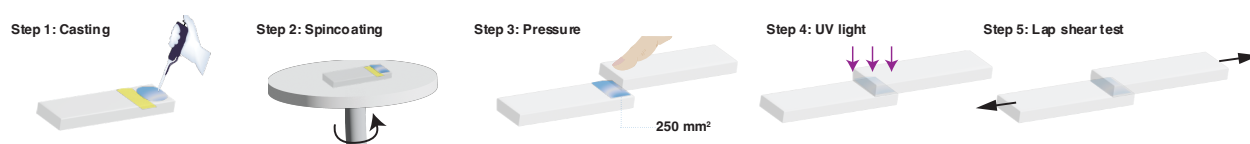
Figure 3.12 Schematic diagram of shear tensile test preparation. This figure is a revised version from Figure 3a of M. Inada *et al.*, 2023. ※

As shown in Fig. 3g, the shear adhesion strength increased with increasing 365 nm light irradiation and a strength of 1.0–1.7 MPa was achieved after the 15 min irradiation. The molecular mechanism of light-driven adhesives can be broadly categorized into three main categories: photoisomerization, photocyclization, and photolysis. Studies have shown that photoisomerization and photocyclization reactions exhibit a distinct distribution pattern, particularly when compared to other parameters such as adhesive strength and switching time. In our study, we employed the use of a coumarin adhesive and found that it displayed adhesive

strength comparable to that of photocyclization reactions. Notably, the adhesion forces of the samples after irradiation for more than 30 min appeared too strong to be measured without substrate failure; glass breaking occurred at an average force of ~1.7 MPa, which is lower than the shear adhesion force of the samples. Moreover, surface observations of the samples after the lap-shear test revealed that the adhesives remained on both substrates (adherends) in all cases, confirming that the mode of failure was cohesive (Fig. 3.13).
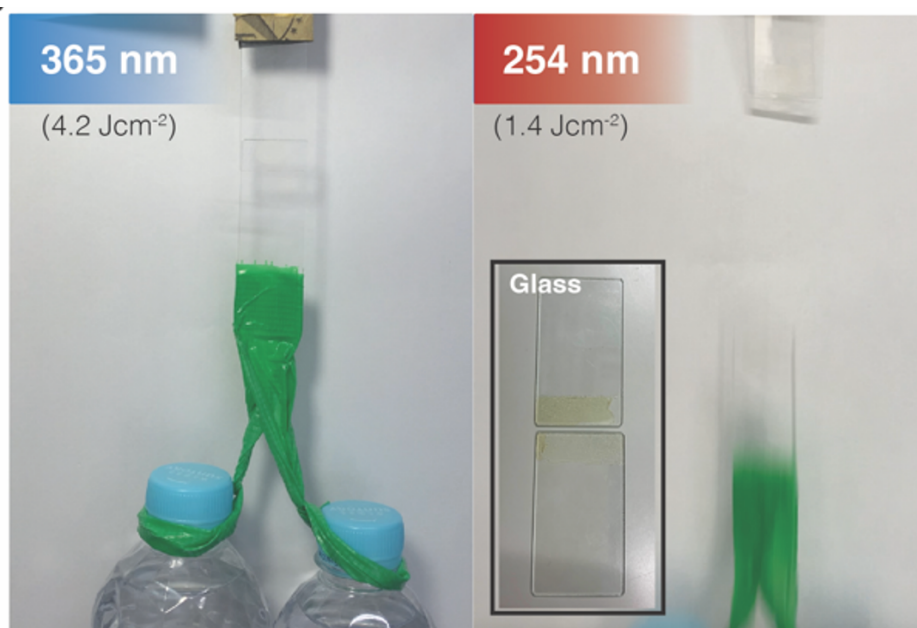
Figure 3.13 Photo of photoinduced DoD adhesives and the surface of the glass after a shear tensile test. (Left)365 nm irradiation for 15 min (4.2 Jcm^{-2}), (Right) 254 nm irradiation for 5 min (1.4 Jcm^{-2}). This figure is a reprinted version from Figure 3b of M. Inada *et al.*, 2023. [※]
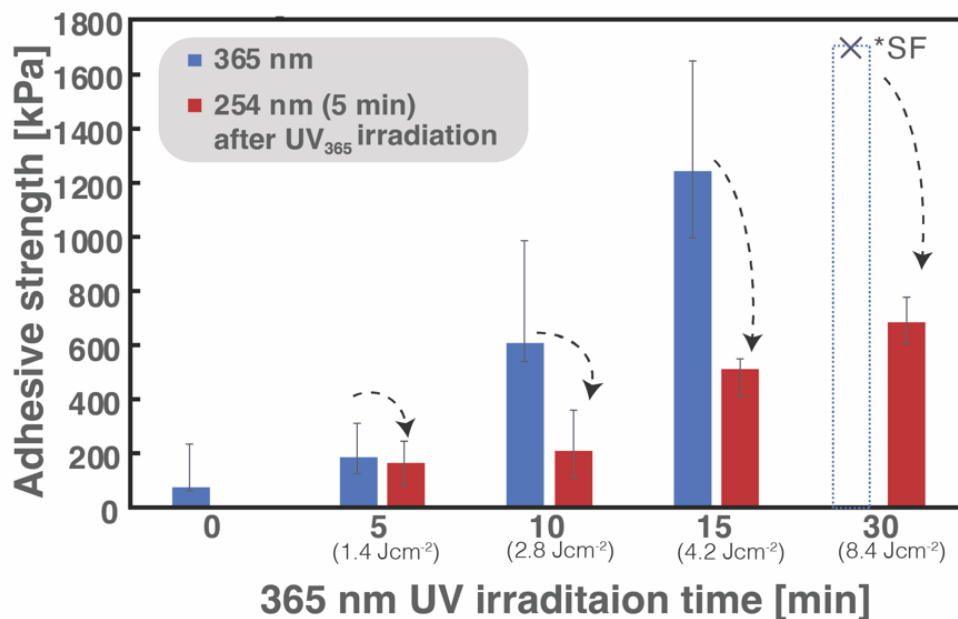
Figure 3.14 Average adhesion strengths of shear stress test upon prolonged UV exposure (>360 nm); the cross mark in the graph denotes the average of the glass breaking (substrate failure strength (see text). This figure is a reprinted version from Figure 3c of M. Inada *et al.*, 2023. ※

For each sample irradiated at 365 nm for a specific period, subsequent 254 nm UV irradiation for 5 min decreased the bond strength by ~33% (Fig. 3.14). Notably, the samples after 30 min irradiation at 365 nm, of which the adhesive strength was unmeasurable owing to substrate failure, exhibited an adhesiveness as high as ~0.7 MPa, even after subsequent irradiation for 5 min at 254 nm. The decrease in adhesiveness is related to the change in T_g associated with the crosslinked density, and to the change in the stiffness of the film. The decrease in adhesiveness is related to the change in T_g, and thus, to the change in the stiffness of the film. In addition, Fig. 3.15 shows the frequency dependence of the dynamic modulus (G': storage modulus, G": loss modulus) in the nonirradiated and UV-irradiated samples at 365 and 254 nm. In the nonirradiated state, G' was significantly lower than G", suggesting that the monomer was in a liquid state. Subsequently, following crosslinking by photoirradiation, the corresponding values of G' and G" were reversed, implying that the stiffness increased. After further irradiation at 254 nm, G' was higher than G" in the low-frequency region; however, after 30 Pa, G' was lower than G" in the high-frequency region. This rheological behavior indicates that the adhesive strength is not only owing to microscopic intermolecular bonding, but also to light-induced changes in the macroscopic stiffness of the overall material.
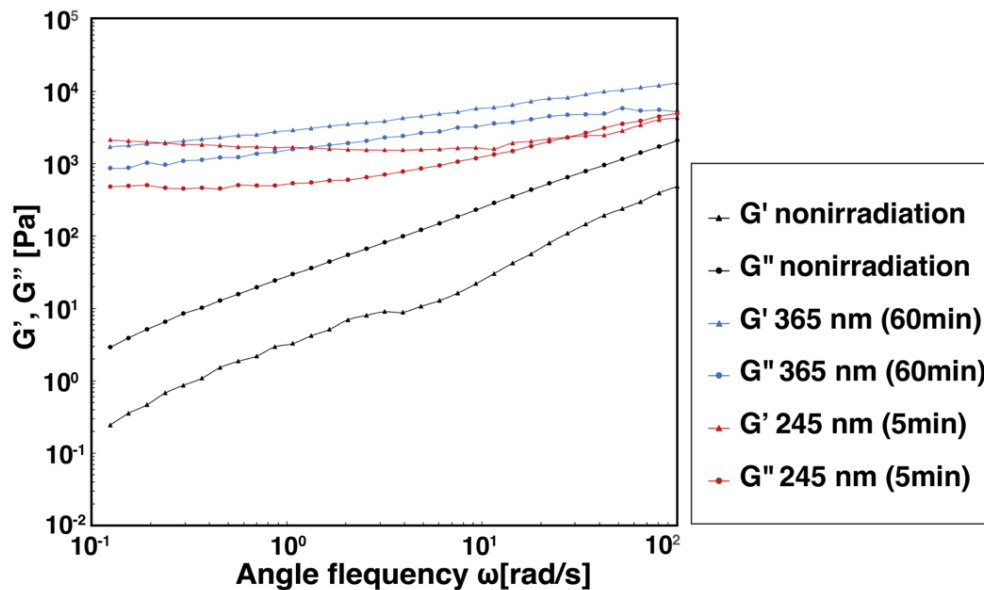
Figure 3.15 The rheological properties of **SS1** before irradiation, 365nm irradiation for 60 min, and 254 nm irradiation for 5 min depending on frequency. *G'*: storage modulus, *G''*: loss modulus. This Figure is a reprinted version from Figure S5 of M. Inada *et al.*, 2023. ※

Furthermore, a series of lap-shear tests were performed by returning the two separated glass slides to an originally bonded state and alternately switching the irradiation wavelength between 365 and 254 nm; this is done by repeating Steps 3–5 in Fig. 3.16 by alternately switching the two wavelengths for UV irradiation. Representative results are shown in Fig. 3h. The adhesive strength of the **SS1** film, determined to be ~1.1 and 0.2 MPa for the initial crosslinked and subsequent decrosslinked states, respectively, recovered to ~0.8 MPa by recrosslinking (after the second 365 nm irradiation). Thus, the reworkability of the **SS1** film as a detachable adhesive was successfully demonstrated. The recovery of adhesiveness from ~0.1 MPa at the second decrosslinked state to ~0.3 MPa by the third crosslinking indicates that the bond strength can be cyclically controlled, even though the bond strength gradually decreased. As indicated by the UV-vis spectroscopy and solubility results, photodimerization and photocleavage transitions, including loop monomers which were produced by intramolecular [2+2] cycloaddition reactions, were observed in only 70% of cases. This resulted in a cumulative decline in strength with repeated test cycles. However, these UV-vis spectroscopy results suggest the reactivity of the coumarin motif, and other motif defects may also lead to reduced adhesion. For instance, it is plausible that the cyclic siloxane backbone may undergo degradation The chemical composition of adhesives should be analyzed after repeated testing to identify any potential issues. This repeated reduction and recovery of adhesiveness is suggestive of the promising potential of photo-reversible cycloaddition systems, such as **SS1** in this study, for DoD adhesives.
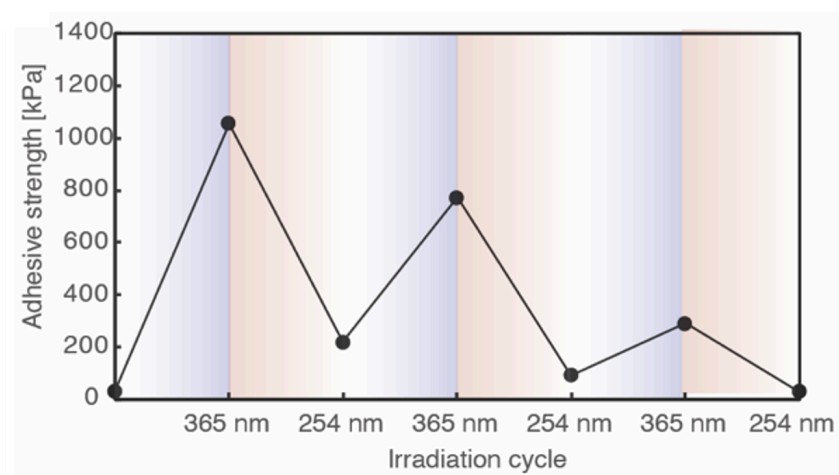
Figure 3.16 Shear adhesion of **SS1** reversibly crosslinked by repeated photocrosslinking. The **SS1** adhesives were irradiated by 365 nm UV light for 15 min and 254 nm for 5 min. This figure is a reprinted version from Figure 3d of M. Inada *et al.*, 2023. ※
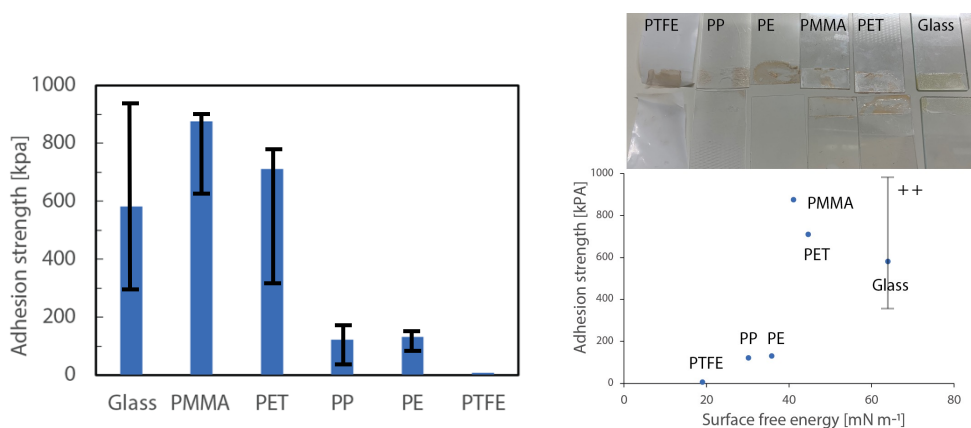
Figure 3.17 Adhesive strength for different substrates.

Different substrates transmitting 365 nm light were prepared, and their respective adhesion levels were measured. Figure 3.17 shows **SS1** adhered firmly to various substrates, such as glass, polymethyl methacrylate (PMMA), and Polyethylene Terephthalate (PET). Conversely, the results suggest that polymers such as polypropylene (PP), polyethylene (PE), and polytetrafluoroethylene (PTFE) have low adhesive strength. The adhesive strength was indicated by the surface free energy of the substrate, and the adhesive strength increased as the surface free energy increased. In a glass, the large number of hydroxyl groups provides interaction sites for hydrogen bonding with O sites in the adhesive. Only weak cross-linking interactions and interactions at the interface are suggested for other substrates. Also, as shown

in the top photo, the exfoliated interface of the low surface energy polymer is detached from the adherend interface. However, the exfoliated interface of the high surface energy polymer is detached from the adherend interface. Accordingly, the adhesive strength is highly dependent on the surface free energy of the base material. The interface with low surface energy and the adhesive peeled away from the interface where the adhesive adhered, resulting in a final freestanding film. On the other hand, for glass, PET, and PMMA adherends, adhesive failure was brought about by the cohesive mode or a combination of these two failure modes, as the adhesive remained thinly adhered to both adherends (Fig.3.18).
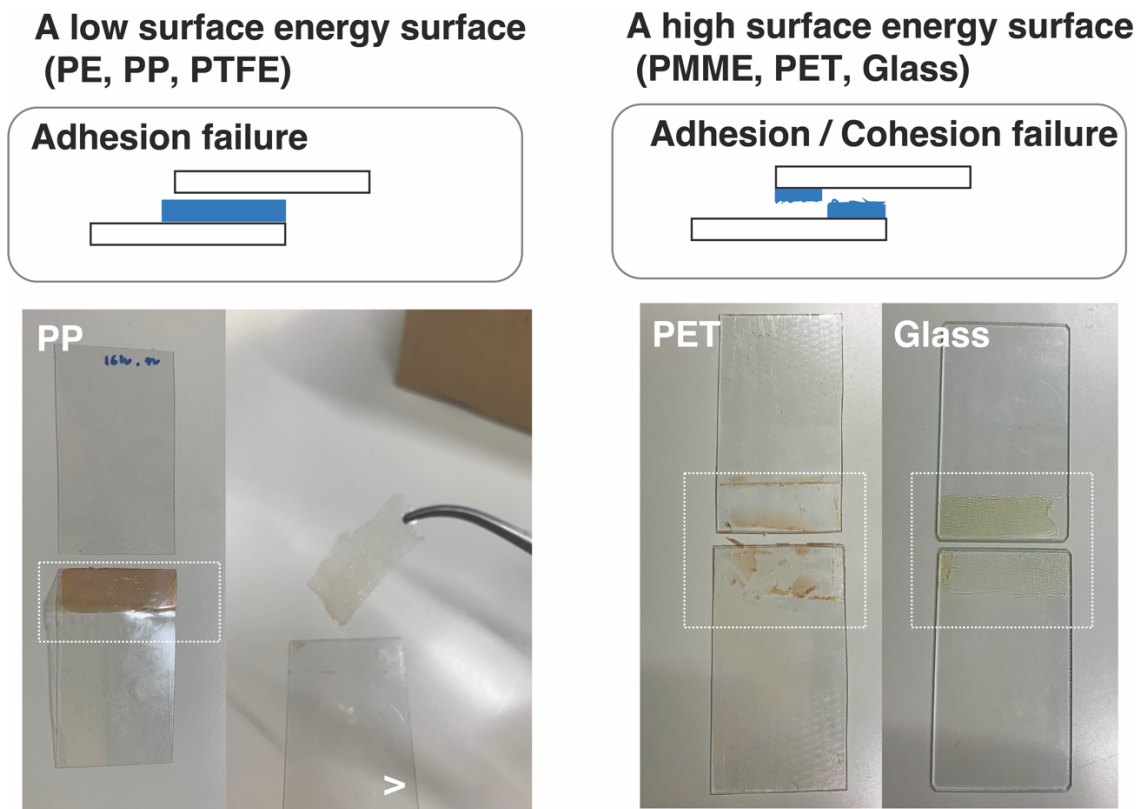
Figure 3.18 The picture of failures after the lap-shear test.

3.3.7 Studying dynamic processes and modeling of the photoproducts

To understand the dynamic behavior of **SS1** monomer and photoproduct, NMR relaxation time measurement and Density functional theory (DFT) calculation were conducted.

NMR relaxation time measurement

To discuss the fluidity of the side chains in the bulk state, pulsed NMR was measured, and the time taken from the excited state to the ground state was measured as T1 (longitudinal relaxation time, spin-lattice relaxation time) and T2 (transverse relaxation time, spin-spin relaxation time). NMR measurements using a T2 filter can be performed to signal can be reduced and the signal from components with longer relaxation times can be enhanced. These results are related to molecular mobility. Thus, as Figure 3.19 shows, in solution, the terminal Coumarin molecule is highly mobile and the molecules near the cyclic siloxane have low molecular mobility.
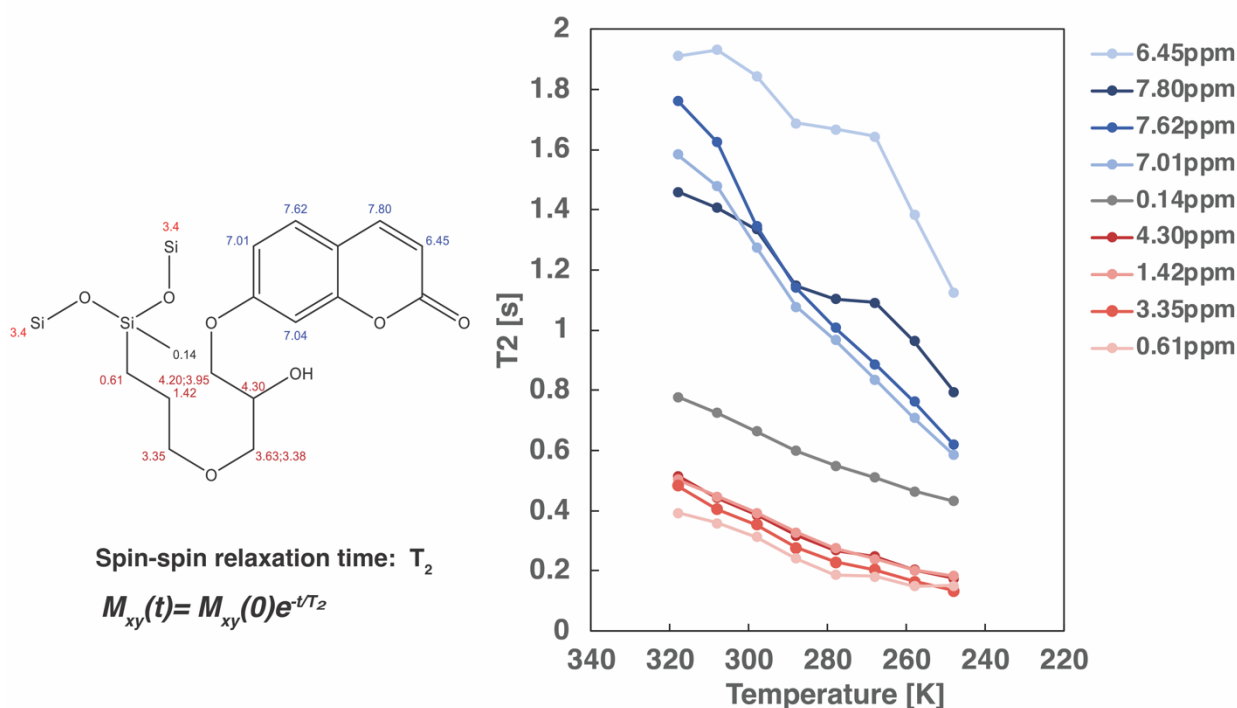
Figure 3.19 Temperature dependence of T2.

Density functional theory (DFT) calculation

To understand the behavior of photo [2+2] polymerization, it is necessary to clarify the optimal structure of the photo-polymerized state, which may provide a guideline for future molecular design.

Calculation of the most stable structure and energy level of the modeled molecule based on theoretical calculations: As mentioned above, there are isomers of coumarin photodimer, and differences in the distance between molecules may lead to dimerization in two ways: intermolecular/intramolecular reactions.[58] Therefore, the most stable structures and energy levels of the four possible isomers were calculated. The energy diagrams were calculated by DFT at the wB97XD/6-31G(d,p) level using the Gaussian program. The energies of the optimized structures were calculated in vacuum.

1. intramolecular [2+2] cycloaddition reactions
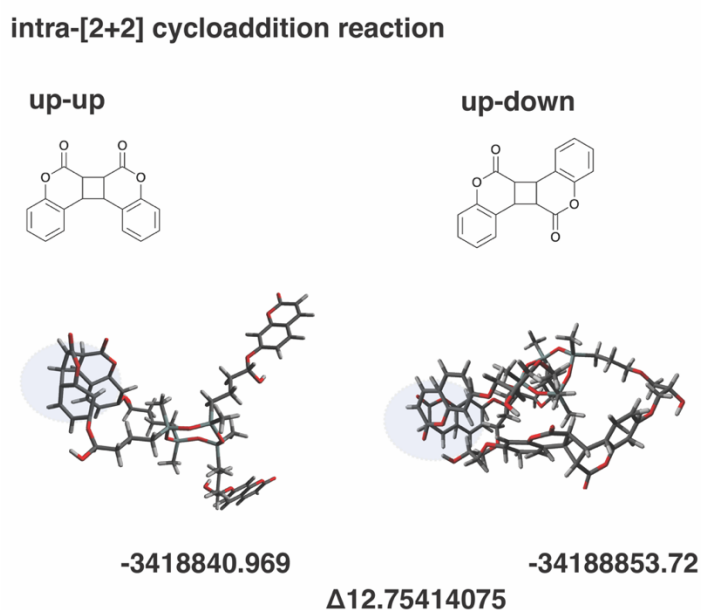
Figure 3.20 Most stable structures and energy levels in intramolecular [2+2] cycloaddition reactions of **SS1**.

Table 3.2 Summary of energy levels in intramolecular [2+2] cycloaddition reactions of **SS1**.

KCAL/MOL		E	zero correct E	Gibbs correct E
	up-up	-3419632.24	-3418751.362	-3418840.969
	up-down	-3419652.2	-3418769.75	-3418853.723
DELTA KCAL/MOL		19.95983808	18.3879255	12.75414075

2. intermolecular [2+2] cycloaddition reaction
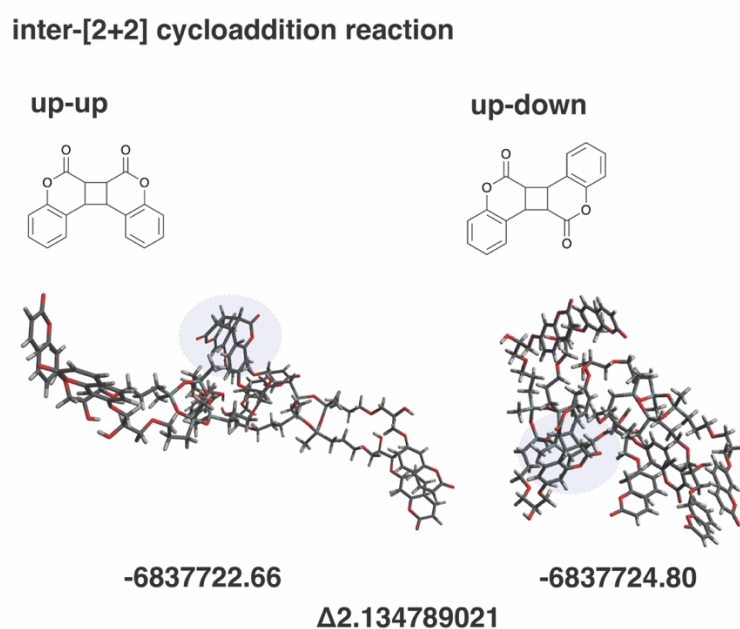
Figure 3.21 Most stable structures and energy levels in intermolecular [2+2] cycloaddition reactions of **SS1**.

Table 3.3 Summary of energy levels in intermolecular [2+2] cycloaddition reactions of **SS1**.

		E	zero correct E	Gibbs correct E
	up-up	-6839329.063	-6837564.598	-6837722.66
	up-down	-6839345.526	-6837579.115	-6837724.795
DELTA KCAL/MOL		16.46209734	14.51744385	2.134789021

Figures 3.21 and 3.22 show the most stable structures and energy levels in intra- and inter-molecular [2+2] cycloaddition reactions of **SS1**, respectively. This result indicates that the up-down conformation is the preferred stable conformation for the [2+2]-addition isomer in both inter- and intramolecular photoreactions. This supports the hypothesis that arm length plays a role in promoting intramolecular [2+2]-cycloaddition reactions. However, this approach also has the disadvantage of compromising the inherent fluidity of the monomer when the side chains of the molecule are shortened. Therefore, further research is required to fully understand the correlation between arm length and the propensity for intramolecular [2+2]-cycloaddition reactions. It is worth noting that these calculations were performed under vacuum conditions and do not consider bulk conditions, which may affect the comparability with experimental results.

3.4 Conclusion

This study proposed the utilization of photo-reversible cycloaddition reactions to DoD adhesives and demonstrated its potential using a newly synthesized coumarin-functionalized four-arm cyclosiloxane monomer (**SS1**). This simple **SS1** system exhibited photoinduced reversible crosslinking and decrosslinking with irradiation at 365 and 254 nm under ambient conditions, and the resultant two states exhibited T_g values higher and lower than the room temperature, respectively. In addition, the **SS1** films exhibited alternating increases and decreases in adhesiveness with changes in crosslink density upon light irradiation at two different wavelengths. The results enable the feasible application of simple siloxane-based reversible cycloaddition systems, represented by **SS1**, as sustainable DoD adhesives in industrial processes.
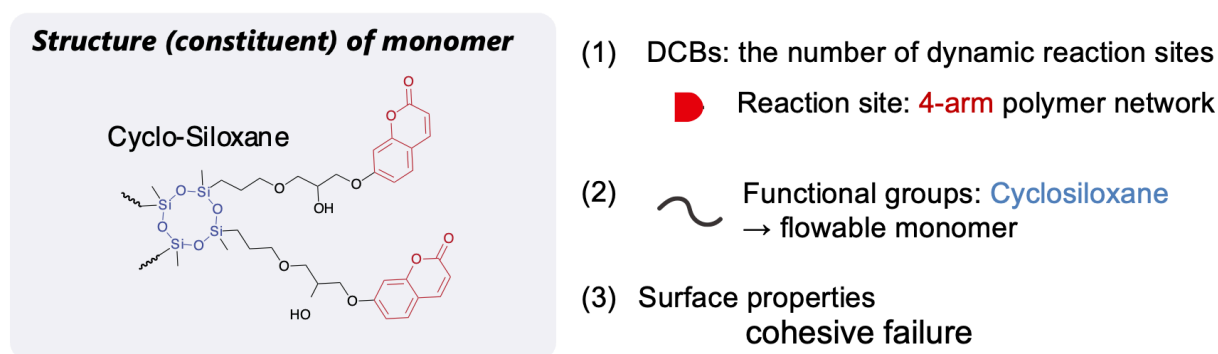
Figure 3.22 Monomer design for the formation of crosslinked polymer structures.

Molecule design

A four-arm monomer was incorporated as a monomer design to produce a dynamic crosslinked polymer (Figure 3.22).

(1) DCB sites
For intermolecular [2+2] photocycloaddition reactions to occur in the bulk state, it is necessary to kinetically increase the number of contacts between molecules. Therefore, this study aimed to design a reaction system with a highly branched monomer and relatively high contact establishment at the reaction site. As expected, **SS1** showed differences in dynamic properties induced by light

(2) Functional groups
Cyclicsiloxane was used as the central backbone to achieve a flowable structure in the monomer state. Further viscosity adjustments may be possible by increasing the length of the side chains and the molecular weight of Si. However, low-molecular-weight cyclic siloxanes cannot be readily degraded, raising concerns about them as novel environmental pollutants. [195] Therefore, functional cyclic siloxanes with recyclability, which can be used repeatedly without

being disposed of into the environment, have a great advantage from an environmental standpoint.

(3) Surface properties
According to tensile tests, the adhesive strength can be controlled by light intensity, and photocrosslinking can be accelerated by light exposure time. Further, it showed that insufficient cohesion within the adhesive results in adhesion failure, whereas excessive photocrosslinking results in substrate failure. These results suggest that **SS1** is a functional adhesive that 1) contributes to chemical bonding through the interaction between the adhesive and the substrate and 2) controls the degree of bonding through dynamic photo-crosslinking.

Polymer properties

The dynamically crosslinked polymers obtained by photopolymerization showed polymer-like properties. For understanding the properties of polymers, especially crosslinked polymers, the topology of the polymer network should be considered. In this study, these polymer properties were demonstrated by thermal analysis and rheological measurements. DSC measurements showed that the T_g increased above room temperature after light irradiation, and the high and low T_g indicate how difficult it is for segments to move. The glass transition temperature above room temperature indicates that the crosslinked polymer was rigid, which means that the segments were hard to move. A rheology measurement is an analytical method to determine the behavior of polymers and other complex systems under simplified deformation. This study investigated the viscoelastic properties of polymers by measuring the frequency dependence of the rheological behavior. Light-induced alterations in rheological behavior were observed, indicating that light stimulation was also involved in the macroscopic stiffness of the overall material.

Chapter 4

General conclusions and future and industrial perspectives

4.1 General conclusions
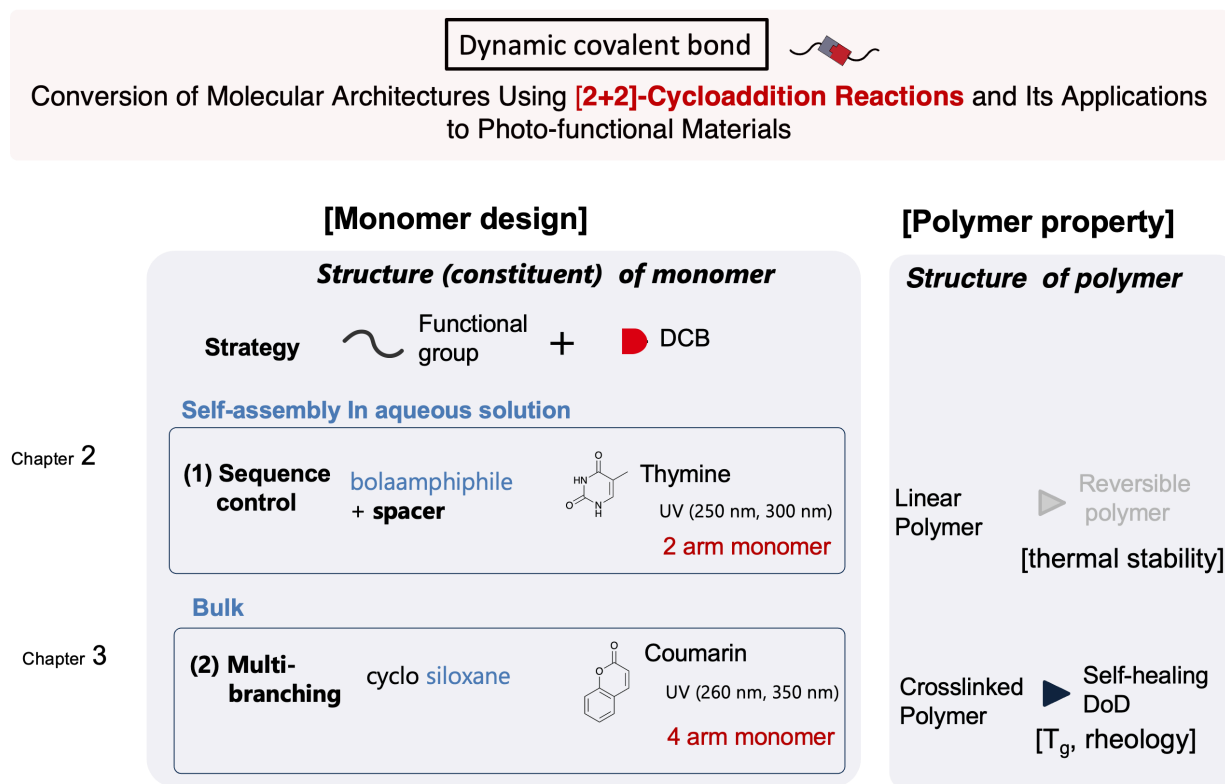
Figure 4.1 Summary of conclusion.

The results of this study are shown in Figure 4.1. In the design of monomers constituting polymers using dynamic covalent bonding, the arrangement of the binding sites in the reaction field and their chemical structures are important and contribute directly to the polymer structure. In particular, the precise molecular design of monomers leads to the control of intra-/inter-molecular reactivity through [2+2] cycloaddition reactions, which is shown to be an important factor in the design of materials.

The following were shown to be essential for obtaining the intended dynamic covalent polymeric structures by [2+2]-cycloaddition reactions.

(1) Monomer design
The monomer structural framework design and the arrangement of photoreaction sites should adhere to a strategy for efficient reaction progression.

Strategy (reaction fields**)**: [2+2] polymerizations were attempted in different reaction fields. In Chapter 2, for creating a linear polymer structure, the focus was on molecular arrangement. [2+2] cycloaddition reactions were carried out within a flexible self-assembled structure, considering the development of applications in various fields, rather than within a crystal structure confined to the packed state as previously reported. In Chapter 3, to produce

dynamically crosslinked polymers, hyperbranched monomers were synthesized to facilitate the formation of networks. Hyperbranched monomers with intrinsically branched points have the advantages of 1) simple (one-step) reaction steps and 2) easy to keep the heterogeneity of the network. [99] Moreover, the design of the main backbone has enabled successful photopolymerization in a solvent-free state, where the monomer state is a liquid state.

Functional group: In Chapter 2, the molecules were synthesized with a polyethylene glycol (PEG) introduced at the terminal end for the formation of self-assembly. A spacer was used between the photoreactive groups to control the intramolecular/intermolecular [2+2] cycloaddition reactions. Moreover, the use of aromatic rings as the spacer, added functionality (p-p stacking) and enabled desirable self-assembly. In Chapter 3, siloxane was used as the central framework for molecular design, and a solvent-free photoreaction was successfully performed.

DCBs: In Chapter 2, thymine was selected for its relatively high photo-reversibility. In Chapter 3, the DCB molecule was changed to coumarin to further advance its application. In Chapter 2, thymine was selected as the dynamic covalent bonding site, and coumarin was selected for its reaction at higher wavelengths closer to sunlight and for a shorter reaction time. The number of ends bounding DCBs was varied depending on the application. Linear polymers have two bonding points for chain linkage, and crosslinked polymers have four bonding points to intrinsically provide a branching point.

(2) Polymer properties

In Chapter 2, the results are insufficient to show that a high molecular weight was formed since only up to a pentamer was observed upon photoirradiation. Thus, the specific properties of the polymer could not be confirmed. However, the self-assemblies that created continuous covalent structures were found to be thermally stable. This suggests that the physical properties of the self-assembly were transformed by light stimulus. This result may contribute to future research on supramolecules, since the self-assembly (supramolecule), which is easily destroyed by heat, was transformed into a rigid structure by an external stimulus. In Chapter 3, thermal analysis and rheological measurements confirmed that the photoresponsive dynamic crosslinked polymers have polymeric properties. These dynamic photocrosslinked polymers can be applied as self-healing and national defense materials due to their different physical properties by light stimulation.

4.2 Future perspectives

Based on these results, further development of this study is discussed. For designing monomers to obtain the intended dynamic covalent polymers, a design scheme was proposed as shown in Figure 4.2.

Design Scheme

Structure (constituent) of monomer | *Structure of polymer*

primary structure | photoreaction site (DCB) | +(other) functional moieties | ▶ for additional/future functionalization

Primary structure ✓ Increase the wide range of polymers introduced into the main chain

Photoreaction site (DCB) ✓ Blue-shift the reaction wavelength →high applicability

+

(Other) functional moieties ✓ Dual functional materials

for additional/future functionalization

Figure 4.2 Summary of future perspectives.

Monomer design is critical for the development of smart polymers and environmentally sustainable materials in the future.
Future challenges include:
(1) Further investigation of versatile monomer design,
(2) Bottlenecks to the practical application due to photoreaction by UV control
(3) Additional Features

A roadmap for the further development of sustainable materials in the future is described below.

(1) Primary structure

The first step is to broaden the range of polymers to be introduced into the main chain that forms the backbone of the dynamic covalent polymer. The introduction of versatile polymers into this main chain backbone, including the siloxane backbone, can be used in industrial processes, where it is practical and can be recycled more efficiently. Nakagawa and Yoshie have listed the polymer main skeletons used in the star polymer network (Figure 4.3).
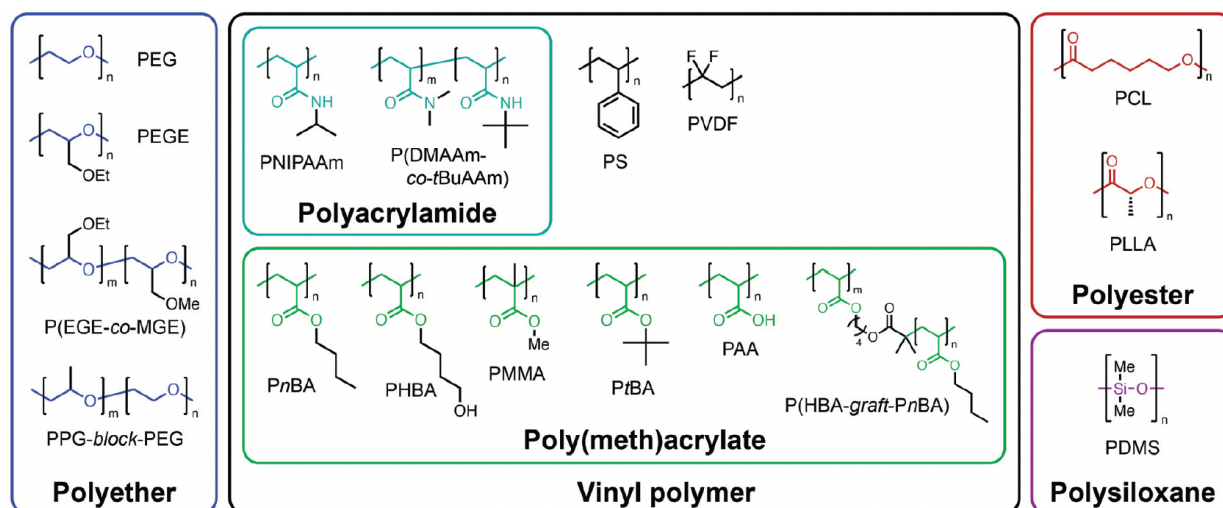
Figure 4.3 Summary diagram of the main chain structures used in the star polymer network reprinted in part from ref 99, with permission from Royal Society of Chemistry [99]

(2) Photoreaction sites

Regarding [2+2] cycloaddition reactions, redshifted photocycloadditions can be studied for applications requiring low wavelengths, which is expected to lead to a high degree of applicability. Previously, photocycloaddition reactions have required UV light to induce bond/cleavage. The use of photo-light above 400 nm, which is biologically acceptable, has been desirable considering the application.[196] In recent years, two different approaches have attempted to account for the redshifted photocycloadditions. The first is the red-shift strategy by extended conjugation. [196, 197] The second is the pioneering of synthetic reactions using visible light photocatalytic redox catalysis, which can be excited by long-wavelength light. [198, 199] However, dynamic behavior induced by visible light has the disadvantage that the sample cannot be precisely controlled under the sun. Therefore, a strategy to broaden the wavelength of switching may help to create materials that are stable under visible light without overlapping wavelength ranges in response to switching.

(3) Dual-functional materials

Finally, the development of bifunctional materials that respond to different stimuli can be expected to give rise to smart polymers with additional functions in the future. In this study, functional materials have been developed using light-based stimuli. In the future, it will be possible to combine further functional molecules with monomers to develop highly functional

smart polymers that create more complex behavior. The combination of two or more different crosslinking ingredients in one system is defined as a dual dynamic network (DDN). [200] As a pioneering study, dual dynamic network polymers are being investigated. [201-205] DDNs allow the design of materials with tailored thermal, rheological, and mechanical properties compared to single crosslinked materials. Compared to single crosslinking, these DDN polymers pose a more difficult challenge in terms of how to control individual responses to different dynamic behaviors and how to quantitatively characterize them.[162] The combination of dynamic behavior, including the above issues, is one of the key points for the future.

In building a sustainable resource-recycling process, these materials should be upcycled as raw materials or similar monomers when they are reintroduced for recycling. Furthermore, in upcycling, the generation of raw material is also important, but methods for further separation of this material should also be considered. Further material development may be possible by developing the above attempts to broaden the scope of our research.

4.3 Industrial Perspectives

A strategy incorporating elements of resource recycling at the material design stage would significantly contribute to "separation, refining, and recycling that reduces the generation of greenhouse gases, CO_2, and other pollutants, thereby reducing environmental impact."

(1) Light-driven dynamic covalent bonding

Photochemical reactions are promising as environmentally adaptive materials since green synthetic pathways are available under ambient temperatures and pressure, and the properties of materials could be efficiently controlled by adjusting light parameters (wavelength, intensity, and irradiation time). The coumarin used in this process is suitable for use with visible light, including sunlight, as it has irradiation conditions near the visible light spectrum. By designing functional polymer materials that utilize non-depleting energy sources such as sunlight, it is possible to move towards creating a more resource-recycling society. The reverse reaction can be initiated at a wavelength as low as 254 nm, which is only a small fraction of natural light, making it easier to control.

(2) Materials function

External stimuli materials can be controlled by applying stimuli to the completed product and can approach areas that are artificially difficult to control. Such materials are expected to be deployed in a wide range of fields, such as aerospace, electronic skin, energy, and bionics, as these materials are highly versatile. Dynamic covalent polymers can be organized by external stimuli after polymerization and are expected to be applied as shape memory polymers, self-healing materials, and de-attachable adhesives. In this study, reversible linear polymers with the possibility of chemical recycling and crosslinked polymers for the creation of externally responsive materials were implemented.

(3) Reversibility

In Chapters 2 and 3, UV spectroscopy demonstrated the reversibility of the [2+2] cycloaddition reaction at the molecular level. However, to design sustainable materials following the principles of a circular economy, it is necessary to examine the overall process of separation and recovery of these chemicals, with a focus on minimizing waste production. In collecting raw materials, it is considered that degrading polymers to their original monomers is the most effective process. Therefore, it is necessary to develop a methodology for separating and recovering by-products from [2+2] cycloaddition reactions to proceed with these reactions efficiently.

(4) Application

SS1 crosslinked polymers are expected to be applied as a photoresponsivity adhesive material because of the different viscosities of the monomer and polymer. These adhesives can be cured with light irradiation, and their bonds can be broken by changing the wavelength, allowing for easy disassembly and potential reuse. In the semiconductor industry, it is suggested that synthetic polymers can be applied to photomasks and component adhesion within the semiconductor sputtering process. Although the adhesive efficacy of polymers has been ensured within the process, there are issues, such as the compatibility between the adhesive and the substrate, the adhesive application method, and the need to improve the reversibility as a de-adhesive material further.

The material is expected to develop as ink for 3D printers to facilitate the development of material applications. The development of 4D-printing technology, which external stimuli can alter after printing, is in the limelight and is expected to be a sustainable material for mass production, taking advantage of the flexibility of the polymeric materials design in this study. As described above, the molecular-level approach, which introduces photodynamic covalent bonds and a strategy to incorporate elements of resource recycling at the material design stage, effectively converts the linear manufacturing flow into a circular cycle.

In manufacturing, the development of a photomask that can be repeatedly bonded and peeled off can significantly improve efficiency and versatility in the production process. There are four key elements to be considered to realize this goal. The first is precise control of the adhesive's viscosity, which can be achieved by modifying the molecular structure of monomers based on the results shown in this dissertation and adjusting the concentration of monomers in the solution. The second is a practical method satisfying the requirement for thin-film bonding in photo-curable polymers. Hence, techniques like spin-coating of thin films and droplet conditioning for casting should be utilized to guarantee proper application. The third is a flexible and adaptable system for shaping, particularly in the semiconductor industry that requires handling of photomasks with micrometer-level precision. The fourth is the design of adhesives to be peeled off from the substrate. Achieving successful exfoliation is essential to modify the interfacial interaction between the substrate and adhesive for separation. In the future, the focus of controlling should shift from the internal structure of adhesives to the features of the substrate and interface. This strategy can be achieved by modifying the surface of the polymer/substrate using monomers containing dynamic covalent bonds. Additionally, functional groups must be introduced using dynamic covalent bonding with two compatible

functionalities to ensure adhesion properties. This approach will enable precise control of the exfoliation properties of the polymer/substrate while ensuring adequate adhesion.

Acknowledgments

First, I would like to express my deepest gratitude to my principal supervisor, Prof. Toru Asahi, for his kind guidance and encouragement. He not only supported my research but also gave me many experiences in my personal life and off-campus events. I would also like to express my deepest gratitude to Prof. Kei Saito of Kyoto University, who supervised me as a collaborator, for his guidance and encouragement. I would also like to thank the members of Saito Laboratory for warmly accepting me to Australia abroad program at Monash University. Without their support, I would not have been able to make progress in my study abroad and subsequent research. I am also very grateful to Dr. Akihiro Udagawa, a graduate from Waseda University, for his research guidance and insightful advice.

I am also deeply grateful to Prof. Sota Sato at the University of Tokyo, Prof. Toshinori Fujie, and Dr. Tatsuhiro Horii of the Tokyo Institute of Technology, for their valuable advice and discussions throughout the research period. I was involved in this project as a joint research project and were able to make significant progress in our research.

I am grateful to Prof. Kenichi Oyaizu of Waseda University, Prof. Kenji Miyatake of the University of Yamanashi, Dr. Hidehito Obayashi of Hitachi High-Tec Corporation and Nissan Chemical Industries, Ltd, and Prof. Takuya Nakanishi of Waseda University for their insightful discussions and opinions as referees.

I would also like to thank the members of the Asahi Laboratory and the secretary, Ms. Aiko Maeda, for their support and encouragement during my doctoral studies.

Finally, I would like to thank my parents and my partner for their support and understanding.

February 2023

Moeka Inada

References

1 S. J. Rowan, S. J. Cantrill, G. R. L. Cousins, J. K. M. Sanders and J. F. Stoddart, Dynamic Covalent Chemistry, *Angew. Chem. Int. Ed.,* 2002, **41**, 898-952 (DOI:10.1002/1521-3773(20020315)41:6).

2 P. T. Corbett, J. Leclaire, L. Vial, K. R. West, J. Wietor, J. K. M. Sanders and S. Otto, Dynamic Combinatorial Chemistry, *Chemical reviews,* 2006, **106**, 3652-3711 (DOI:10.1021/cr020452p).

3 T. Aida and E. W. Meijer, Supramolecular polymers – we've come full circle, *Israel journal of chemistry,* 2020, **60**, 33-47 (DOI:10.1002/ijch.201900165).

4 N. Zheng, Y. Xu, Q. Zhao and T. Xie, Dynamic Covalent Polymer Networks: A Molecular Platform for Designing Functions beyond Chemical Recycling and Self-Healing, *Chem. Rev.,* 2021, **121**, 1716–1745 (DOI:10.1021/acs.chemrev.0c00938).

5 N. Roy, B. Bruchmann and J. Lehn, DYNAMERS: dynamic polymers as self-healing materials, *Chem. Soc. Rev.,* 2015, **44**, 3786-3807 (DOI:10.1039/c5cs00194c).

6 M. Behl and A. Lendlein, Shape-memory polymers, *Materials Today,* 2007, **10**, 20 (DOI:10.1016/s1369-7021(07)70047-0).

7 X. Luo, Z. Wei, B. Seo, Q. Hu, X. Wang, J. A. Romo, M. Jain, M. Cakmak, B. W. Boudouris, K. Zhao, J. Mei, B. M. Savoie and L. Dou, Circularly Recyclable Polymers Featuring Topochemically Weakened Carbon–Carbon Bonds, *J. Am. Chem. Soc.,* 2022, **144**, 16588 (DOI:10.1021/jacs.2c06417).

8 Y. Jin, Q. Wang, P. Taynton and W. Zhang, Dynamic Covalent Chemistry Approaches Toward Macrocycles, Molecular Cages, and Polymers, *Accounts of chemical research,* 2014, **47**, 1575-1586 (DOI:10.1021/ar500037v).

9 T. Maeda, H. Otsuka and A. Takahara, Dynamic covalent polymers: Reorganizable polymers with dynamic covalent bonds, *Progress in polymer science,* 2009, **34**, 581-604 (DOI:10.1016/j.progpolymsci.2009.03.001).

10 大塚 英幸 and 青木 大輔, 動的共有結合を有する反応性ポリウレタン, *日本接着学会誌,* 2019, (DOI:10.11618/adhesion.55.168).

11 P. Chakma and D. Konkolewicz, Dynamic Covalent Bonds in Polymeric Materials, *Angewandte Chemie,* 2019, **131**, 9784-9797 (DOI:10.1002/ange.201813525).

12 S. Peng, Y. Sun, C. Ma, G. Duan, Z. Liu and C. Ma, Recent advances in dynamic covalent bond-based shape memory polymers, *e-Polymers,* 2022, **22**, 285 (DOI:10.1515/epoly-2022-0032).

13 K. Hawkins, A. K. Patterson, P. A. Clarke and D. K. Smith, Catalytic Gels for a Prebiotically Relevant Asymmetric Aldol Reaction in Water: From Organocatalyst Design to Hydrogel Discovery and Back Again, *J. Am. Chem. Soc.,* 2020, **142**, 4379-4389 (DOI:10.1021/jacs.9b13156).

14 W. J. Svirbely and J. F. Roth, Carbonyl Reactions. I. The Kinetics of Cyanohydrin Formation in Aqueous Solution,1953, **75**, 3106–3111 (DOI:10.1021/ja01109a020).

15 C. A. Smith, M. R. Narouz, P. A. Lummis, I. Singh, A. Nazemi, C. Li and C. M. Crudden, N-Heterocyclic Carbenes in Materials Chemistry, *Chem. Rev.,* 2019, **119**, 4986-5056 (DOI:10.1021/acs.chemrev.8b00514).

16 J. W. Kamplain and C. W. Bielawski, Dynamic covalent polymers based upon carbene dimerization, *Chemical communications,* 2006, **16**, 1727-1729 (DOI:10.1039/b518246h).

17 C. Giordano, M. Villa and R. Annunziata, Mild and Reversible Friedel-Crafts Acylation: Synthesis of 6-Acyl-2-methoxynaphthalenes, *Synthetic Communications,* 1990, **20**, 383-392 (DOI:10.1080/00397919008052779).

18 R. Cramer, Olefin Coordination Compounds of Rhodium: The Barrier to Rotation of Coordinated Ethylene and the Mechanism of Olefin Exchange, *Journal of the American Chemical Society,* 1964, **86**, 217-222 (DOI:10.1021/ja01056a022).

19 O. Diels and K. Alder, Synthesen in der hydroaromatischen Reihe, *Justus Liebigs Ann. Chem.,* 1928, **460**, 98-122 (DOI:10.1002/jlac.19284600106).

20 H. B. Kagan and O. Riant, Catalytic asymmetric Diels Alder reactions, *Chemical reviews,* 1992, **92**, 1007-1019 (DOI:10.1021/cr00013a013).

21 H. Frisch, D. E. Marschner, A. S. Goldmann and C. Barner-Kowollik, Wavelength-Gated Dynamic Covalent Chemistry, *Angewandte Chemie (International ed.),* 2018, **57**, 2036-2045 (DOI:10.1002/anie.201709991).

22 J. Singh, *Photochemistry and pericyclic reactions*, New Age International, 2005.

23 K. Acharyya and P. S. Mukherjee, Organic Imine Cages: Molecular Marriage and Applications, *Angewandte Chemie,* 2019, **131**, 8732-8745 (DOI:10.1002/ange.201900163).

24 H. Erguven, E. N. Keyzer and B. A. Arndtsen, A Versatile Approach to Dynamic Amide Bond Formation with Imine Nucleophiles, *Chemistry : a European journal,* 2020, **26**, 5709-5716 (DOI:10.1002/chem.202001140).

25 R. Brachvogel and M. von Delius, The Dynamic Covalent Chemistry of Esters, Acetals and Orthoesters, *European journal of organic chemistry,* 2016, **2016**, 3662-3670 (DOI:10.1002/ejoc.201600388).

26 N. Kihara and K. Kidoba, Dynamic Covalent Chemistry of the Nicholas Ether-Exchange Reaction, *Org. Lett.,* 2009, **11**, 1313-1316 (DOI:10.1021/ol900095d).

27 Á Beltrán, E. Álvarez, M. M. Díaz-Requejo and P. J. Pérez, Direct Synthesis of Hemiaminal Ethers via a Three-Component Reaction of Aldehydes, Amines and Alcohols, *Adv. Synth. Catal.,* 2015, **357**, 2821-2826 (DOI:10.1002/adsc.201500588).

28 H. OTSUKA, Reorganization of polymer structures based on dynamic covalent chemistry: polymer reactions by dynamic covalent exchanges of alkoxyamine units, *Polymer journal,* 2013, **45**, 879-891 (DOI:10.1038/pj.2013.17).

29 K. Vanherck, P. Vandezande, S. O. Aldea and I. F. J. Vankelecom, Cross-linked polyimide membranes for solvent resistant nanofiltration in aprotic solvents, *Journal of membrane science,* 2008, **320**, 468-476 (DOI:10.1016/j.memsci.2008.04.026).

30 C. Saiz, P. Wipf, E. Manta and G. Mahler, Reversible Thiazolidine Exchange: A New Reaction Suitable for Dynamic Combinatorial Chemistry, *Org. Lett.,* 2009, **11**, 3170-3173 (DOI:10.1021/ol901104a).

31 B. H. Northrop, S. H. Frayne and U. Choudhary, Thiol–maleimide "click" chemistry: evaluating the influence of solvent, initiator, and thiol on the reaction mechanism, kinetics, and selectivity, *Polymer chemistry,* 2015, **6**, 3415-3430 (DOI:10.1039/C5PY00168D).

32 S. Belbekhouche, M. Guerrouache and B. Carbonnier, Thiol–Maleimide Michael Addition Click Reaction: A New Route to Surface Modification of Porous Polymeric Monolith, *Macromol. Chem. Phys.,* 2016, **217**, 997-1006 (DOI:10.1002/macp.201500427).

33 T. Debsharma, V. Amfilochiou, A. A. Wróblewska, I. De Baere, W. Van Paepegem and F. E. Du Prez, Fast Dynamic Siloxane Exchange Mechanism for Reshapable Vitrimer Composites, *J. Am. Chem. Soc.,* 2022, **144**, 12280-12289 (DOI:10.1021/jacs.2c03518).

34 A. Canal-Martín and R. Pérez-Fernández, Biomimetic selenocystine based dynamic combinatorial chemistry for thiol-disulfide exchange, *Nature Communications,* 2021, **12**, 163 (DOI:10.1038/s41467-020-20415-6).

35 M. O. Saed and E. M. Terentjev, Siloxane crosslinks with dynamic bond exchange enable shape programming in liquid-crystalline elastomers, *Scientific Reports,* 2020, **10**, 6609 (DOI:10.1038/s41598-020-63508-4).

36 T. Debsharma, V. Amfilochiou, A. A. Wróblewska, I. De Baere, W. Van Paepegem and F. E. Du Prez, Fast Dynamic Siloxane Exchange Mechanism for Reshapable Vitrimer Composites, *J. Am. Chem. Soc.,* 2022, **144**, 12280-12289 (DOI:10.1021/jacs.2c03518).

37 F. Schaufelberger and O. Ramström, Kinetic Self-Sorting of Dynamic Covalent Catalysts with Systemic Feedback Regulation, *J. Am. Chem. Soc.,* 2016, **138**, 7836-7839 (DOI:10.1021/jacs.6b04250).

38 P. Chen, Designing Sequence Selectivity into a Ring-Opening Metathesis Polymerization Catalyst, *Acc. Chem. Res.,* 2016, **49**, 1052-1060 (DOI:10.1021/acs.accounts.6b00085).

39 A. Matsumoto and Y. Miyahara, 'Borono-lectin' based engineering as a versatile platform for biomedical applications, *Science and Technology of Advanced Materials,* 2018, **19**, 18-30 (DOI:10.1080/14686996.2017.1411143).

40 C. D. Meyer, C. S. Joiner and J. F. Stoddart, Template-directed synthesis employing reversible imine bond formation, *Chemical Society Reviews,* 2007, **36**, 175-1723 (DOI:10.1039/b513441m).

41 J. I. Seeman, Woodward–Hoffmann's Stereochemistry of Electrocyclic Reactions: From Day 1 to the JACS Receipt Date (May 5, 1964 to November 30, 1964), *J. Org. Chem.,* 2015, **80**, 11632-11671 (DOI:10.1021/acs.joc.5b01792).

42 K. Fukui, The path of chemical reactions - the IRC approach, *Acc. Chem. Res.,* 1981, **14**, 363-368 (DOI:10.1021/ar00072a001).

43 S. Chatani, C. J. Kloxin and C. N. Bowman, The power of light in polymer science: photochemical processes to manipulate polymer formation, structure, and properties, *Polym. Chem.,* 2014, **5**, 2187-2201 (DOI:10.1039/C3PY01334K).

44 F. D. Jochum and P. Theato, Temperature- and light-responsive smart polymer materials, *Chem. Soc. Rev.,* 2013, **42**, 7468-7483 (DOI:10.1039/C2CS35191A).

45 F. Ercole, T. P. Davis and R. A. Evans, Photo-responsive systems and biomaterials: photochromic polymers, light-triggered self-assembly, surface modification, fluorescence modulation and beyond, *Polym. Chem.,* 2010, **1**, 37-54 (DOI:10.1039/B9PY00300B).

46 Z. Zhang, K. G. Demir and G. X. Gu, Developments in 4D-printing: a review on current smart materials, technologies, and applications, *International Journal of Smart and Nano Materials,* 2019, **10**, 205-224 (DOI:10.1080/19475411.2019.1591541).

47 H. M. D. Bandara and S. C. Burdette, Photoisomerization in different classes of azobenzene, *Chem. Soc. Rev.,* 2012, **41**, 1809-1825 (DOI:10.1039/C1CS15179G).

48 G. Kaur, P. Johnston and K. Saito, Photo-reversible dimerisation reactions and their applications in polymeric systems, *Polymer chemistry,* 2014, **5**, 2171-2186 (DOI:10.1039/c3py01234d).

49 D. Frackowiak, The Jablonski diagram, *Journal of Photochemistry and Photobiology B: Biology,* 1988, **2**, 399 (DOI:10.1016/1011-1344(88)85060-7).

50 J. Fritzsche, Ueber die festen Kohlenwasserstoffe des Steinkohlentheers, *J. Prakt. Chem.,* 1867, **101**, 333-343 (DOI:10.1002/prac.18671010147).

51 C. N. Riiber, Das directe Ueberführen der Zimmtsäure in α-Truxillsäure, *Ber. Dtsch. Chem. Ges.,* 1902, **35**, 2908-2909 (DOI:10.1002/cber.19020350373).

52 G. Ciamician and P. Silber, Chemische Lichtwirkungen, *Ber. Dtsch. Chem. Ges.,* 1908, **41**, 1928-1935 (DOI:10.1002/cber.19080410272).

53 N. D. Heindel and M. A. Pfau, A profitable partnership: Giacomo Ciamician and Paul Silber, *J. Chem. Educ.,* 1965, **42**, 383 (DOI:10.1021/ed042p383).

54 F. R. de Gruijl, Skin cancer and solar UV radiation, *Eur. J. Cancer,* 1999, **35**, 2003-2009 (DOI:10.1016/S0959-8049(99)00283-X).

55 C. Barner-Kowollik and A. J. Inglis, Has Click Chemistry Lead to a Paradigm Shift in Polymer Material Design? *Macromolecular chemistry and physics,* 2009, **210**, 987-992 (DOI:10.1002/macp.200900139).

56 S. S. Labana, Photopolymerization, *Journal of Macromolecular Science, Part C,* 1974, **11**, 299-319 (DOI:10.1080/15583727408546026).

57 D. Bailey, N. Seifi and V. E. Williams, Steric effects on [4+4]-photocycloaddition reactions between complementary anthracene derivatives, *Dyes and pigments,* 2011, **89**, 313-318 (DOI:10.1016/j.dyepig.2010.05.016).

58 S. R. Trenor, A. R. Shultz, B. J. Love and T. E. Long, Coumarins in Polymers: From Light Harvesting to Photo-Cross-Linkable Tissue Scaffolds, *Chemical reviews,* 2004, **104**, 3059-3078 (DOI:10.1021/cr030037c).

59 R. Anet, THE PHOTODIMERS OF COUMARIN AND RELATED COMPOUNDS, *Canadian journal of chemistry,* 1962, **40**, 1249-1257 (DOI:10.1139/v62-193).

60 R. Alcántara and S. Y. Wang, PHOTOCHEMISTRY OF THYMINE IN AQUEOUS SOLUTION, *Photochemistry and Photobiology (England),* 1965, **4**, 473-476 (DOI:10.1111/j.1751-1097.1965.tb09762.x).

61 D. Sun, S. M. Hubig and J. K. Kochi, Oxetanes from [2+2] Cycloaddition of Stilbenes to Quinone via Photoinduced Electron Transfer, *Journal of organic chemistry,* 1999, **64**, 2250-2258 (DOI:10.1021/jo981754n).

62 J. Desvergne and H. Bouas-Laurent, *Chapter 13 - Cycloaddition Reactions Involving 4n Electrons: (2+2) Cycloaddition; Molecules with Multiple Bonds Incorporated in or Linked to Aromatic Systems*, Elsevier Science, Amsterdam, 2003.

63 N. D. Epiotis, The Theory of Pericyclic Reactions, *Angew. Chem. Int. Ed Engl.,* 1974, **13**, 751-780 (DOI:10.1002/anie.197407511).

64 J. Ashenhurst, HOMO and LUMO In the Diels Alder Reaction, accessed 20 November 2022.<https://www.masterorganicchemistry.com/2018/03/23/molecular-orbitals-in-the-diels-alder-reaction/>.

65 P. Johnston, Doctoral thesis, Monash University, 2012.

66 D. L. MITCHELL and R. S. NAIRN, THE BIOLOGY OF THE (6–4) PHOTOPRODUCT, *Photochem. Photobiol.,* 1989, **49**, 805-819 (DOI:10.1111/j.1751-1097.1989.tb05578.x).

67 H. Kobayashi, H. Morioka, T. Torizawa, K. Kato, I. Shimada, O. Nikaido and E. Ohtsuka, Specificities and Rates of Binding of Anti-(6–4) Photoproduct Antibody Fragments to Synthetic Thymine Photoproducts, *Journal of biochemistry (Tokyo),* 1998, **123**, 182-188 (DOI:10.1093/oxfordjournals.jbchem.a021908).

68 P. Clivio, Inconsistencies in the specific nucleobase pairing motif prone to photodimerization in a MOF nanoreactor, *Nature Communications,* 2021, **12**, 6981 (DOI:10.1038/s41467-021-27196-6).

69 E. Adman and L. H. Jensen, The crystal and molecular structure of the cis-syn photodimer of uracil, *Acta Crystallographica Section B,* 1970, **26**, 1326-1334 (DOI:10.1107/S0567740870004077).

70 G. Ciamician and P. Silber, Chemische Lichtwirkungen, *Ber. Dtsch. Chem. Ges.,* 1902, **35**, 1992-2000 (DOI:10.1002/cber.190203502148).

71 X. Hou, Z. Wang, J. Lee, E. Wysocki, C. Oian, J. Schlak and Q. R. Chu, Synthesis of polymeric ladders by topochemical polymerization, *Chem. Commun.,* 2014, **50**, 1218-1220 (DOI:10.1039/C3CC47379A).

72 K. Hema, A. Ravi, C. Raju, J. R. Pathan, R. Rai and K. M. Sureshan, Topochemical polymerizations for the solid-state synthesis of organic polymers, *Chem. Soc. Rev.,* 2021, **50**, 4062-4099 (DOI:10.1039/D0CS00840K).

73 A. Matsumoto, T. Tanaka, T. Tsubouchi, K. Tashiro, S. Saragai and S. Nakamoto, Crystal Engineering for Topochemical Polymerization of Muconic Esters Using Halogen−Halogen and CH/π Interactions as Weak Intermolecular Interactions, *J. Am. Chem. Soc.,* 2002, **124**, 8891-8902 (DOI:10.1021/ja0205333).

74 G. K. Kole and J. J. Vittal, Solid-state reactivity and structural transformations involving coordination polymers, *Chemical Society reviews,* 2013, **42**, 1755-1775 (DOI:10.1039/C2CS35234F).

75 K. Hema, A. Ravi, C. Raju and K. M. Sureshan, Polymers with advanced structural and supramolecular features synthesized through topochemical polymerization, *Chemical science,* 2021, **12**, 5361-538 (DOI:10.1039/d0sc07066a).

76 R. Medishetty, I. Park, S. S. Lee and J. J. Vittal, Solid-state polymerisation via [2+2] cycloaddition reaction involving coordination polymers, *Chemical communications,* 2016, **52**, 3989-41 (DOI:10.1039/c5cc08374e).

77 B. Zimmermann, G. Baranović and J. Macan, IR study of temperature induced rearrangements of dehydrobenzoannulenes, *Vibrational Spectroscopy,* 2007, **43**, 38-45 (DOI:10.1016/j.vibspec.2006.06.007).

78 G. M. J. Schmidt, Topochemistry. Part III. The crystal chemistry of some trans-cinnamic acids, *Journal of the Chemical Society (Resumed),* 1964, 2014-2021 (DOI:10.1039/JR9640002014).

79 G. M. J. Schmidt, Photodimerization in the solid state, *Pure and applied chemistry,* 1971, **27**, 647-678 (DOI:10.1351/pac197127040647).

80 S. Skoulika, M. G. Siskos and A. Michaelides, 2D to 3D solvent mediated transformation of a photoreactive lanthanum MOF: a case of three parallel photo-cycloaddition reactions, *CrystEngComm,* 2019, **21**, 1137-1142 (DOI:10.1039/C8CE01983E).

81 S. Kusaka, A. Kiyose, H. Sato, Y. Hijikata, A. Hori, Y. Ma and R. Matsuda, Dynamic Topochemical Reaction Tuned by Guest Molecules in the Nanospace of a Metal–Organic Framework, *J. Am. Chem. Soc.,* 2019, **141**, 15742 (DOI:10.1021/jacs.9b07682).

82 M. Bui, I. Gunawan, V. Verheyen, P. Feron, E. Meuleman and S. Adeloju, Dynamic modelling and optimisation of flexible operation in post-combustion CO2 capture plants—A review, *Comput. Chem. Eng.,* 2014, **61**, 245-265 (DOI:10.1016/j.compchemeng.2013.11.015).

83 R. Pallach, J. Keupp, K. Terlinden, L. Frentzel-Beyme, M. Kloß, A. Machalica, J. Kotschy, S. K. Vasa, P. A. Chater, C. Sternemann, M. T. Wharmby, R. Linser, R. Schmid and S. Henke, Frustrated flexibility in metal-organic frameworks, *Nature communications,* 2021, **12**, 4097 (DOI:10.1038/s41467-021-24188-4).

84 H. Yu, D. T. L. Alexander, U. Aschauer and R. Häner, Synthesis of Responsive Two-Dimensional Polymers via Self-Assembled DNA Networks, *Angewandte Chemie (International ed.),* 2017, **56**, 5040-5044 (DOI:10.1002/anie.201701342).

85 F. Ishiwari, Y. Shoji and T. Fukushima, Supramolecular scaffolds enabling the controlled assembly of functional molecular units, *Chemical Science,* 2018, **9**, 228-241 (DOI:10.1039/c7sc04340f).

86 T. Aida and E. W. Meijer, Supramolecular polymers – we've come full circle, *Israel journal of chemistry,* 2020, **60**, 33-47 (DOI:10.1002/ijch.201900165).

87 E. Jahnke, I. Lieberwirth, N. Severin, J. P. Rabe and H. Frauenrath, Topochemical Polymerization in Supramolecular Polymers of Oligopeptide-Functionalized Diacetylenes, *Angewandte Chemie (International ed.),* 2006, **45**, 5383-5386 (DOI:10.1002/anie.200600610).

88 J. Seo, J. F. Joung, S. Park, Y. J. Son, J. Noh and J. Kim, Light-directed trapping of metastable intermediates in a self-assembly process, *Nature communications,* 2020, **11**, 6260 (DOI:10.1038/s41467-020-20172-6).

89 M. Zhu, L. Yin, Y. Zhou, H. Wu and L. Zhu, Engineering Rotaxane-Based Nanoarchitectures via Topochemical Photo-Cross-Linking, *Macromolecules,* 2018, **51**, 746-754 (DOI:10.1021/acs.macromol.7b02736).

90 M. A. Villalobos and J. Debling, Bulk and Solution Processes in Handbook of Polymer Synthesis, Characterization, and Processing, *Wiley Online Books,* 2013, **13**, 273-294 (DOI:10.1002/9781118480793.ch13).

91 P. Johnston, M. T. W. Hearn and K. Saito, Solid-State Photoreversible Polymerization of n -Alkyl-Linked Bis-Thymines using Non-Covalent Polymer-Templating, *Australian journal of chemistry,* 2010, **63**, 631-639 (DOI:10.1071/CH09619).

92 S. Honda and T. Toyota, Photo-triggered solvent-free metamorphosis of polymeric materials, *Nature Communications,* 2017, **8**, 502 (DOI:10.1038/s41467-017-00679-1).

93 T. Hughes, G. P. Simon and K. Saito, Light-Healable Epoxy Polymer Networks via Anthracene Dimer Scission of Diamine Crosslinker, *ACS Applied Materials & Interfaces,* 2019, **11**, 19429-19443 (DOI:10.1021/acsami.9b02521).

94 J. Dahlke, S. Zechel, M. D. Hager and U. S. Schubert, How to Design a Self-Healing Polymer: General Concepts of Dynamic Covalent Bonds and Their Application for Intrinsic Healable Materials, *Adv. Mater. Interfaces,* 2018, **5**, 1800051 (DOI:10.1002/admi.201800051).

95 Q. Yu, M. Li, J. Gao, P. Xu, Q. Chen, D. Xing, J. Yan, M. J. Zaworotko, J. Xu, Y. Chen, P. Cheng and Z. Zhang, Fabrication of Large Single Crystals for Platinum-Based Linear Polymers with Controlled-Release and Photoactuator Performance, *Angew. Chem. Int. Ed.,* 2019, **58**, 18634-18640 (DOI:10.1002/anie.201910749).

96 X. Luo, Z. Wei, B. Seo, Q. Hu, X. Wang, J. A. Romo, M. Jain, M. Cakmak, B. W. Boudouris, K. Zhao, J. Mei, B. M. Savoie and L. Dou, Circularly Recyclable Polymers Featuring Topochemically Weakened Carbon–Carbon Bonds, *J. Am. Chem. Soc.,* 2022, **144**, 16588 (DOI:10.1021/jacs.2c06417).

97 T. Hughes, G. P. Simon and K. Saito, Chemistries and capabilities of photo-formable and photoreversible crosslinked polymer networks, *Materials horizons,* 2019, **6**, 1762-1773 (DOI:10.1039/c9mh00217k).

98 Y. Tezuka and H. Oike, Topological Polymer Chemistry: Systematic Classification of Nonlinear Polymer Topologies, *J. Am. Chem. Soc.,* 2001, **123**, 11570-11576 (DOI:10.1021/ja0114409).

99 S. Nakagawa and N. Yoshie, Star polymer networks: a toolbox for cross-linked polymers with controlled structure, *Polymer chemistry,* 2022, **13**, 274-217 (DOI:10.1039/d1py01547h).

100 J. E. Mark and P. -. Sung, Model polyurethane networks prepared from poly(ethylene oxide) and poly(tetramethylene oxide), *European Polymer Journal,* 1980, **16**, 1223-1227 (DOI:10.1016/0014-3057(80)90029-4).

101 G. Hild, Model networks based on `endlinking' processes: synthesis, structure and properties, *Progress in Polymer Science,* 1998, **23**, 1019-1149 (DOI:10.1016/S0079-6700(97)00055-5).

102 M. Mohadjer Beromi, C. R. Kennedy, J. M. Younker, A. E. Carpenter, S. J. Mattler, J. A. Throckmorton and P. J. Chirik, Iron-catalysed synthesis and chemical recycling of telechelic 1,3-enchained oligocyclobutanes, *Nature chemistry,* 2021, **13**, 156-162 (DOI:10.1038/s41557-020-00614-w).

103 J. M. Hoyt, V. A. Schmidt, A. M. Tondreau and P. J. Chirik, Iron-catalyzed intermolecular [2+2] cycloadditions of unactivated alkenes, *Science,* 2015, **349**, 960-963 (DOI:10.1126/science.aac7440).

104 A. Ahmed, S. Arya, V. Gupta, H. Furukawa and A. Khosla, 4D printing: Fundamentals, materials, applications and challenges, *Polymer,* 2021, **228**, 123926 (DOI:10.1016/j.polymer.2021.123926).

105 A. Lendlein, H. Jiang, O. Jünger and R. Langer, Light-induced shape-memory polymers, *Nature,* 2005, **434**, 879-882 (DOI:10.1038/nature03496).

106 S. Zechel, M. D. Hager and U. S. Schubert, *Self-Healing Polymers: From Biological Systems to Highly Functional Polymers*, Springer International Publishing, Cham, 2019.

107 S. Wang and M. W. Urban, Self-healing polymers, *Nature reviews. Materials,* 2020, **5**, 562-583 (DOI:10.1038/s41578-020-0202-4).

108 Y. Yang, X. Ding and M. W. Urban, Chemical and physical aspects of self-healing materials, *Progress in Polymer Science,* 2015, **49-50**, 34-59 (DOI:10.1016/j.progpolymsci.2015.06.001).

109 S. Banerjee, R. Tripathy, D. Cozzens, T. Nagy, S. Keki, M. Zsuga and R. Faust, Photoinduced Smart, Self-Healing Polymer Sealant for Photovoltaics, *ACS Applied Materials & Interfaces,* 2015, **7**, 2064-2072 (DOI:10.1021/am508096c).

110 M. Abdallh, C. Yoshikawa, M. T. W. Hearn, G. P. Simon and K. Saito, Photoreversible Smart Polymers Based on $2\pi + 2\pi$ Cycloaddition Reactions: Nanofilms to Self-Healing Films, *Macromolecules,* 2019, **52**, 2446-2455 (DOI:10.1021/acs.macromol.8b01729).

111 T. Hughes, G. P. Simon and K. Saito, Photocuring of 4-arm coumarin-functionalised monomers to form highly photoreversible crosslinked epoxy coatings, *Polymer chemistry,* 2019, **10**, 2134-2142 (DOI:10.1039/C8PY01767K).

112 T. Hughes, G. P. Simon and K. Saito, Improvement and tuning of the performance of light-healable polymers by variation of the monomer content, *Polymer chemistry,* 2018, **9**, 5585-5593 (DOI:10.1039/C8PY01203B).

113 S. Kaiser, S. V. Radl, J. Manhart, S. Ayalur-Karunakaran, T. Griesser, A. Moser, C. Ganser, C. Teichert, W. Kern and S. Schlögl, Switching "on" and "off" the adhesion in stimuli-responsive elastomers, *Soft matter,* 2018, **14**, 2547-2559 (DOI:10.1039/C8SM00284C).

114 M. Inada, A. Udagawa, S. Sato, T. Asahi and K. Saito, Photo-conversion of self-assembled structures into continuous covalent structures via [2 + 2]-cycloaddition reactions, *Photochemical & Photobiological Sciences,* 2022, **21**, 2169-2177 (DOI:10.1007/s43630-022-00286-0).

115 K. Petkau - Milroy and L. Brunsveld, Supramolecular chemical biology : bioactive synthetic self-assemblies, *Org. Biomol. Chem.,* 2013, **11**, 219-232 (DOI:10.1039/c2ob26790j).

116 K. H. Park, K. Jang and S. U. Son, Synthesis, Optical Properties, and Self-Assembly of Ultrathin Hexagonal In2S3 Nanoplates, *Angewandte Chemie,* 2006, **118**, 4724-4728 (DOI:10.1002/ange.200601031).

117 G. M. Whitesides and B. Grzybowski, Self-Assembly at All Scales, *Science,* 2002, **295**, 2418-2421 (DOI:10.1126/science.1070821).

118 G. M. Whitesides, J. P. Mathias and C. T. Seto, Molecular self-assembly and nanochemistry: a chemical strategy for the synthesis of nanostructures, *Science,* 1991, **254**, 1312-1319 (DOI:10.1126/science.1962191).

119 J. Lehn, Supramolecular chemistry: from molecular information towards self-organization and complex matter, *Reports on progress in physics,* 2004, **67**, 249-265 (DOI:10.1088/0034-4885/67/3/R02).

120 N. V. Solodkov, J. Shim and J. C. Jones, Self-assembly of fractal liquid crystal colloids, *Nature Communications,* 2019, **10**, 198 (DOI:10.1038/s41467-018-08210-w).

121 J. Motoyanagi, T. Fukushima, N. Ishii and T. Aida, Photochemical Stitching of a Tubularly Assembled Hexabenzocoronene Amphiphile by Dimerization of Coumarin Pendants, *Journal of the American Chemical Society,* 2006, **128**, 4220-4221 (DOI:10.1021/ja060593z).

122 D. Gçrl and F. Würthner, Entropically Driven Self-Assembly of Bolaamphiphilic Perylene Dyes in Water, *Angew. Chem. Int. Ed.,* 2016, **55**, 12094 (DOI:10.1002/anie.201606917).

123 B. Maiti, A. Abramov, R. Pérez-Ruiz and D. Díaz Díaz, The Prospect of Photochemical Reactions in Confined Gel Media, *Acc. Chem. Res.,* 2019, **52**, 1865 (DOI:10.1021/acs.accounts.9b00097).

124 B. Adhikari, X. Lin, M. Yamauchi, H. Ouchi, K. Aratsu and S. Yagai, Hydrogen-bonded rosettes comprising π-conjugated systems as building blocks for functional one-dimensional assemblies, *Chemical communications,* 2017, **53**, 9663-9683 (DOI:10.1039/c7cc04172a).

125 Q. Zhang, D. Qu and H. Tian, Photo-Regulated Supramolecular Polymers: Shining Beyond Disassembly and Reassembly, *Advanced optical materials,* 2019, **7**, 1900033 (DOI:10.1002/adom.201900033).

126 M. Yoshizawa, M. Tamura and M. Fujita, Diels-Alder in Aqueous Molecular Hosts: Unusual Regioselectivity and Efficient Catalysis, *Science,* 2006, **312**, 251-254 (DOI:10.1126/science.1124985).

127 M. Yoshizawa, Y. Takeyama, T. Kusukawa and M. Fujita, Cavity-Directed, Highly Stereoselective [2+2] Photodimerization of Olefins within Self-Assembled Coordination Cages, *Angewandte Chemie International Edition,* 2002, **41**, 1347 (DOI:10.1002/1521-3773(20020415)41:8<1347::aid-anie1347>3.0.co;2-x).

128 I. Park, R. Medishetty, H. Lee, C. E. Mulijanto, H. S. Quah, S. S. Lee and J. J. Vittal, Formation of a Syndiotactic Organic Polymer Inside a MOF by a [2+2] Photo-Polymerization Reaction, *Angewandte Chemie,* 2015, **127**, 7421-7425 (DOI:10.1002/ange.201502179).

129 H. Frisch, J. P. Menzel, F. R. Bloesser, D. E. Marschner, K. Mundsinger and C. Barner-Kowollik, Photochemistry in Confined Environments for Single-Chain Nanoparticle Design, *J. Am. Chem. Soc.,* 2018, **140**, 9551 (DOI:10.1021/jacs.8b04531).

130 H. Frisch, F. R. Bloesser and C. Barner-kowollik, Controlling Chain Coupling and Single-Chain Ligation by Two Colours of Visible Light, *Angew. Chem. Int. Ed.,* 2019, **58**, 3604 (DOI:10.1002/anie.201811541).

131 A. S. Al-Shereiqi, B. J. Boyd and K. Saito, Photo-responsive self-assemblies based on bio-inspired DNA-base containing bolaamphiphiles, *Chemical communications,* 2015, **51**, 5460-5462 (DOI:10.1039/C4CC08580A).

132 P. Johnston, C. Braybrook and K. Saito, Topochemical photo-reversible polymerization of a bioinspired monomer and its recovery and repolymerization after photo-depolymerization, *Chemical science (Cambridge),* 2012, **3**, 2301 (DOI:10.1039/c2sc20380d).

133 A. Udagawa, P. Johnston, H. Uekusa, H. Koshima, K. Saito and T. Asahi, Solid-State Photochemical Reaction of Multisubstituted Thymine Derivatives, *ACS sustainable chemistry & engineering,* 2016, **4**, 6107-6114 (DOI:10.1021/acssuschemeng.6b01529).

134 A. Udagawa, P. Johnston, A. Sakon, R. Toyoshima, H. Uekusa, H. Koshima, K. Saito and T. Asahi, Crystal-to-crystal photo-reversible polymerization mechanism of bis-thymine derivative, *RSC advances,* 2016, **6**, 107317-107322 (DOI:10.1039/C6RA24229D).

135 A. S. Al-Shereiqi, B. J. Boyd and K. Saito, Photo-Switchable Self-Assemblies Based on Thymine-Containing Bolaamphiphiles, *ChemPlusChem (Weinheim, Germany),* 2017, **82**, 1135-1144 (DOI:10.1002/cplu.201700207).

136 A. Udagawa, Doctoral thesis, Waseda University, 2017.

137 M. Banno, T. Yamaguchi, K. Nagai, C. Kaiser, S. Hecht and E. Yashima, Optically Active, Amphiphilic Poly(meta-phenylene ethynylene)s: Synthesis, Hydrogen-Bonding Enforced Helix Stability, and Direct AFM Observation of Their Helical Structures, *J. Am. Chem. Soc.,* 2012, **134**, 8718-8728 (DOI:10.1021/ja303204m).

138 C. A. Scarff, M. J. G. Fuller, R. F. Thompson and M. G. Iadaza, Variations on Negative Stain Electron Microscopy Methods: Tools for Tackling Challenging Systems, *Journal of Visualized Experiments,* 2018, **132**, 57199 (DOI:10.3791/57199).

139 H. Kobayashi, H. Morioka, T. Torizawa, K. Kato, I. Shimada, O. Nikaido and E. Ohtsuka, Specificities and Rates of Binding of Anti-(6–4) Photoproduct Antibody Fragments to Synthetic Thymine Photoproducts, *Journal of biochemistry (Tokyo),* 1998, **123**, 182-188 (DOI:10.1093/oxfordjournals.jbchem.a021908).

140 N. Tohnai, M. Miyata, N. Yasui, E. Mochizuki, Y. Kai and Y. Inaki, Photodimerization of Thymine Derivatives in Single Crystal, *Journal of Photopolymer Science and Technology,* 1998, **11**, 59-64 (DOI:10.2494/photopolymer.11.59).

141 D. K. Hohl and C. Weder, (De)bonding on Demand with Optically Switchable Adhesives, *Advanced Optical Materials,* 2019, **7**, 1900230 (DOI:10.1002/adom.201900230).

142 B. T. Michal, E. J. Spencer and S. J. Rowan, Stimuli-Responsive Reversible Two-Level Adhesion from a Structurally Dynamic Shape-Memory Polymer, *ACS Applied Materials & Interfaces,* 2016, **8**, 11041-11049 (DOI:10.1021/acsami.6b01251).

143 H. Zhu, A. Demirci, Y. Liu, J. Gong and M. Mitsuishi, Robust, Reusable, and Antioxidative Supramolecular Adhesive to Inorganic Surfaces Based on Water-Stimulated

Hydrogen Bonding, *ACS Applied Polymer Materials,* 2022, **4**, 1586-1594 (DOI:10.1021/acsapm.1c01353).

144 Z. Liu and F. Yan, Switchable Adhesion: On-Demand Bonding and Debonding, *Advanced Science,* 2022, **9**, 2200264 (DOI:10.1002/advs.202200264).

145 N. D. Blelloch, H. J. Yarbrough and K. A. Mirica, Stimuli-responsive temporary adhesives: enabling debonding on demand through strategic molecular design, *Chemical Science,* 2021, **12**, 15183-15205 (DOI:10.1039/d1sc03426j).

146 Y. Zhao, S. Song, X. Ren, J. Zhang, Q. Lin and Y. Zhao, Supramolecular Adhesive Hydrogels for Tissue Engineering Applications, *Chem. Rev.,* 2022, **122**, 5604-5640 (DOI:10.1021/acs.chemrev.1c00815).

147 K. R. Mulcahy, A. F. R. Kilpatrick, G. D. J. Harper, A. Walton and A. P. Abbott, Debondable adhesives and their use in recycling, *Green Chem.,* 2021, **24**, 36-61 (DOI:10.1039/d1gc03306a).

148 Y. Choi, K. Kang, D. Son and M. Shin, Molecular Rationale for the Design of Instantaneous, Strain-Tolerant Polymeric Adhesive in a Stretchable Underwater Human–Machine Interface, *ACS Nano,* 2022, **16**, 1368-1380 (DOI:10.1021/acsnano.1c09393).

149 Y. Lu, J. Broughton and P. Winfield, A review of innovations in disbonding techniques for repair and recycling of automotive vehicles, *Int J Adhes Adhes,* 2014, **50**, 119-127 (DOI:10.1016/j.ijadhadh.2014.01.021).

150 M. D. Banea, L. F. M. Silva and R. J. C. Carbas, Debonding on command of adhesive joints for the automotive industry, *Int J Adhes Adhes,* 2015, **59**, 14-20 (DOI:10.1016/j.ijadhadh.2015.01.014).

151 C. Zhang, M. Wang, C. Jiang, P. Zhu, B. Sun, Q. Gao, C. Gao and R. Liu, Highly adhesive and self-healing γ-PGA/PEDOT:PSS conductive hydrogels enabled by multiple hydrogen bonding for wearable electronics, *Nano Energy,* 2022, **95**, 106991 (DOI:10.1016/j.nanoen.2022.106991).

152 C. Shao, L. Meng, C. Cui and J. Yang, An integrated self-healable and robust conductive hydrogel for dynamically self-adhesive and highly conformable electronic skin, *Journal of Materials Chemistry C,* 2019, **7**, 15208-15218 (DOI:10.1039/c9tc05467g).

153 H. Memon, Y. Wei and C. Zhu, Recyclable and reformable epoxy resins based on dynamic covalent bonds – Present, past, and future, *Polym. Test.,* 2022, **105**, 107420 (DOI:10.1016/j.polymertesting.2021.107420).

154 M. A. Rahman, C. Bowland, S. Ge, S. R. Acharya, S. Kim, V. R. Cooper, X. C. Chen, S. Irle, A. P. Sokolov, A. Savara and T. Saito, Design of tough adhesive from commodity thermoplastics through dynamic crosslinking, *Science Advances,* 2021, **7**, eabk2451 (DOI:10.1126/sciadv.abk2451).

155 R. J. Wojtecki, M. A. Meador and S. J. Rowan, Using the dynamic bond to access macroscopically responsive structurally dynamic polymers, *Nature Materials,* 2011, **10**, 14-27 (DOI:10.1038/nmat2891).

156 S. Das, S. Samitsu, Y. Nakamura, Y. Yamauchi, D. Payra, K. Kato and M. Naito, Thermo-resettable cross-linked polymers for reusable/removable adhesives, *Polymer Chemistry,* 2018, **9**, 5559-5565 (DOI:10.1039/c8py01495g).

157 J. H. Aubert, Note: Thermally removable epoxy adhesives incorporating thermally reversible diels-alder adducts, *The Journal of Adhesion,* 2010, **79**, 609-616 (DOI:10.1080/00218460309540).

158 K. K. Oehlenschlaeger, N. K. Guimard, J. Brandt, J. O. Mueller, C. Y. Lin, S. Hilf, A. Lederer, M. L. Coote, F. G. Schmidt and C. Barner-Kowollik, Fast and catalyst -free hetero-Diels–Alder chemistry for on demand cyclable bonding/debonding materials, *Polymer Chemistry,* 2013, **4**, 4348-4355 (DOI:10.1039/c3py00476g).

159 A. J. Inglis, L. Nebhani, O. Altintas, F. G. Schmidt and C. Barner-Kowollik, Rapid Bonding/Debonding on Demand: Reversibly Cross-Linked Functional Polymers via Diels−Alder Chemistry, *Macromolecules,* 2010, **43**, 5515-5520 (DOI:10.1021/ma100945b).

160 H. Tsai, Y. Nakamura, W. Hu, T. Fujita and M. Naito, Mechanochromism of dynamic disulfide bonds as a chromophoric indicator of adhesion strength for epoxy adhesive, *Materials Advances,* 2021, **2**, 5047-5051 (DOI:10.1039/d1ma00252j).

161 H. Zhang, C. Cai, W. Liu, D. Li, J. Zhang, N. Zhao and J. Xu, Recyclable Polydimethylsiloxane Network Crosslinked by Dynamic Transesterification Reaction, *Scientific Reports,* 2017, **7**, 11833 (DOI:10.1038/s41598-017-11485-6).

162 N. Ishikawa, M. Furutani and K. Arimitsu, Adhesive Materials Utilizing a Thymine–Adenine Interaction and Thymine Photodimerization, *ACS Macro Letters,* 2015, **4**, 741-744 (DOI:10.1021/acsmacrolett.5b00359).

163 L. Wang, X. Ma, L. Wu, Y. Sha, B. Yu, X. Lan, Y. Luo, Y. Shi, Y. Wang and Z. Luo, Coumarin derivative trigger controlled photo-healing of ion gels and photo-controlled reversible adhesiveness, *European Polymer Journal,* 2021, **144**, 110213 (DOI:10.1016/j.eurpolymj.2020.110213).

164 S. R. Trenor, T. E. Long and B. J. Love, Development of a Light-Deactivatable PSA Via Photodimerization, *The Journal of Adhesion,* 2005, **81**, 213-229 (DOI:10.1080/00218460590922011).

165 J. Ling, M. Z. Rong and M. Q. Zhang, Photo-stimulated self-healing polyurethane containing dihydroxyl coumarin derivatives, *Polymer,* 2012, **53**, 2691-2698 (DOI:10.1016/j.polymer.2012.04.016).

166 H. Akiyama, Y. Okuyama, T. Fukata and H. Kihara, Reversible Photocuring of Liquid Hexa-Anthracene Compounds for Adhesive Applications, *The Journal of Adhesion,* 2018, **94**, 1-15 (DOI:10.1080/00218464.2017.1383244).

167 S. Kaiser, S. V. Radl, J. Manhart, S. Ayalur-Karunakaran, T. Griesser, A. Moser, C. Ganser, C. Teichert, W. Kern and S. Schlögl, Switching "on" and "off" the adhesion in stimuli-responsive elastomers, *Soft Matter,* 2018, **14**, 2547-2559 (DOI:10.1039/c8sm00284c).

168 Z. Wang, L. Guo, H. Xiao, H. Cong and S. Wang, A reversible underwater glue based on photo- and thermo-responsive dynamic covalent bonds, *Materials Horizons,* 2019, **7**, 282-288 (DOI:10.1039/c9mh01148j).

169 Z. Liu, G. Wang, J. Cheng and J. Zhang, Crystalline segments in a photo-detachable adhesive, *European Polymer Journal,* 2021, **152**, 110472 (DOI:10.1016/j.eurpolymj.2021.110472).

170 L. Shen, J. Cheng and J. Zhang, Reworkable adhesives: Healable and fast response at ambient environment based on anthracene-based thiol-ene networks, *European polymer journal,* 2020, **137**, 109927 (DOI:10.1016/j.eurpolymj.2020.109927).

171 Z. Liu, J. Cheng and J. Zhang, An Efficiently Reworkable Thermosetting Adhesive Based on Photoreversible [4+4] Cycloaddition Reaction of Epoxy-Based Prepolymer with Four Anthracene End Groups, *Macromolecular Chemistry and Physics,* 2021, **222**, 2000298 (DOI:10.1002/macp.202000298).

172 G. Xu, S. Li, C. Liu and S. Wu, Photoswitchable Adhesives Using Azobenzene-Containing Materials, *Chemistry – An Asian Journal,* 2020, **15**, 547-554 (DOI:10.1002/asia.201901655).

173 J. T. Lai, D. Filla and R. Shea, Functional Polymers from Novel Carboxyl-Terminated Trithiocarbonates as Highly Efficient RAFT Agents, *Macromolecules,* 2002, **35**, 6754-6756 (DOI:10.1021/ma020362m).

174 Y. Amamoto, J. Kamada, H. Otsuka, A. Takahara and K. Matyjaszewski, Repeatable Photoinduced Self-Healing of Covalently Cross-Linked Polymers through Reshuffling of Trithiocarbonate Units, *Angewandte Chemie International Edition,* 2011, **50**, 1660-1663 (DOI:10.1002/anie.201003888).

175 K. J. Arrington, S. C. Radzinski, K. J. Drummey, T. E. Long and J. B. Matson, Reversibly Cross-linkable Bottlebrush Polymers as Pressure-Sensitive Adhesives, *ACS Applied Materials & Interfaces,* 2018, **10**, 26662-26668 (DOI:10.1021/acsami.8b08480).

176 J. J. Gallagher, M. A. Hillmyer and T. M. Reineke, Acrylic Triblock Copolymers Incorporating Isosorbide for Pressure Sensitive Adhesives, *ACS Sustainable Chemistry & Engineering,* 2016, **4**, 3379-3387 (DOI:10.1021/acssuschemeng.6b00455).

177 Y. Yang and M. W. Urban, Self-healing polymeric materials, *Chem. Soc. Rev.,* 2013, **42**, 7446-7467 (DOI:10.1039/c3cs60109a).

178 A. V. Menon, G. Madras and S. Bose, The journey of self-healing and shape memory polyurethanes from bench to translational research, *Polym. Chem.,* 2019, **10**, 4370-4388 (DOI:10.1039/C9PY00854C).

179 S. Wang and M. W. Urban, Self-healing polymers, *Nature Reviews Materials,* 2020, **5**, 562-583 (DOI:10.1038/s41578-020-0202-4).

180 T. Hughes, G. P. Simon and K. Saito, Improvement and tuning of the performance of light-healable polymers by variation of the monomer content, *Polymer Chemistry,* 2018, **9**, 5585-5593 (DOI:10.1039/c8py01203b).

181 T. Hughes, G. P. Simon and K. Saito, Chemistries and capabilities of photo-formable and photoreversible crosslinked polymer networks, *Materials Horizons,* 2019, **6**, 1762-1773 (DOI:10.1039/c9mh00217k).

182 M. Abdallh, C. Yoshikawa, M. T. W. Hearn, G. P. Simon and K. Saito, Photoreversible Smart Polymers Based on 2π + 2π Cycloaddition Reactions: Nanofilms to Self-Healing Films, *Macromolecules,* 2019, **52**, 2446-2455 (DOI:10.1021/acs.macromol.8b01729).

183 J. Ling, M. Z. Rong and M. Q. Zhang, Coumarin imparts repeated photochemical remendability to polyurethane, *Journal of Materials Chemistry,* 2011, **21**, 18373-18380 (DOI:10.1039/c1jm13467a).

184 S. Peng, Y. Sun, C. Ma, G. Duan, Z. Liu and C. Ma, Recent advances in dynamic covalent bond-based shape memory polymers, *e-Polymers,* 2022, **22**, 285-300 (DOI:10.1515/epoly-2022-0032).

185 A. Lendlein, H. Jiang, O. Jünger and R. Langer, Light-induced shape-memory polymers, *Nature,* 2005, **434**, 879-882 (DOI:10.1038/nature03496).

186 Q. Zhao, W. Zou, Y. Luo and T. Xie, Shape memory polymer network with thermally distinct elasticity and plasticity, *Science Advances,* 2016, **2**, e1501297 (DOI:10.1126/sciadv.1501297).

187 T. Defize, J. Thomassin, H. Ottevaere, C. Malherbe, G. Eppe, R. Jellali, M. Alexandre, C. Jérôme and R. Riva, Photo-Cross-Linkable Coumarin-Based Poly(ε-caprolactone) for Light-Controlled Design and Reconfiguration of Shape-Memory Polymer Networks, *Macromolecules,* 2019, **52**, 444-456 (DOI:10.1021/acs.macromol.8b02188).

188 H. Zhu, A. Demirci, Y. Liu, J. Gong and M. Mitsuishi, Robust, Reusable, and Antioxidative Supramolecular Adhesive to Inorganic Surfaces Based on Water-Stimulated Hydrogen Bonding, *ACS Applied Polymer Materials,* 2022, **4**, 1586-1594 (DOI:10.1021/acsapm.1c01353).

189 H. Sun, C. P. Kabb, Y. Dai, M. R. Hill, I. Ghiviriga, A. P. Bapat and B. S. Sumerlin, Macromolecular metamorphosis via stimulus-induced transformations of polymer architecture, *Nature Chemistry,* 2017, **9**, 817-823 (DOI:10.1038/nchem.2730).

190 D. Aoki, S. Uchida and T. Takata, Star/Linear Polymer Topology Transformation Facilitated by Mechanical Linking of Polymer Chains, *Angewandte Chemie International Edition,* 2015, **54**, 6770-6774 (DOI:10.1002/anie.201500578).

191 A. U. Alrayyes, Y. Hu, R. F. Tabor, H. Wang and K. Saito, Photo-switchable membranes constructed from graphene oxide/star-PDMS nanocomposites for gas permeation control, *Journal of Materials Chemistry A,* 2021, **9**, 21167-21174 (DOI:10.1039/d1ta05947e).

192 R. B. Woodward and R. Hoffmann, The Conservation of Orbital Symmetry, *Angewandte Chemie International Edition in English,* 1969, **8**, 781-853 (DOI:10.1002/anie.196907811).

193 S. Inacker, J. Fanelli, S. I. Ivlev and N. A. Hampp, Intramolecular Coumarin-Dimer Containing Polyurethanes: Optical Tuning via Single- and Two-Photon Absorption Processes, *Macromolecules,* 2022, **55**, 8461-8471 (DOI:10.1021/acs.macromol.2c01374).

194 D. Van-Pham, M. T. Nguyen, K. Ohdomari, H. Nakanishi, T. Norisuye and Q. Tran-Cong-Miyata, Controlling the nano-deformation of polymer by a reversible photo-cross-linking reaction, *Advances in Natural Sciences: Nanoscience and Nanotechnology,* 2017, **8**, 025003 (DOI:10.1088/2043-6254/aa690d).

195 X. Xiang, N. Liu, L. Xu and Y. Cai, Review of recent findings on occurrence and fates of siloxanes in environmental compartments, *Ecotoxicol. Environ. Saf.,* 2021, **224**, 112631 (DOI:10.1016/j.ecoenv.2021.112631).

196 V. X. Truong and C. Barner-Kowollik, Photodynamic covalent bonds regulated by visible light for soft matter materials, *Trends in chemistry,* 2022, **4**, 291-304 (DOI:10.1016/j.trechm.2022.01.011).

197 D. E. Marschner, H. Frisch, J. T. Offenloch, B. T. Tuten, C. R. Becer, A. Walther, A. S. Goldmann, P. Tzvetkova and C. Barner-Kowollik, Visible Light [2 + 2] Cycloadditions for Reversible Polymer Ligation, *Macromolecules,* 2018, **51**, 3802 (DOI:10.1021/acs.macromol.8b00613).

198 S. Ha, Y. Lee, Y. Kwak, A. Mishra, E. Yu, B. Ryou and C. Park, Alkyne–Alkene [2 + 2] cycloaddition based on visible light photocatalysis, *Nature communications,* 2020, **11**, 2509 (DOI:10.1038/s41467-020-16283-9).

199 J. M. R. Narayanam and C. R. J. Stephenson, Visible light photoredox catalysis: applications in organic synthesis, *Chemical Society reviews,* 2010, **4**, 12-113 (DOI:10.1039/b913880n).

200 L. Hammer, N. J. Van Zee and R. Nicolaÿ, Dually Crosslinked Polymer Networks Incorporating Dynamic Covalent Bonds, *Polymers,* 2021, **13**, 396 (DOI:10.3390/polym13030396).

201 X. Niu, F. Wang, X. Kui, R. Zhang, X. Wang, X. Li, T. Chen, P. Sun and A. Shi, Dual Cross-linked Vinyl Vitrimer with Efficient Self-Catalysis Achieving Triple-Shape-Memory Properties, *Macromol. Rapid Commun.,* 2019, **40**, 1900313 (DOI:10.1002/marc.201900313).

202 J. Xu, Y. Chen, L. Wu, C. Tung and Q. Yang, Dynamic Covalent Bond Based on Reversible Photo [4 + 4] Cycloaddition of Anthracene for Construction of Double-Dynamic Polymers, *Organic letters,* 2013, **15**, 6148-6151 (DOI:10.1021/ol403015s).

203 J. Han, X. Dai, H. Wang, H. Zhang and Y. Liu, Dual-Stimulus Supramolecular Luminescent Switch Based on Cyanostilbene-Bridged Bis(Dibenzo-24-Crown-8) and a Diarylethene Derivative, *Adv. Optical Mater.,* 2022, **10**, 2102390 (DOI:10.1002/adom.202102390).

204 J. Leng, X. Lan, Y. Liu and S. Du, Shape-memory polymers and their composites: Stimulus methods and applications, *Progress in materials science,* 2011, **56**, 1077-1135 (DOI:10.1016/j.pmatsci.2011.03.001).

205 S. Lee, S. Shin and D. Lee, Self-healing of cross-linked PU via dual-dynamic covalent bonds of a Schiff base from cystine and vanillin, *Materials & Design,* 2019, **172**, 10774 (DOI:10.1016/j.matdes.2019.107774).

Academic achievements

List of publications

○<u>Moeka Inada</u>, Tatsuhiro Horii, Toshinori Fujie, Takuya Nakanishi, Toru Asahi, and Kei Saito, "Debonding-on-demand adhesive based on photo-reversible cycloaddition reactions", *Materials Advances*, DOI: 10.1039/D2MA01048H (2023.1).

○<u>Moeka Inada</u>, Akihiro Udagawa, Sota Sato, Toru Asahi, Kei Saito, "Photo-Conversion of Self Assembled Structures into Continuous Covalent Structures via [2+2]-Cycloaddition Reactions", *Photochemical & Photobiological Sciences*, 2022, **12**, 2169-2177 (2022.12).

List of conferences

<u>稲田萌花</u>, 朝日透, 齋藤敬,"光動的共有結合を有した自己修復性高分子フィルムの創出", 第 11 回 JACI/GSC シンポジウム, 2022 年 6 月, Poster Presentation (online)

<u>Moeka Inada</u>, Akihiro Udagawa, Sota Sato, Toru Asahi, Kei Saito, "Photo-conversion of 3D self assembly structure into continuous covalent structure via [2+2] cycloaddition reaction", Pacifichem 2021, December 2021, Poster Presentation (online)

<u>稲田 萌花</u>, 朝日 透, 齋藤 敬,"シロキサンを有する 4 分岐架橋ポリマー/銀ナノ複合材料の作製と自己修復性評価", 第 70 回高分子討論会, 2021 年 9 月, Poster Presentation (online)

<u>稲田 萌花</u>, 宇田川 瑛弘, 佐藤 宗太, 朝日 透, 齋藤 敬, "チミン誘導体の自己集合体形成と可逆的光化学反応に基づく省エネルギー・低環境負荷型材料の探索", 第 9 回 JACI/GSC シンポジウム, 2020 年 6 月, Poster Presentation (online)

<u>Moeka Inada</u>, Udagawa Akihiro, Kei Saito, Hideko Koshima, Toru Asahi, "Photochemical Reaction of Amphiphile Bis-Thymine Derivatives in Self-assembly Structure", 第 68 回高分子学会年次大会, May 2019, Oral Presentation (大阪府立国際会議場, 大阪)

<u>Moeka Inada,</u> Udagawa Akihiro, Kei Saito, Hideko Koshima, Toru Asahi, "Photochemical Reaction and Self-assembly of Chiral Bis-Thymine Derivatives", the 4th Molecular Chirality Asia, Harbin Engineering University, July 2018, Poster Presentation (Harbin, China)

<u>稲田 萌花</u>, 宇田川 瑛弘, 齋藤 敬, 小島 秀子, 朝日 透, "ビスチミン誘導体の自己集合体内の光化学反応と形態変化", 光化学討論会, 2018 年 9 月, Oral Presentation(関西学院大学上ケ原キャンパス, 西宮)

稲田 萌花, 宇田川 瑛弘, Al-Shereiqi Ahmed S, 齋藤 敬, 小島 秀子, 朝日 透, "水素結合を有するキラル Bis-Thymine 誘導体の自己集合化と光反応", 日本化学会 第 98 春季年会, 2018 年 3 月, Oral Presentation (日本大学理工学部船橋キャンパス, 船橋)

Akihiro Udagawa, Moeka Inada, Al-Shereiqi Ahmed S, Hideko Koshima, KOSHIMA, Kei Saito, Toru Asahi, "Photochemical Reaction of Bis-Thymine Derivatives in Self-assembly", 光化学討論会, September 2017, Poster presentation (東北大学青葉山キャンパス, 仙台)

List of symposiums

Moeka Inada, Akihiro Udagawa, Sota Sato, Toru Asahi, Kei Saito, "Recyclable Photopolymerization of Bis-Thymine Derivatives in Self-assembly", University of Waseda Day Individual Research Workshop on Advanced Research for Ageing Society, May 2019, Oral Presentation (Bonn University, Bonn, Germany)

Moeka Inada, Udagawa Akihiro, Kei Saito, Hideko Koshima, Toru Asahi, "Photochemical Reaction of Amphiphile Bis-Thymine Derivatives in Self-assembly Structure", 5th Core-to-Core International Symposium "3D Lab-Exchange Program", February 2019, Poster Presentation (Okinawa Institute of Science and Technology Graduate University, Onna, Okinawa).

Moeka Inada, Udagawa Akihiro, Kei Saito, Hideko Koshima, Toru Asahi," Photochemical Reaction of Amphiphile Bis-Thymine Derivatives in Self-assembly Structure", Joint Symposium of Peking University & Waseda University on Energy and nanomaterials, January 2019, Poster Presentation (Peking University, Begin, China).

Moeka Inada, Udagawa Akihiro, Kei Saito, Hideko Koshima, Toru Asahi, "The photochemical reaction of self-assembled bis-thymine derivatives", Monash-Waseda Joint Workshop on "Energy and Nanomaterials", November 2018, Poster Presentation (Waseda University, Tokyo).